ABSTRACT

BURNS, VIRGINIA ABIGAIL. Evolution of Cyclic Peptide Scaffolds to Target Nucleic Acids. (Under the direction of Dr. Christian Melander)

Given the great strides that have taken place over the past few decades in our understanding of nucleic acid's role in cellular processes, it has become abundantly clear that DNA and RNA can provide a great tool and target for drug development. The human genome project has provided a major impetus in identifying human genes implicated in diseases and has opened the door to new possibilities with DNA-based therapeutics. Further developments in transcriptomics and proteomics will provide additional momentum for the advancement of therapeutics by supplying novel targets for drug design, screening, and selection. As new discoveries are made and our knowledge of nucleic acid's role in life processes is expanding, the area of chemistry focused on learning how to target and exploit these nucleic acids for control of their relative processes is also expanding. New strategies to develop molecules that can both identify DNA or RNA targets and modulate their activity are of great interest to medicinal chemistry. The goal of this research was to delineate an efficient approach to targeting nucleic acids that yields cell permeable, biologically stable molecules that can be exploited *in vivo* applications.

Herein describes our approach which utilizes cyclic peptide phage display for the evolution of novel cyclic peptide scaffolds that target a given oligonucleotide. Evolved scaffolds are then tested *in vitro* as discrete entities to assess their binding capabilities. Given that the phage display scaffolds employ a disulfide linker for cyclization, alternative redox stable

macrocylic linkers were developed and synthesized. Generated analogues were subsequently assessed for the retention of the desired binding activity.

The details of this pragmatic approach were developed using the bTAR RNA oligo as a model system. Results indicated that not only could we evolve bTAR binders from a pool of 1.2 billion possible scaffolds in a relatively short time, but that these scaffolds bound with affinities in the low micromolar range when tested as discrete entities. We were also successful in developing an alternative dicarbon macrocyclic linker to yield redox stable analogues. Subsequent testing of the analogue scaffolds indicated the retention of the desired binding properties.

Evolution of Cyclic Peptide Scaffolds to Target Nucleic Acids

by
Virginia Abigail Burns

A dissertation submitted to the Graduate Faculty of
North Carolina State University
In partial fulfillment of the
Requirements for the degree of
Doctor of Philosophy

Chemistry

Raleigh, North Carolina

2008

APPROVED BY:

Dr. Christian Melander
Committee Chair

Dr. Reza Ghiladi

Dr. John Cavanagh

Dr. Tatyana Smirnova

DEDICATION

I would like to dedicate this work….

To all of the wonderful people who have helped me to achieve this goal. Thank you for the countless hours of love, support, and motivation.

To all of the amazing friends I have met along the way

To my grandma Keeton who inspires me to be a better person

To my Mom and Dad, who have stood by me through thick and thin

To my loving husband who makes me laugh, smile, and remember that there is more to life than work.

BIOGRAPHY

The author, Virginia A. Burns, was born on December 7th, 1976 in Booneville, MO. After graduating from the North Carolina School of Science and Mathematics in 1995, she attended North Carolina State University where she earned both a B.S. degree in Biochemistry and a B.A. degree in Chemistry. In August of 2004 she returned to academia to begin her doctoral studies at North Carolina State University under the advisement of Dr. Christian Melander. Virginia has taken a position at Duke Translational Research Institute working as a project leader for the Cellular Therapies Core. In this capacity, she will be working with researchers by streamlining efforts to translate basic science discoveries into therapeutics.

ACKNOWLEDGMENTS

Main Entry: 1fam·i·ly

Pronunciation: fam-lē, fa-mə-lē

Function: noun

Inflected Form(s): plural fam·i·lies

1 a group of individuals living under one roof and usually under one head: household
2 (a) group of persons of common ancestry: clan (b) a people or group of peoples regarded as deriving from a common stock
3 a group of people united by certain convictions or a common affiliation
4 a group of things related by common characteristics such as (a) a closely related series of elements or chemical compounds (b) a group of soils with similar chemical and physical properties (as texture, pH, and mineral content) that comprise a category ranking above the series and below the subgroup in soil classification (c) a group of related languages descended from a single ancestral language
5 (a) the basic unit in society traditionally consisting of two parents rearing their children; also: any of various social units differing from but regarded as equivalent to the traditional family "a single-parent family' (b) spouse and children "want to spend more time with my family"
6 a group of related plants or animals forming a category ranking above a genus and below an order and usually comprising several to many genera bin livestock breeding (1) the descendants or line of a particular individual especially of some outstanding female (2) an identifiable strain within a breed
7 a set of curves or surfaces whose equations differ only in parameters
8 a unit of a crime syndicate (as the Mafia) operating within a geographic area

TABLE OF CONTENTS

LIST OF TABLES

LIST OF FIGURES

CHAPTER 1: INTRODUCTION

Nucleic acids provide the fundamental basis for life. It has long been known that their chemical composition serves as the blueprint for the structure and function of all cellular and multicellular processes. Crick eloquently delineated this role when he first enunciated the concept of the Central Dogma of Molecular Biology which defines the flow of information in cellular processes as DNA $\longrightarrow$ RNA $\longrightarrow$ Protein.[1] According to this doctrine, DNA (deoxyribonucleic acid) is the permanent storage place for genetic information in the nucleus of the cell. RNA (ribonucleic acid) is transcribed from DNA and further processed by other enzymes. The resulting processed RNA, termed messenger RNA (mRNA) transmits genetic information encoded by the DNA to the protein synthesizers in the cell, and then serves as the template for translation of genes into proteins.

In recent years, it has also been discovered that nucleic acids have capabilities that far exceed their function to store and transmit genetic information. Although the majority of all DNA is found as a B-form double helical structure, DNA has been shown to form alternative secondary and tertiary structures that can serve as protein binding sites.[2-10] Through the recruitment of protein binding factors, these regions have been shown to exert regulatory control of transcription.[11] Other non-coding regions of DNA located in the telomeres and centromeres have been shown to contribute to chromosome stability.[12-16] The human genome project has also provided a major impetus in identifying human genes implicated in diseases and has opened the door to new possibilities with DNA-based therapeutics.[17] It has also given insight by elucidating the genetic markers responsible for patient response to drug therapy, drug interactions, and potential drug side effects.[18] Further developments in human genomics, transcriptomics, and proteomics will provide an additional impetus for the advancement of therapeutics by supplying novel targets for drug design, screening, and selection.

Ever-increasing evidence indicates that RNA can adopt an array of structural variations and can perform a wide range of cellular functions including the ability to function as direct sensors of biochemical physical signals without the involvement of proteins within an organism.[1, 19, 20] Cech and Altman won the 1989 Noble Prize in Chemistry for their groundbreaking work that showed that RNA can fold into complex shapes and are capable of catalyzing biochemical reactions, a function previously thought to be restricted to protein enzymes. These RNA enzymes, termed ribozymes, prove that RNA is sometimes an active participant in the chemistry of life, not just a passive messenger. Other interesting discoveries demonstrating a role for RNA beyond that of a simple messenger or transfer molecule include the importance of small nuclear ribonucleoproteins (snRNPs) in the processing of pre-mRNA and RNA editing, and reverse transcription from RNA in the maintenance of telomeres in the telomerase reaction.

Historically, molecules that target RNA have had far reaching application to human medicine and have been an attractive target for molecular medicine.[21] For example, bacterial ribosomal RNA (rRNA) has provided a valuable target for the development of new anti-infective agents.[22] Also, crucial protein/RNA interactions that drive the life cycle of many pathogenic viruses[23] offer an abundance of currently un-exploited targets for drug discovery.[21] One of the best elucidated examples would be that of the work done with HIV therapeutics. A number of potential therapies to control HIV replication rely upon disrupting either the Tat/TAR[24] or Rev/RRE[25] interaction. As such, there is a large body of scientific literature that has documented these research efforts to target RNA.[23, 25-27]

Given the great strides that have taken place over the past few decades in our understanding of nucleic acid's roles in cellular processes, it has become abundantly clear that DNA and RNA can provide a great tool and target for drug development. As new discoveries are made and our knowledge of nucleic acid's role in life processes is expanding, the area of chemistry focused on learning how to target and exploit these nucleic acids for control of their relative processes is also expanding. New strategies to develop molecules that can both identify DNA or RNA targets and modulate their activity are of great interest to medicinal chemistry. Our goal is to delineate an efficient approach that yields cell permeable, biologically stable molecules that can target a given nucleic acid for *in vivo* applications.

Although we would like to develop an approach that can be implemented universally to target all nucleic acid based structures, we chose to focus on RNA for our developmental phase and proof of concept experiment given the logistical difficulty of working with RNA due to its inherent instability and the myriad of secondary and tertiary structures it adopts.

Our premise is that if the methodology can be implemented successfully with RNA, then those principles should be able to be translated to DNA targets.

Targeting RNA

The emerging area of RNA as a tool and target for drug development requires that new methodologies be developed to identify biologically active cell permeable molecules that can specifically target RNA for therapeutic applications. There have been a plethora of strategies that have been developed to target RNA with cell permeable molecules.[28-30] These strategies include derivatization of the aminoglycoside backbone,[31] high throughput screening of chemical libraries,[28] and the use of linear peptides [29]and peptide conjugates.[21, 22, 32, 33] The approaches are summarized below and the well-documented limitations of each approach are highlighted.

Aminoglycosides (**Figure 1.1**) are naturally occurring RNA-binding scaffolds that bind in a pH-dependent manner and have disassociation constants in the high nanomolar to low micromolar range for RNA targets at physiological pH.[34] These polysaccharides provide a reliable starting point for analog design,[35] and have been studied extensively for RNA recognition. Structural modification of the core aminoglycoside scaffold can provide an RNA-binding ligand that binds in the low nanomolar range.[36] However, molecular complexity and the difficulty of derivative synthesis have prohibited the aminoglycoside scaffold from providing a widely applicable RNA recognition motif.

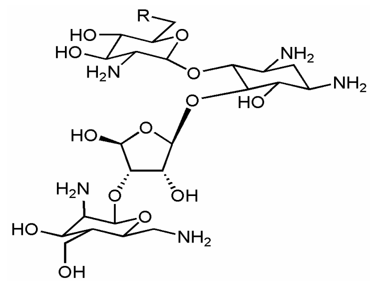

Figure 1.1. Aminoglycoside scaffold.

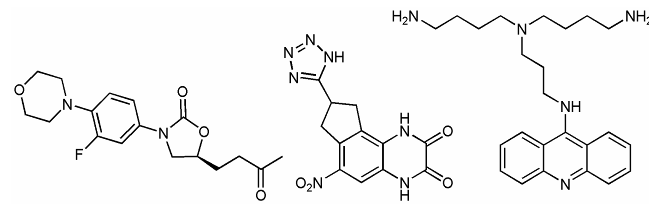

Figure 1.2. RNA-binding ligands identified by HTS screening.

High throughput screening (HTS) approaches have also been employed to identify small molecules that target predetermined RNA sequences (**Figure 1.2**).[27] In this approach, a molecular library is screened against the RNA target in a multi-well format. In each case, a small molecule has been identified that binds the RNA oligonucleotide. The HTS approach, however, suffers from a low hit rate and poor sequence discrimination of the identified hits. These limitations can be attributed to the fact that the libraries screened were originally designed for protein targets and do not represent optimal nucleic acid ligands.[37]

The myriad of secondary and tertiary structures that RNA oligonucleotides adopt[24] are, arguably, the biggest hurdle to surmount when designing molecules to target predetermined RNA sequences. Libraries of cell permeable molecules designed to bind proteins would not necessarily provide the optimal binding properties for targeting RNA. Ligands that bind nucleic acids with high affinity typically have more hydrogen bond donor/acceptor pairs than libraries designed under Lipinski's rules,[38] and possess a significantly larger architecture that is required to span and discriminate the larger binding surfaces presented by an oligonucleotide target. These principals have already been shown through previous work to develop sequence specific DNA binders.[39-41] In this approach, a basic polyamide scaffold, that was shown to be a modest DNA binder, could be derivatized to acquire sequence specificity through engineering optimal hydrogen bond donor/acceptor pair contacts with the base pairs of the DNA duplex.

This powerful hydrogen bond engineering approach can theoretically be applied to target RNA with one major caveat. In contrast to targeting DNA, which is primarily a static, B-form helix whose structure does not significantly alter based on sequence content, an approach to targeting RNA would have to be able to identify a unique scaffold for each RNA target. Since each potential RNA oligonucleotide target will have a unique secondary and tertiary structure, it would follow that each RNA oligonucleotide would require a unique scaffold for binding. Structure-based design could then be applied to each scaffold to augment both affinity and specificity as seen with DNA.[42, 43]

Nature has evolved its own RNA binding scaffold: proteins. In efforts to learn from nature's example, many researchers have developed approaches to employ peptides and peptide conjugates to target nucleic acids. Linear peptide RNA ligands have been derived from three general sources: 1) combinatorial libraries,[41, 44-49] 2) selection-based approaches,[50-56] and 3) the use of peptidomimetics and peptide fragments from RNA-binding proteins.[57-62] In each case, binding peptides have been identified. The limitation of this approach stems from the fact that linear peptides suffer from poor pharmacokinetics, are rapidly degraded in the gut, and often suffer from poor cell permeability.

Peptides for Targeting Nucleic Acids

There are many things to consider in the design of the small molecule library that is to be screened for RNA binding capabilities and determination of unique binding scaffolds. The library needs to be composed of small molecules that can potentially bind RNA with high specificity and that are stable to metabolic conditions in order to be used as therapeutic agents. Proteins have proven to be highly responsive sensors to biological and environmental signals, and are known to bind RNA in a sequence specific manner with biological function[63] indicating that short peptide sequences possess the necessary chemical attributes to effectively bind mRNA.[26, 64, 65] However, as noted with previous attempts to target RNA with linear peptides and peptide conjugates, linear peptides suffer from poor bioavailability and cell permeability.

Linear peptides exhibit poor drug metabolism and pharmacokinetics (DMPK) properties. One of their main drawbacks is their poor metabolic stability and inability to cross membrane barriers.[26, 64, 66-68] Specifically, linear peptides display very little stability towards proteolysis by peptidases in the gastrointestinal tract and in the serum with $t_{1/2}$ on the order of minutes. This is compounded by rapid excretion of linear peptides through the liver and/or kidneys. Linear peptides also display poor transport properties from the intestines to the blood and across the blood-brain barrier due to their high molecular weight and lack of specific transport systems.

Linear peptides also have shown limited ability for sequence specific recognition and discrimination between target molecules and negative controls. The lack of structural constraints within the peptide is responsible for lowering the binding specificity.[69] Linear peptides are inherently flexible which enables interactions with multiple receptors, not just the intended target. This could result in an array of undesired side effects if used as therapeutics. The lack of structural constraints within the peptide also lowers the peptide's activity because binding comes at an entropic loss.[69] Poor bioavailabilities combined with decreased specificity do not make linear peptides good candidates for small molecule design scaffolds to target RNA. The introduction of conformational constraints in a peptide, however, has been shown to increase bioavailability and specificity of binding. One way to apply conformational constraints within a peptide library is by the use of a cyclic peptide motif for small molecule design scaffold (**Figure 1.3**).

Linear peptides	Vs.	Cyclic peptides
• Lower binding specificity because of lack of structural constraints		• Conformational restraints due to cyclization increase binding specificity
• Inability to readily cross membrane barriers		• Allow for greater membrane permeability (> 5X larger)
• Poor metabolic stability, susceptible to chemical, thermal and enzymatic degradation		• Increased stability towards chemical, thermal and enzymatic degradation.
• Low activity because enforcing bioactive conformation is at an entropic cost		• Higher oral bioavailability and increased activity *in vivo*

Figure 1.3. Summary of the advantages of a cyclic vs. linear peptide scaffold

Cyclic peptides are at the forefront of current research in medicinal chemistry and are well-established therapeutics.[70] A short list of currently available cyclic peptide drugs include: actinomycin D (cancer chemotherapeutic), cyclosporin A (immunosuppresant),[23] oxytocin (labor induction),[27] polymyxin E (antibiotic),[26] and octreotide (growth hormone antagonist). Cyclic peptides have increased stability towards chemical, thermal and enzymatic degradation. Most enzymatic degradation pathways are initiated through either the amino or carboxy terminus of the peptide. Since cyclic peptides lack these termini, the rate of degradation by peptidases and other enzymes is greatly reduced in comparison to their linear counterparts.[43] Research has also shown that cyclic peptides show an increase in cell permeability which also contributes to higher bioavailability,[42, 66] along with increased binding specificity and activity.[71] Conformationally restrained structures eliminate the inherent flexibility observed with linear peptides and, therefore, minimize binding to non-target molecules and enhance the activity at the desired target.

Cyclic Peptide Phage Display

After careful consideration of the properties that were necessary to achieve a bioavailable, RNA binding, cell permeable molecule, we determined that the cyclic peptide motif would be employed as our binding scaffold. Critical thought was given as to how to screen our library of compounds for specific RNA binding. The use of a random cyclic peptide phage display library allows for the evolution of binding scaffolds in a manner that is not limited by conventional thoughts of what comprises a good RNA binder. In phage display, the library is directly encoded into a biological vector. This allows for high throughput screening using the virus as a biological workhorse for amplification and easy identification of any given member of the library through sequencing. Phage display techniques are also relatively cheap and easy to implement at preliminary stages for the development of this new methodology.

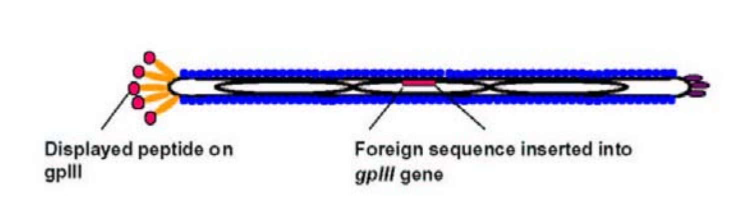

Figure 1.4. M13: A single-stranded filamentous DNA

Phage display technology involves the expression of exogenous proteins, peptides or peptide libraries on the surface of bacteriophage. The design of random peptide phage display libraries typically involves the in-frame insertion of a short random peptide into the M13 minor coat protein, gpIII, the functional activity of which remains intact (**Figure 1.4**). As a result, the peptide is displayed on the surface of the bacteriophage and the phage remains infectious for *E. coli*. Phage display libraries can then be subjected to an *in vitro* selection technique that enables phage that display polypeptides with desired properties to be selected and extracted from a larger collection of variants (**Figure 1.5**). The direct phenotype/genotype link of the genetically encoded library then enables rapid identification of selected clones. Since this methodology was originally described,[33] it has become established as a powerful method for identification of polypeptides with novel properties.[72-75]

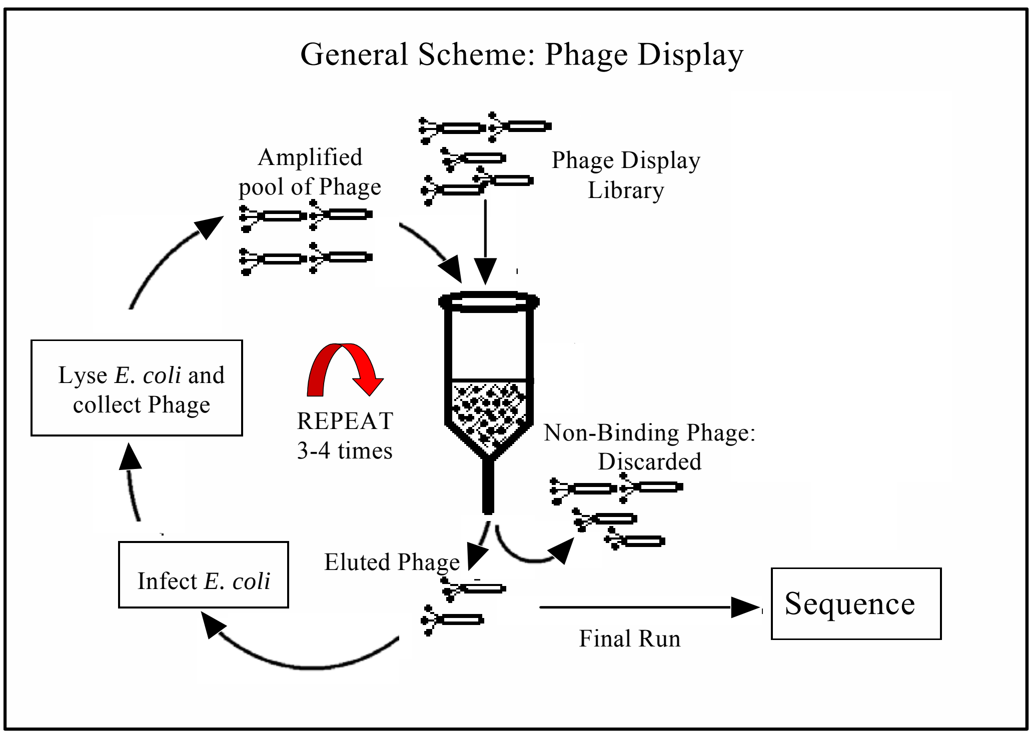

Figure 1.5. General *in vitro* selection scheme for "Positive" phage selection cycle. Step **1**, the phage library is incubated with the biotinylated RNA target. Step **2**, bound phage are captured with streptavidin. Step **3**, unbound phage are washed away. Step **4**, the bound phage are eluted and amplified to create an enriched phage library for the subsequent selection round. After 3-4 iterative rounds of selection, the final eluent is sequenced to identify binding motifs.

Cyclic peptide phage display libraries have previously been shown to be effective for targeting biological macromolecules.[30] Unlike linear phage display libraries, the randomized sequence is flanked by a pair of cysteines that can form a disulfide linkage (**Figure 1.6**). The disulfide-constrained peptides are engineered at the N-terminus of the pIII coat protein and followed by a short spacer (Gly-Gly-Gly-Ser) followed by the wild-type pIII sequence. Under nonreducing conditions the cysteines will spontaneously form a disulfide cross-link, resulting in phage display of cyclized peptides. Cysteine-constrained phage libraries have been utilized to map structural epitopes,[76-78] to identify mirror image ligands for D-amino acids,[79] and to generate leads for peptide-based therapeutics;[80-82] however, they have not been applied to the identification of discrete cyclic peptides that target pre-determined RNA sequences.

gIII leader sequence…TGT NNN NNN NNN $(NNN)_n$ TGC GGT GGA GGT TCG…. gIII wildtype

C----Randomer Sequence ----C---Gly---Gly---Gly---Ser---pIII wildtype

Disulfide linkage

Figure 1.6. Engineering of cysteine constrained cyclic peptide phage libraries

Previous reports that have investigated RNA binding with linear phage display libraries have demonstrated a correlation between peptide length and the ability to select RNA binding ligands. In initial studies, Schimmel[35] reported that they failed to select binding peptides from a random 10mer library when the library was screened against a hairpin microhelix containing 25 nucleotides. To overcome this hurdle, they flanked the N- and C-terminius of the 10mer library with a generic RGG motif of 9 amino acids (total peptide length = 28 amino acids). RGG peptides are known to bias RNA binding and, after performing multiple rounds of selection with this second generation construct, they were able to isolate and characterize a novel RNA-binding peptide. The individually synthesized peptide KRGGKRGGKMSVAMEAENVKRGGKRGGK had a K_d for its RNA target of 300 nM. Subsequently, studies by Agris have revealed that screening longer, 15mer peptide libraries negates the need to flank the peptide with the RGG motif, and sequence-specific RNA-binding phage can be selected.[48, 49] Individually synthesized 15mer peptides displayed dissociation constants of 1.3 – 45.4 μM for their target RNA oligonucleotide.[48] Interestingly, in both of these cases, selected peptides were not arginine/lysine rich, indicating that the sequence space of RNA-binding peptides is not limited to the highly charged character displayed by the well-studied arginine rich motif. More recent results have shown that it is possible to generate linear peptide binders with a 7-random amino acid phage library; however, subsequent biophysical characterization of these peptides revealed that the selected peptides had modest affinities to their RNA target (K_d = 25-35 μM).[49] Again, paralleling the work of Schimmel[35] and Agris,[48, 49] the selected peptides were not arginine/lysine rich.

As one of the ultimate goals for the development of this particular methodology was to identify biologically active, cell permeable ligands that bind discrete RNA sequences *in vivo*, the peptide length required to achieve sequence-specific recognition in these previous cases has prompted us to consider membrane permeability of our cyclic peptide library. Although there is no direct correlation between cyclic peptide size and cell permeability, the general guideline is to minimize size. It has been hypothesized that cysteine-constrained libraries that were of comparable length to either the Schimmel library (28 amino acids)[35] or the Agris library (15 amino acids)[48, 49] could be too large to be efficiently transported through a cell membrane. The size of the 7-random amino acid library was attractive, and led us to consider whether these shorter peptides, in cyclic form, could be utilized to target RNA for *in vivo* applications. Previous studies have shown that cyclic peptides can have superior recognition properties over their linear counterparts due to a reduction in the entropic loss upon binding.[40] Therefore, it was posited that these superior recognition properties would overcome the modest affinity demonstrated by the shorter, linear peptides,[45] and the use of cysteine-constrained libraries would allow for the identification of cyclic peptide scaffolds that had affinities that were comparable to the longer, linear peptides that both Schimmel[35] and Agris[48, 49] had selected (high nM to low μM).

Based upon this hypothesis, we elected to focus our initial efforts on cysteine-constrained libraries containing a seven amino acid variable region flanked by two cysteines. Seven variable amino acids results in a theoretical library diversity of 20^7, or 1.28×10^9 different cyclic peptides, and the 9 amino acid core (2 cysteines plus the 7 variable amino acids) gives an average MW of 1035 amu (for comparison, cyclosporin A has a MW of 1203 amu, while actinomycin D has a MW of 1255 amu).

Summary

My goal is to develop a new and streamlined approach to targeting nucleic acids. I hypothesize that cyclic peptide phage display can be exploited to efficiently identify novel cyclic peptide scaffolds from a comprehensive library that can specifically target a given RNA or DNA sequence. The cyclic peptide scaffold provides the necessary elements to specifically target nucleic acids and can easily make the transition to *in vivo* applications with its potentially more favorable DMPK properties.

Using a comprehensive, cysteine constrained, heptamer cyclic peptide library for selection allows for the evolution of novel cyclic peptide scaffolds that bind a target RNA, not based on or limited to preconceived ideas of what properties mitigate binding. These cysteine constrained scaffolds can subsequently be tested *in vitro* to characterize their binding properties and determine their binding affinities for the target oligonucleotide. Since the disulfide bond is the Achilles' heel of our molecular scaffold and would most likely be cleaved in a cellular environment, investigational studies of alternative, non-cleavable macrocyclic linkages are important to determine an alternative linkage that will elicit greater cellular stability without distorting the cysteine constrained peptide structure. Second generation scaffolds employing the alternative macrocyclic linkage were synthesized and subsequently tested for retention of desired binding properties.

After completing the proof of concept studies and refining the approach, there are many potential applications and directions to explore. In contrast to the peptidomimetic approach, this methodology is not hinged on a priori knowledge of an existing binder for the target sequence. This opens the door to use our methodology for any RNA or DNA target, including that of engineered RNA aptamers such as riboswitches

CHAPTER 2: DEVELOPMENT OF SELECTION SCHEME USING BTAR RNA

I. Introduction

The first phase of the development of a general nucleic acid targeting approach is the validation and refinement of methodology. Bovine Immunodeficiency Virus (BIV) Transactivating Response Sequence, bTAR, provides a well-characterized RNA target[32, 36, 45] that allows us to develop the basic science that will drive the ability to generate ligands that target predetermined RNA sequences. Once this methodology is developed, it can be applied to any other predetermined RNA sequence to generate potential therapeutics for targets of more medicinal importance.

The BIV model system was chosen rather than the HIV model system because human cells are not susceptible to BIV infection and have not been shown to seroconvert upon exposure to BIV, lowering the biological hazards associated with working with this virus. However, BIV is genetically and antigenically related to Human Immunodeficiency Virus-1 (HIV-1) with extremely high sequence homology (**Figure 2.1**). The two viruses are so structurally similar that they display cross reactivities with antibodies of each other when exposed to TAR RNA. The cross reactivities of antibodies likely represent reactivities to conserved epitopes found on BIV and HIV. [83]

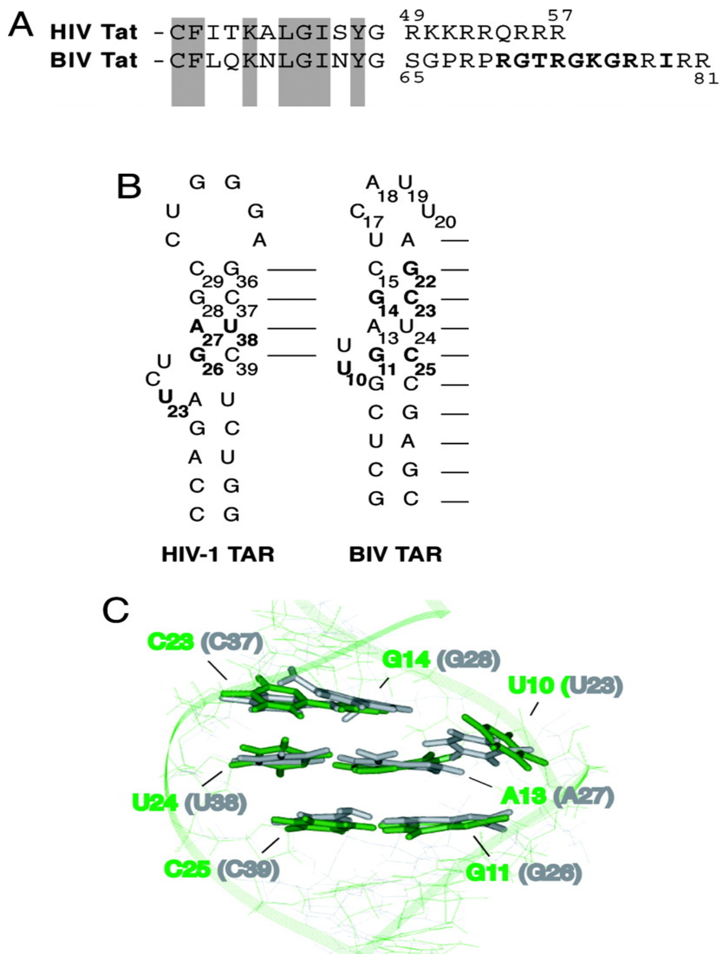

Figure 2.1. Taken from Calabro, Valerie et al. (2005) Proc. Natl. Acad. Sci. USA 102, 6849-6854. (*A*) The HIV-1 and BIV Tat ARM domains are aligned based on homology between the N-terminal activation domains (partially shown, with conserved residues shaded). (*B*) Secondary structures of the HIV-1 and BIV hairpins. Sequence identity is indicated by the lines, and nucleotides in HIV-1 and BIV TARs important for binding by the cognate protein are shown in bold. (*C*) Superimposition of the Tat binding sites in BIV TAR (green) and HIV-1 TAR (gray) in their bound conformations, from NMR models of the HIV-1 TAR-arginamide (19) and BIV Tat–TAR (28) complexes. The structures were superimposed by using all bases known to be important for binding of each, and the corresponding base numbering is shown for both RNAs.

The TAR RNA element is located at the 5'-terminus of the viral genome and functions as a responsive sequence for viral transcription initiation and/or elongation from the LTR promotor.[84] TAR RNA forms a conserved secondary structure of a hairpin stem-loop with a side bulge that binds the endogenous regulatory protein named the transcriptional transactivator or Tat (**Figure 2.2**). Stimulation of polymerase elongation results from interactions between Tat and serine kinase CDK9, which phosphorylates the carboxyl-terminal domain of RNA polymerase II[74] allowing full-length transcripts to be produced. In the absence of Tat expression, BIV/HIV has been shown to be capable of generating only short (less than 100 nucleotides in length) truncated transcripts. The Tat/TAR complex is one of two viral regulatory elements, both of which are essential for BIV/HIV gene expression,[75] and disrupting this interaction has been a target for drug discovery efforts.[44, 61] As a result,

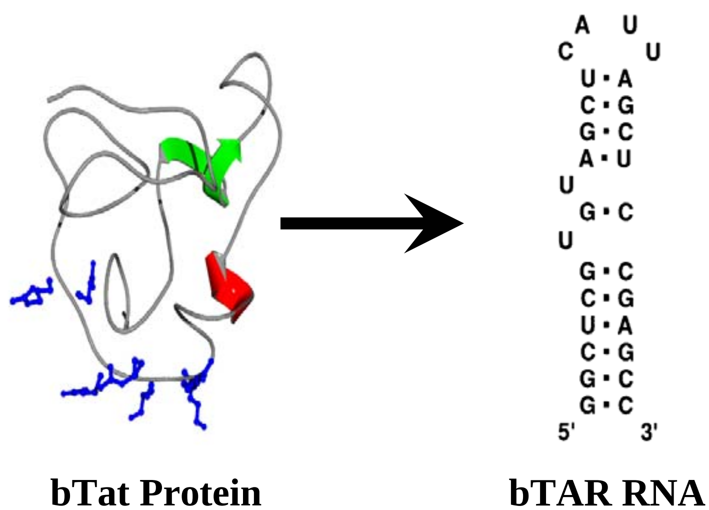

bTat: 103 amino acids protein

NH_2-MPGPWVAMIMLPQPKESFGGKPIGWLFWNTCKGPRRDCPHCCCPICSWHC
QLCFLQKNLGVNYGSGPRPRGTRGKGRRIRRTASGEDQRREADSQRSFTNMDQ-
CO_2H

Theoretical pI = 9.75
Mw = 11739.55
Image: RCSB PDB # 1MNB

Figure 2.2. bTAT / bTAR interaction. bTat protein binds bTAR RNA *in vivo* to initiate transcription. BTat sequence shown with Arginine rich region responsible for binding interaction depicted in red.

there is a plethora of structural and biophysical characterization associated with the Tat/TAR interaction that we can utilize as a platform for ligand development. The NMR structure of BIV TAR complexed with a binding peptide derived from BIV Tat has been solved[34, 36] and is available for structure-based studies. Overall, bTAR provides a well-characterized system for the development and evolution of this methodological approach.

Essential to the phage display selection scheme is the ability to separate phage that bind the target RNA from those that do not bind. This is usually accomplished through exploitation of the biotin / streptavidin binding interaction. By biotinylating the target RNA, one can isolate it, along with any bound species, by incubating it with a streptavidin-coated surface. The biotin / streptavidin interaction is very specific with K_a values around 10^{15} M^{-1}. After washing away non-binders, the phage can then be either specifically eluted with a competitive binding ligand or non-specifically eluted via a glycine elution buffer (pH 2.2).

The 5'-biotinylated minimal recognition motif of the bTAR[46] used in initial selection experiments was ordered from Dharmacaon (**Figure 2.3**). Biotin was conjugated to the 5' end of the oligonucleotide by a short linker that spaced the RNA oligonucleotide away from the solid support. This spatial arrangement limits sterics involved in the phage/RNA/solid support complex.

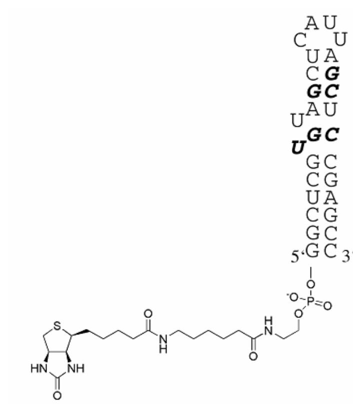

Figure 2.3. Biotinylated BIV TAR. Bases that are involved in Tat recognition are noted in bold italic.

We purchased a commercially available library for our initial investigations that fit the criteria previously proposed. The Ph.D.-C7C™ Phage Display Peptide Library Kit from New England Biolabs (NEB) is based on a combinatorial library of random peptide 7-mers flanked by a pair of cysteine residues fused to a minor coat protein (pIII) of M13 phage. Under nonreducing conditions, the cysteines will spontaneously form a disulfide cross-link, resulting in phage display of cyclized peptides and a scaffold that contains all of the properties that underpin this methodology (**Figure 2.4**). The disulfide-constrained heptapeptides are expressed at the N-terminus of gpIII, with the first cysteine preceded by an alanine residue, and the second cysteine followed by a short spacer (Gly-Gly-Gly-Ser) and then the wild-type gpIII sequence. The comprehensive library was provided as a concentrated stock solution that contained ~200 copies of each sequence per 10 µl of supplied phage. Extensive sequencing of the naive library has revealed a wide diversity of sequences with no obvious positional biases.

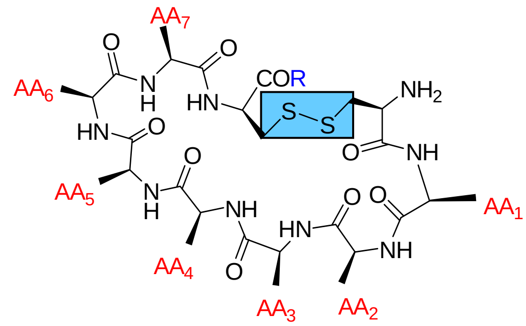

Figure 2.4. Cysteine constrained cyclic peptide library scaffold NH_2-CXXXXXXXC-COR where R represents the continuing pIII polypeptide chain. The disulfide linkage between flanking cysteine residues is highlighted in blue.

This methodology of selecting cysteine-constrained peptides that bind predetermined RNA sequences relies upon alternating between "positive" and "negative" selection cycles. "Positive" selection cycles are used to enrich the library for the pool phage displaying cyclic

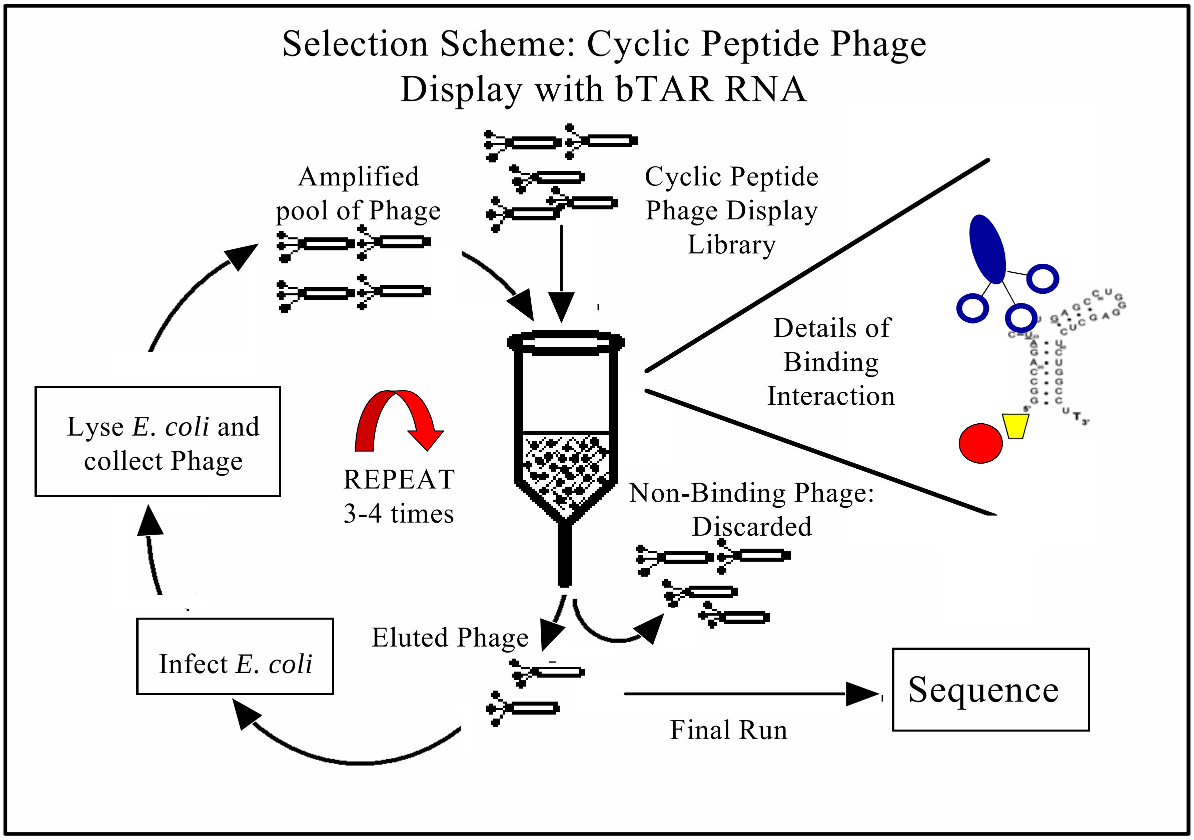

Figure 2.5. Positive selection scheme.

peptides that bind to the sequence of interest, while we utilize "negative" selection cycles to potentially remove phage that display non-specific RNA binding motifs along with phage that display motifs that could bind other elements present during the selection incubation other than our target RNA such as streptavidin, biotin, or the linker. One of the key peptide motifs that we wanted to exclude was that of poly-cationic peptides (such as poly-arginine). These are common RNA-binding motifs that bind RNA oligonucleotides through predominantly electrostatic interactions. Given that poly-arginine is a non-specific RNA binding motif, negative selection rounds are imperative to ensure that the library is biased away from poly-cationic peptides. For negative selection cycles, a 5'-biotinylated randomer [5'–(Biotin)GCAAUGUUGACGACAGUUAGAUUACAGA–3'] was also purchased from Dharmacon. The randomer was designed to be of comparable size to the bTAR minimal recognition motif used for positive selection rounds but with no notable secondary or tertiary structure.

The general approach to "positive" phage selection and amplification is depicted in **Figure 2.5**. Biotinylated bTAR RNA stock is diluted in binding buffer and folded by heating and

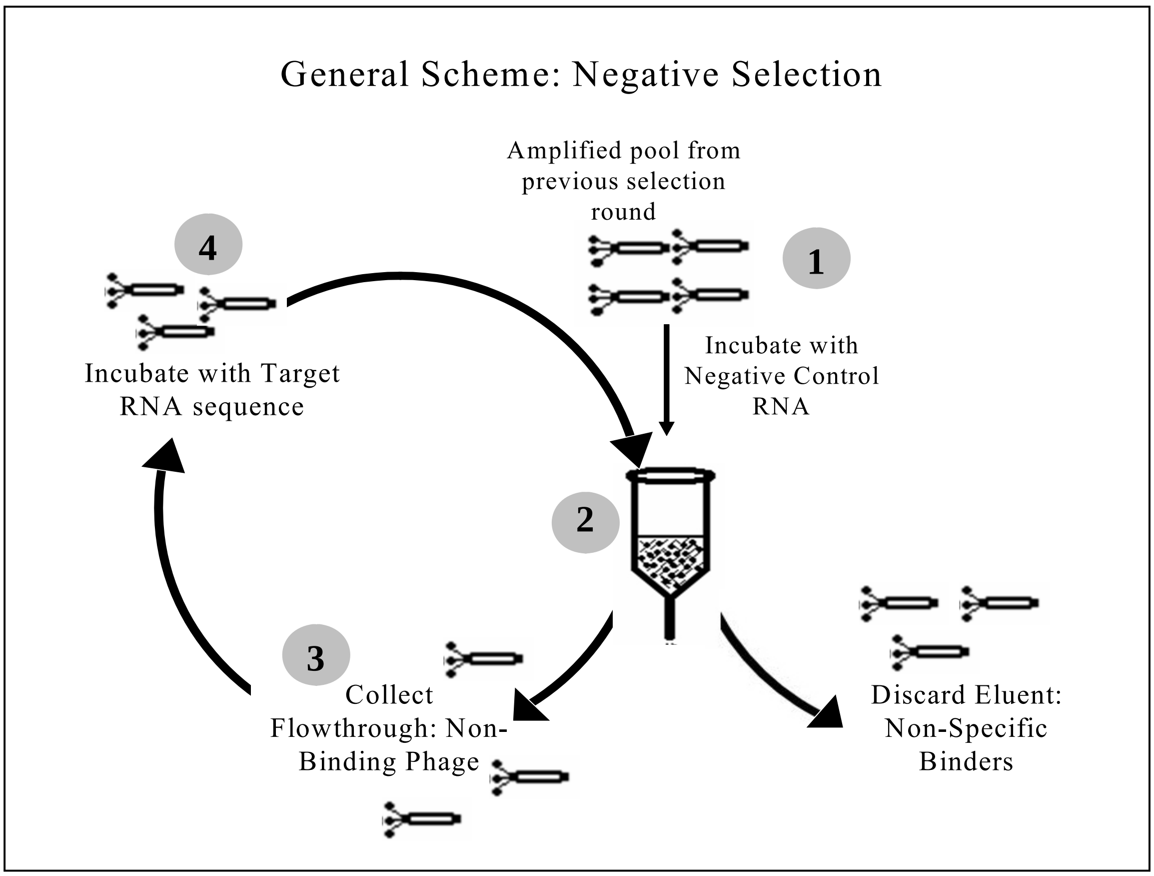

Figure 12. General Scheme for Negative Selection. Step 1. Phage in incubated with biotinylated target to allow for binding interaction. Step 2. phage/target complexes are captured by strepavidin bead. Step 3. Non-bonding phage in solution are collected and taken straight into the next round of positive selection.

then cooling to room temperature. Target bTAR RNA is then incubated with the phage library to allow for binding. Streptavidin coated magnetic bead solution is then added to the RNA/phage solution to capture the target and bound phage. These 1μm non-porous magnetic particles have been previously shown to bind oligonucleotides.[72, 73] The bead/RNA/phage complexes are then magnetically pooled to the bottom of the tube and the supernatant is discarded. The beads are washed with buffer, and the binding phage are eluted. The phage eluent is subsequently amplified for the next round of selection.

The “negative” selection experiment is outlined in **Figure 2.6**. The enriched library, resulting from the amplified pool from previous selection round, is incubated with 5’-biotinylated negative control RNA under the exact same conditions used during positive rounds. Streptavidin coated magnetic beads were used to capture negative control RNA along with bound phage. Non-binding phage were then removed with the supernatant and utilized directly for the subsequent round of positive selection. After refining the pool through iterative rounds of positive and negative selection, individual clones are picked and amplified for sequencing to illuminate binding scaffolds.

Using cysteine constrained cyclic peptide phage display to elucidate cyclic peptide binding scaffolds de novo is the cornerstone of this approach to targeting nucleic acids. The proof of concept target, bTAR RNA, is extremely well characterized, is known to form a discrete secondary structure, and has been used in many other targeting studies. The large body of research conducted regarding bTAR RNA should provide a platform on which to develop and evaluate this approach and the necessary insight to drive this concept to fruition.

II. Results and Discussion

2.1 Development of the Selection Assay Protocol

Although the general approach has been designed to be that of cyclic peptide phage display to target bTAR using the New England Biolabs Phage Display C7C Ph.D. kit, there are many details to consider when developing the actual assay and protocol. First and foremost, when developing a methodology to target RNA, careful consideration must be given to how to mitigate or prevent RNase contamination. Other important points of modification within the procedure to consider are the buffer system, selection conditions (incubation time and temperature), binding scenario (solution binding vs. bead binding), isolation of target / phage complex, and elution conditions. Below is a brief discussion of each.

RNase Mitigation

The stability of the target molecule is of the utmost importance when developing binders through an *in vitro* selection assay. All buffers or tubes that were used during the selection portion of the assay were either purchased as nuclease free and / or baked at 450 ºF overnight to ensure they were RNase free. Also all benchtop surfaces were cleaned and wiped down prior to starting experiments every day. All reagants were purchased at the highest purity and nuclease free where possible, and proper care and technique were used when using these reagents to ensure that they remained RNase free. During the first attempt at selection, SUPERase•In™ was added to the binding buffers in order to mitigate possible RNase contamination. RNAsecure™ was added in the same fashion to all of the wash buffers.

Both of these products were eliminated from the buffers in later selection attempts and not present in the final selection protocol. It was determined that by using the appropriate sterile techniques and nuclease free reagents and containers, these additivites were unnecessary and could potentially complicate the selection protocol. Inherent in the design of an *in vitro* selection protocol is the minimization of additives to the buffer system, thereby increasing the selective pressures for your target. Also, most RNase mitigating products contain reducing agents designed to unfold the active RNase protein and render it inactive. Since the cyclization of the phage coat protein to form the disulfide linked cyclic peptide is impeded in reducing environments, the addition of reducing agents would compromise the integrity of the assay.

Buffer Systems and Selection Conditions

The NEB phage kit protocol was designed to use TBST (0.1% Tween) for the selection portion of the assays. After consulting the literature, I decided to use a Tris-HCl buffer system containing 20 mM KCl (TK buffer) for the RNA studies. TK buffer systems have previously been shown to be applicable to other protein/RNA *in vitro* binding assays including native gel shift experiments involving bTat/bTAR interactions. [85]

There are several variables that can be modulated to control the stringency of the selection conditions. For example, the presence of detergent (typically Tween-20) in the binding and wash buffers reduces nonspecific interactions between the phage and the target and/or blocking agent (BSA). Also, depending on whether the binding interaction is enthalpically or entropically driven, stringency can be increased or decreased, respectively, by raising the temperature of the binding step. For our selection buffers, a low concentration of Tween (0.1%) was added to the TK buffer during the wash steps to aid with the removal of nonspecific binders from the evolved pool. All incubations of the target bTAR RNA and the phage were performed at room temperature.

Alternate binding and elution times can also be used to apply stringency to the selection. With shorter binding times, selection of peptides with rapid on-rates (k_{on}) are favored. Conversely, with longer elution times, selection of peptides with slow off-rates (k_{off}), or tight binders, are favored. Since the equilibrium association constant (K_a) for binding of the peptide to the target is equal to k_{on}/k_{off}, stringency can be increased by shortening the binding time and lengthening the elution time. The assay conditions that were implemented in targeting bTAR were those indicated in the NEB protocol. Binding incubations were allowed to proceed for 20 minutes and elutions were incubated for 10 minutes.

Isolation of Target / Phage Complex

The NEB protocol was slightly modified regarding the isolation of the target and bound phage. The protocol is designed to use SA coated plates to isolate biotinylated targets, but this leads to a rather cumbersome protocol during the isolation phase of the assay. We decided to implement SA coated magnetic beads for our assay. Using the information that came with the beads, in conjunction with the "Alternate Epitope Mapping Procedure" listed as an addendum in the NEB protocol booklet, we devised an overall selection procedure that would provide a scenario for maximum access to target RNA during the recognition phase with a facile isolation of the target along with bound phage.

Binding Scenario: Bead Binding vs. Solution Binding

Two binding scenarios are commonly seen in phage display selection schemes. The first scenario, termed solution binding, allows for free access of phage to the target RNA during the recognition incubation step which can result in improved kinetics as compared to surface binding (bead binding) scenarios. Specifically, biotinylated target RNA is first incubated with the phage library in solution to allow binding of the RNA-phage complex. The complexed RNA is then captured on the streptavidin coated bead in a subsequent step (**Figure 2.7**). Problems can arise if there are more RNA targets in the solution incubation than binding sites on the bead, or if not all of the target RNA is functionalized with the biotin linker. This would result in not sequestering all of the complexed phage and loss of potential binders from the evolved pool. Also, if loading of the bead during the capture step is too high, there is concern that the steric strain could cause dissociation of the phage from the target RNA and the binding phage would be lost in subsequent wash steps.

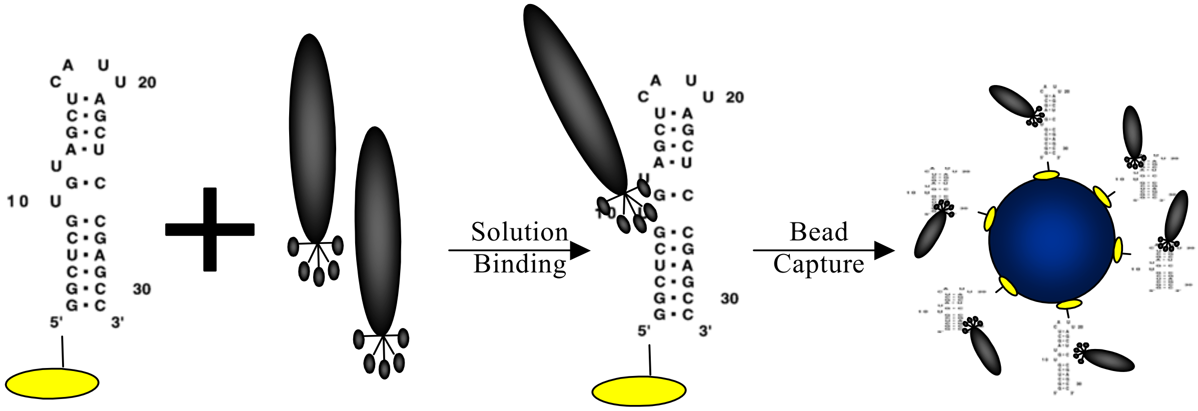

Figure 2.7. Solution Binding Scheme. Phage are incubated with target in solution then subsequently captured on streptavidin coated beads

The second binding scenario, termed bead binding, has its own set of advantages and disadvantages. In the bead binding scenario, the target RNA is first captured onto the streptavidin coated magnetic bead, and then the bead-target complex is incubated with the library for the selection of binders (**Figure 2.8**). Bead binding ensures that all target RNA that is exposed to phage for the selection of binders have already been captured; however, steric hindrance due to being immobilized on the solid surface could inhibit binding if the beads are loaded too densely.

In my completed work with the bTAR RNA target, a solution binding scenario was used. Since the RNA oligonucleotide was synthetically made and purified after functionalization of the 5'-terminus with the biotin linker, it was assumed that the sample was 100% biotinylated. Loss of potential binders due to a lack of capture by the streptavidin coated bead was not of concern. According to the manufacturer, the binding capacity of the streptavidin beads that I used was greater than 500 pmol of single-stranded 20 bp oligonucleotide per mg. Given that

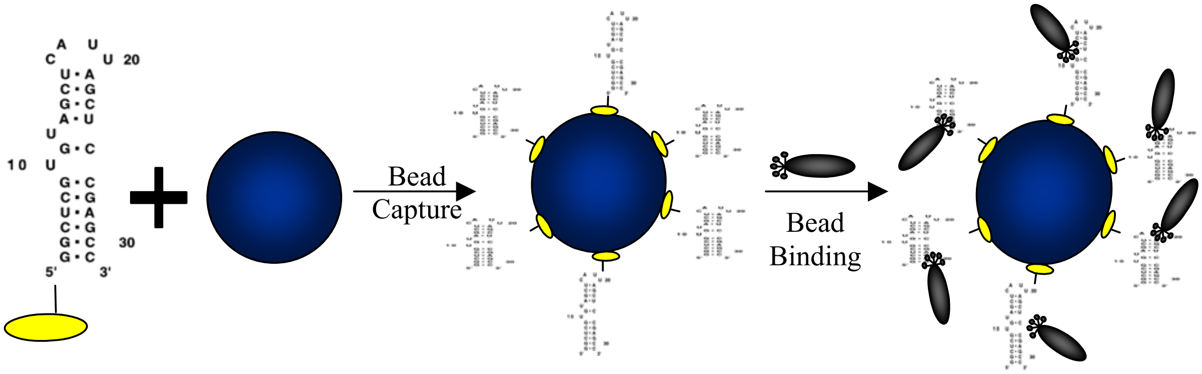

Figure 2.8. Bead binding scheme. Target is first captured by streptavidin coated beads then subsequently incubated with the phage library.

I used 50µL of stock solution / panning round, I calculated that the total binding capacity of the beads used in each round of selection to be approximately 100 pmol of RNA. In accordance with suggested target loading concentrations delineated in the alternate panning procedure addendum of the NEB phage protocol, 200 µL of 10 nM RNA was used during the binding incubations. This results in only 2 pmol of RNA, which is well below (only 2%) the limits of the binding capacity of the SA coated magnetic beads.

Elution conditions

There are three options when eluting the phage or phage / RNA complexes from the SA coated beads. The first approach is to use a non-specific glycine elution buffer, pH 2.2. This disrupts all binding interactions and allows for the dissociation of the aptamer, phage, and bead. The second approach is to use a competitive elution with free biotin. Due to steric effects, free biotin has a higher affinity for the SA sites on the magnetic bead than the biotinylated target and are theoretically capable of displacing the target / phage complex. The third approach also uses a competitive elution and relies on the possession of a known binding ligand for the target. In this approach, the known binding ligand is used to competitively elute those phage that specifically share a common binding site with the ligand.

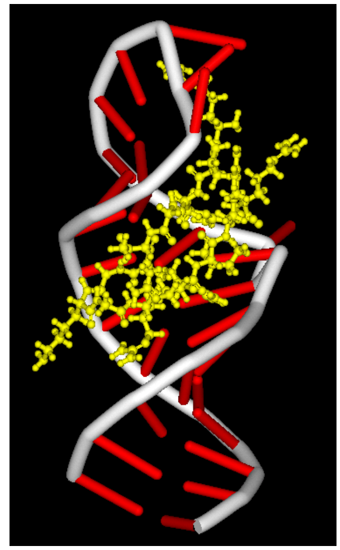
Figure 2.9. bTat peptide binding bTAR bulged stem-loop hairpin

Standard, non-specific conditions (0.2 M glycine-HCl solution, pH = 2.2) were employed for general elution during rounds of selection. In the final round of the final selection experiment, side-by-side selections were performed. One of the selection incubations was eluted with the the non-specific glycine elution buffer while the second was eluted with bTat peptide. The bTat peptide (sequence = H-GPRPRGTRGKGRRIRR-OH, purchased from Sigma Genosys) represents the minimal RNA recognition motif of the bTat protein.[65] This peptide has been extensively characterized, it has high affinity for bTAR (~0.5 nM, **Figure 2.9**),[65] and binds only discrete sequences within the bTAR hairpin (bold sequences, **Figure 2.3**).[58, 68] This final competitive elution protocol with the bTat peptide allows us to determine the subset of the enriched phage pool that specifically targets the same residues as the bTat peptide.

2.2 Characterization of bTAR RNA Stock

Gel Electrophoresis

Phage display involves the evolution of phage constructs that bind a target molecule through an *in vitro* selection process. If there are contaminants or degradation products of the target molecule present during the selection phase of the assay, then the pool can evolve to recognize these molecules rather than the target. The purity of the RNA stock can easily be assessed using denaturing polyacrylamide gel electrophoresis. **Figure 2.10** shows the results of 1 nmol of biotinylated bTAR RNA stock tested on a 10% denaturing PAGE gel. The multiple banding pattern of the bTAR RNA stock is due to the fact that the hairpin bTAR structure was not fully linearized under the denaturing conditions of the gel. The upper band represents the fraction of the sample in its linear while lower bands are in the hairpin form. The bTAR RNA stock does not show any signs of degradation which would have been represented by a low molecular weight smear at the bottom of the gel.

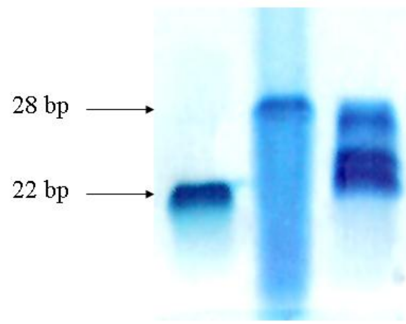

Figure 2.10. bTAR purity assessment by 10% denaturing PAGE gel. Lane 1 contains 1 nmol of 22mer of DNA run as a size marker. Lane 2 contains 1 nmol of 5'-biotinylated 28mer of RNA run as a control. Lane 3 contains 1 nmol Dharmacon ordered 5'-biotinylated 28mer of BIV-TAR RNA.

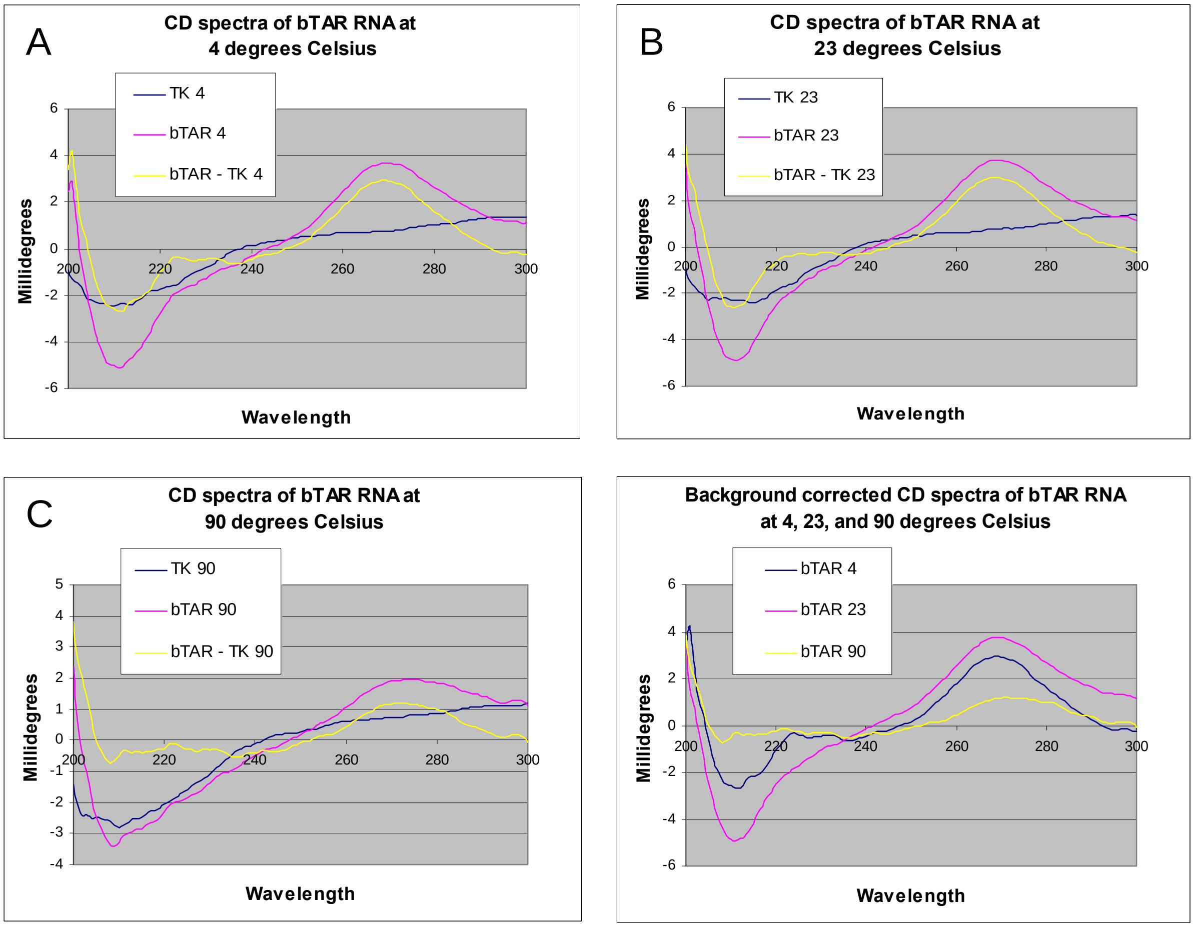

Characterization of bTAR RNA Hairpin by Circular Dichroism

Formation of the bTAR RNA hairpin under assay conditions is crucial to the selection process. In order to evaluate and confirm the presence of the secondary hairpin structure in TK buffer at room temperature, circular dichroism spectroscopy was employed. The first attempt to determine bTAR RNA hairpin structure using circular dischroism spectroscopy was completed in TK-T buffer (0.1% Tween) with RNAsecure™. This attempt was unsuccessful due to the presence of the detergent Tween 20 and, to a larger extent, the

RNAsecure as indicated by the noise and voltage spikes of the TK-T with and without RNAsecure. The second attempt was performed with 20 μM bTAR RNA in TK buffer without Tween or RNAsecure. Samples were tested at 4, 23, and 90 ºC. Background spectra of the TK buffer were also taken at all three temperature set points.

A

experiment 1,16	CHMSTRHQC
experiment 1,18	CHQALNHTC
experiment 1,23	CHQALNHTC
experiment 1,6	CITASNPRC
experiment 1,17	CKPTQSTYC
experiment 1,12	CKPTQSTYC
experiment 1,19	CKPTQSTYC
experiment 1,9	CLEPKMHQC
experiment 1,30	CLPDHTRKC
experiment 1,5	CLPHVMSNC
Experiment 1,7	CNEPRSLQC
experiment 1,28	CNSTNLEQC
experiment 1,25	CQSVHPQTC
experiment 1,24	CTGESLWAC
experiment 1,26	CTQNHPSSC
experiment 1,11	CTTHLKGYC
experiment 1,8	CTVKTAAMC
experiment 1,27	CTVKTAAMC

B

2,53	CNDTTNRXC
2,48	CNDTTNRXC
2,31	CNDTTNRFC
2,21	CTLHHNQQC
2,55	CHPAAHKMC
2,56	CHPAAHKMC
2,47	CPTPHPGKC
2,17	CPSTNPNKC

C

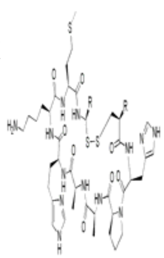

D

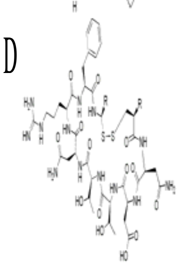

Figure 2.11. CD spectra of bTAR RNA in TK buffer at (**A)** 4 degrees Celsius, (**B)** 23 degrees Celsius, and (**C)** 90 degrees Celsius. Panel **D** is the overlay of the background corrected spectra at each temperature.

CD spectra of double-stranded DNA and RNA are highly sensitive to the conformation of the polynucleotide helix. The CD spectrum of bTAR RNA has previously been shown to have a characteristic peak at 265 nm that is associated with the A-conformation polynucleotide helical structure of the hairpin.[61] The results of the CD temperature study of bTAR RNA in TK buffer shown in **Figure 2.11** indicate that the hairpin secondary structure is forming under the selection conditions. CD data is located in **Appendix A.1**.

2.3 Selection Experiments

Three selection experiments were performed before we developed our final selection protocol. In this trial and error approach, we learned from each attempt and used the information to direct modifications to the protocol for subsequent attempts. The first selection experiment was performed with two additives to the selection process to mitigate any RNase contamination. Thirty plaque forming units (pfu) were isolated and amplified for sequencing. The sequencing results from this selection looked promising; however, it was later realized that the additives would not only unnecessarily complicate the *in vitro* selection process, but that the RNAsecure reagent that was added to the binding buffers was likely to

contain a reducing agent. As previously discussed, this would inhibit the formation of the disulfide linkage that forms the cysteine constrained peptide on the pIII coat protein of the M13 phage. Since the addititives were already added to the bTAR RNA stock tubes, a batch of bTAR RNA was ordered before trying the selection process a second time. The second selection experiment was analoguus to the first selection experiment with the exception of the removal of the RNase mitigating additives from the buffers.

The results from the first and second selection experiments are summarized in **Figure 2.12**. The sequencing results of the second experiment indicated a large degree of wildtype contamination in the evolved pool. There are many reasons why wildtype contamination can occur, including lack of strong selective pressures, increased amplification times, and too many rounds of selection. The gpIII coat protein of the phage plays an important role in the infection of F^+ ER2738 bacteria during amplification. Binding of the F conjugative pilus by the gpIII protein initiates infectivity by causing a retraction of the pilus pulling the pIII terminus into the periplasm. The insertion of the cloned peptide fragment into the gpIII coat protein somewhat attenuates infectivity as compared to that of the wildtype phage and, therefore, small amounts of wildtype contamination can result in domination of the evolved stock following amplification. Sequencing of the clones that were not wildtype in the second selection experiment revealed that there was no overlap with sequences between selection experiment 1 and selection experiment 2.

During the third selection experiment, a negative round of selection was added to the protocol. Negative selection rounds help to remove nonspecific binders and / or binders that have evolved to bind components present in the *in vitro* selection other than the target. A negative randomer oligoncleotide, **N1** (5'–(Biotin) GCAAUGUUGACGACAGUUAGAUU ACAGA–3')**,** was designed to be comparable in size to bTAR RNA (28 nucleotides) but without any notable secondary structure. By incubating the evolved pool of phage with **N1** under the exact selection conditions as used with positive selection rounds**,** any phage capable of binding components other than the RNA should be sequestered along with those that can bind the **N1** RNA. By collecting non-binding phage to take forward to the next round, it is possible to refine the pool to those that are specifically targeting the bTAR RNA.

The impact of the negative round of selection was monitored by pfu counts of the unamplified phage eluent. Previous phage titers yielded a pfu / 10 μL count of 2.5 – 4.1 x 10^{10} for the amplified round 1 stock. 10 μL of the stock was incubated with the biotinylated **N1** RNA and subsequently sequestered by SA coated magnetic beads. The supernatant containing the non-binding phage was collected and titered to give the pfu / 10 μL count for the negative selection of 9.3 x 10^9. These results indicate that the phage pool was reduced by a factor of 4, therefore only ¼ of the phage pool from round 1 were binding bTAR RNA in a specific fashion.

The effect of extending the elution times beyond the 10 minute incubation with the non-specific glycine elution buffer was also tested. As previously discussed, phage displaying peptides with higher affinity for the bTAR RNA target by definition have a slower k_{off} rate. In order to minimize the loss of potential "tight binders" from the evolved pool, it is crucial to make sure that the elution conditions are aggressive enough to recover all phage. Elution conditions were tested by completing sequential 10 min. elutions of the beads during the elution step of the selection and then testing each elution sample for phage concentration by phage titers.

Specifically, 1 mL of glycine elution buffer was added to the phage / RNA / beads and incubated for 10 minutes at room temperature. Beads were then isolated with a magnet, and the supernatant (containing the eluted phage, E1) was removed, neutralized, and titered to determine phage concentration. A second 1 mL aliquot of glycine buffer was then added to the same phage / RNA / beads and allowed to incubate for another 10 min. and subsequently removed, neutralized and titered analogous to the first 10 minute elution (E2). Results showed that phage were recovered during the second 10 minute elution. There was also indication that extension of the elution time plays a larger role in the recovery of phage as the selection experiment progresses as evidenced from the ratio of [E1] : [E2] for round 1 and round 2 (10 and 6.8 respectively). During the *in vitro* selection process, each iterative round of selection refines the pool in terms of binding capabilities for the target molecule, therefore it is expected that later rounds would have a higher percentage of tight binders than earlier rounds.

Final Selection

The final selection experiment was the culmination of everything that was learned in the first three attempts. The selections were performed in TK buffer with 0.1% Tween (no additives). All RNA samples were heated and cooled prior to the binding interaction in order to enforce the hairpin conformation. Solution binding was employed to allow maximum access of phage to the bTAR target molecule during the binding step. RNA / phage complexes were captured via SA coated magnetic beads and nonbinding phage were removed by washing beads 10X with 1 mL TBS-T. Phage were eluted in two consecutive elution steps, each with 1 mL glycine elution incubated with the phage / RNA / beads for 10 minutes at room temperature and then neutralized. Elutions 1 and 2 were then combined and added to mid-log phase ER2738 culture for amplification of the phage stock to take forward to the next round of selection. **Figure 2.13** depicts a schematic of the overall selection process for the final experiment.

I started by performing one round of positive selection experiments, followed by a round of negative selection, and then two more successive rounds of positive selection. At this point, the non-amplified phage titer at the end of the third positive selection cycle showed an increase in colonies when compared to the previous round, which is indicative of convergence in the library. I elected to perform two, parallel positive selection experiments during round 5 – 4th of positive selection where only the elution conditions were varied. In the first experiment, I employed our standard, non-specific conditions (0.2 M glycine-HCl solution, pH = 2.2). In our second experiment, I eluted off the binding phage with the bTat peptide.

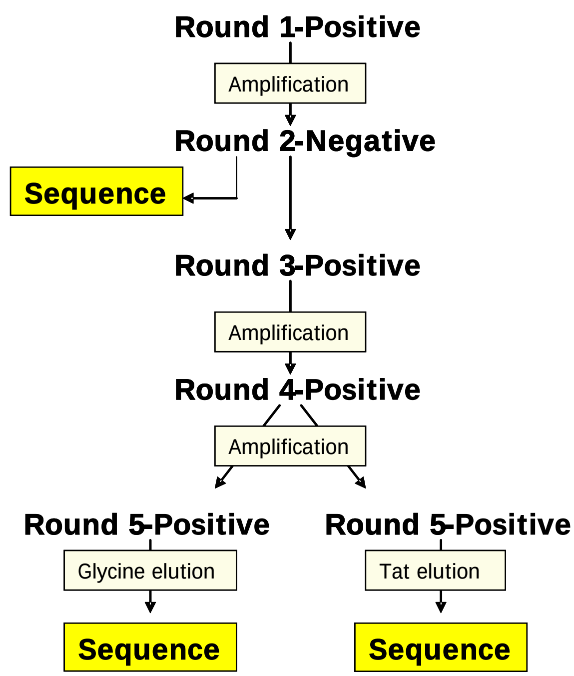

Figure 2.13. Flowchart of the final selection process.

After this last elution step, I plated the eluent on a bacterial lawn (*E. coli* strain ER278 F^+), allowed phage plaques to develop, and then picked random plaques for sequencing. All phage from the library had been engineered to carry the *lacZ* gene, and, as a by-product during their bacterial amplification, all NEB-derived phage developed blue plaques in the presence of IPTG/X-gal. This allows simple blue/white screening to distinguish phage that originated from the NEB library from any wild-type contaminating phage. I picked 21 random blue plaques from the final Tat elution protocol and 35 random blue plaques from the final non-specific elution protocol. In addition, I took the streptavidin beads from the negative selection cycle (which theoretically have bound non-specific RNA binding phage), performed a non-specific elution (0.2 M glycine-HCl solution, pH = 2.2), and plated that eluent on a bacterial lawn. From those non-specific binding phage, I picked 3 random blue plaques. Each plaque was individually amplified in bacterial culture, the phage was subsequently selectively precipitated, and the DNA was isolated for sequencing to determine the library insert. The resulting cyclic peptide sequences have been summarized in **Figure 2.14.**

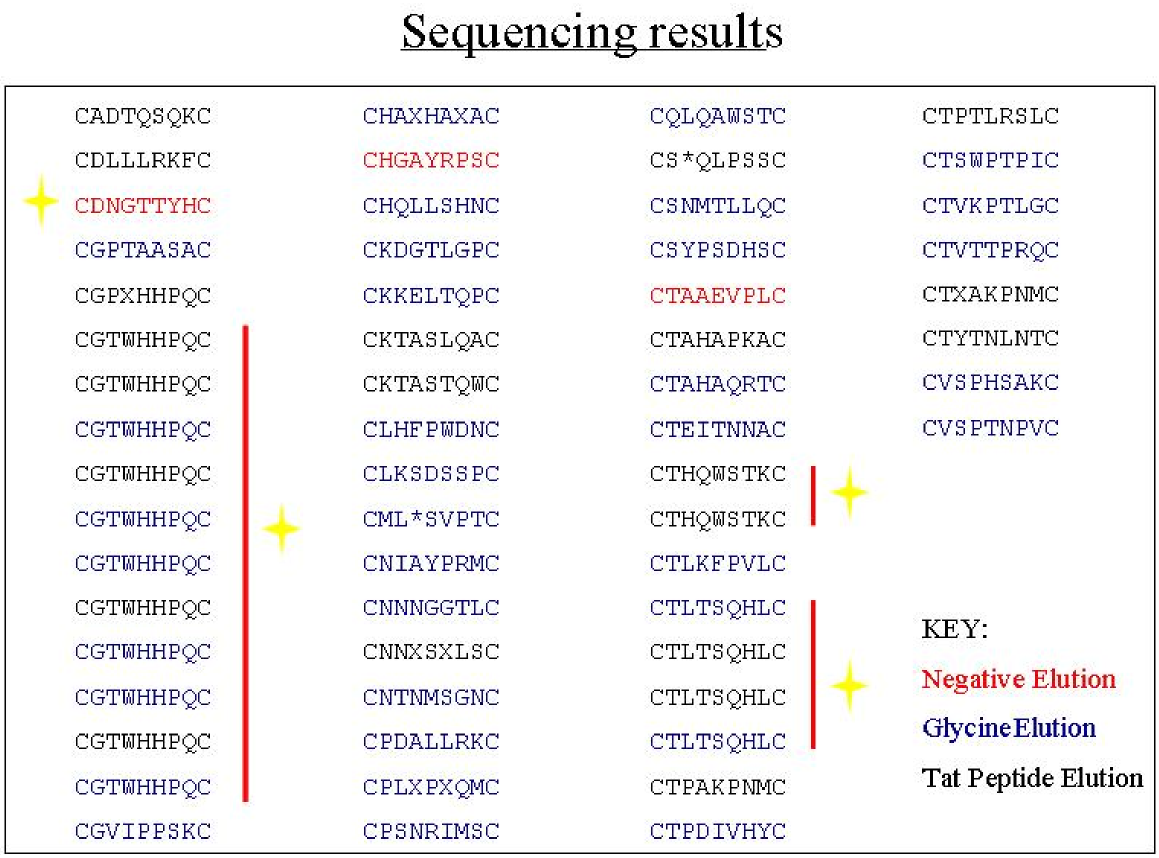

Figure 2.14. Final Sequencing Results. Red vertical lines denote sequences that appeared multiple times in the evolved pool. Yellow stars indicate those scaffolds chosen for synthesis.

Analysis of the initial sequencing results revealed that multiple copies of identical clones were obtained, demonstrating that the use of cysteine-constrained libraries is a viable approach to generating cysteine-constrained peptide scaffolds that can bind a targeted RNA oligonucleotide. I concurrence with previous reports that have documented the use of phage libraries to target RNA motifs,[86-88] the resulting scaffolds are not characterized as being highly poly-cationic in nature. It also revealed that elution with the bTat peptide identified a subset of the binding phage that potentially competed for a biologically relevant interaction. Finally, although only three inserts from the negative selection round were sequenced, it was noted that none of the three negative selection sequences were represented in the non-specific glycine or bTat elution sequences. Based on these results, four of the cyclic peptide scaffolds that were represented multiple times in our sequencing run (starred sequences **Figure 2.14**) were chosen for further investigation of binding properties. One cyclic peptide (**N1**) was chosen from the pool of negative control binding peptides, and three were chosen that exhibited bTAR binding (**P1**, **P2** and **P3**).

III. Summary and Conclusions

Phage display is a powerful tool that extends the range of modern combinatorial screening techniques, allowing the evolution and characterization of peptides that interact with a desired target. It allows for the rapid and effective discovery of scaffolds that can be exploited for therapeutics, diagnostics and targeting agents. We have demonstrated that it is possible to generate novel cyclic peptide motifs that bind with relatively high affinity to a predetermined RNA target by use of cysteine-constrained phage libraries. These peptides represent a base scaffold that may be refined for specificity or function in future structure-based design efforts. Given the flexibility of the phage methodology, it should be possible to use this approach to generate novel, cyclic peptide scaffolds for any predetermined RNA motif. Furthermore, this approach is not limited to or reliant upon a known binding motif.

CHAPTER 3: *IN VITRO* ANALYSIS OF CYSTEINE CONSTRAINED CYLIC PEPTIDE SCAFFOLDS

I. Introduction

In order to ensure that binding properties of the cyclic peptide scaffolds are maintained when the peptides are tested as discrete entities (not as a component of the phage pIII coat protein), cysteine constrained synthetic analogues of the four identified binding scaffolds were purchased from Biopeptide for analysis of bTAR RNA binding properties (**Figure 3.1**). Four different *in vitro* approaches were attempted for biophysical characterization of binding for synthetic constructs: Electrophoretic Mobility Shift Assays, Isothermal Titration Calorimetry (ITC), UV Thermal Denaturation analysis, and Fluorescence quenching assays. *In silico*

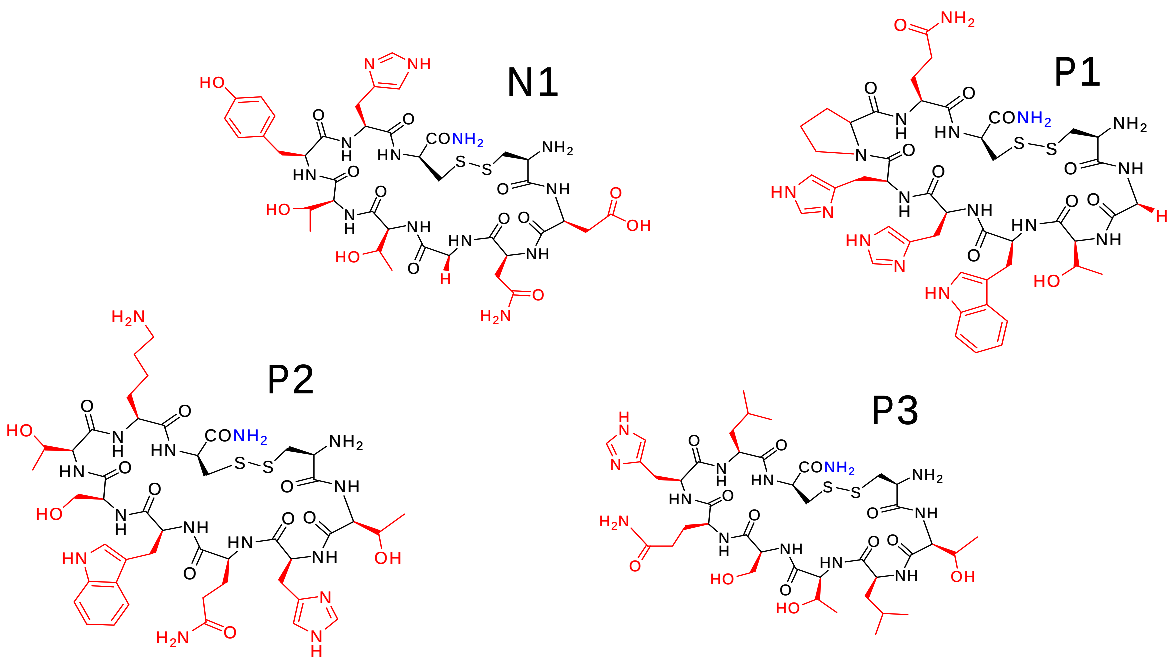

Figure 3.1. Synthetic cysteine constrained cyclic peptides identified by cyclic peptide phage display as potential bTAR RNA binders.

techniques using the computer modeling software HADDOCK were also used by collaborators to model peptide RNA interactions.

EMSA

An electrophoretic mobility shift assay (EMSA) is a common *in vitro* biochemical technique used to study protein-DNA or protein-RNA interactions because of its relative simplicity and small sample requirements.[58] This technique can elucidate if a protein or mixture of proteins is capable of binding to a given DNA or RNA sequence, and can sometimes indicate if more than one protein molecule is involved in the binding complex. EMSA generally involves the electrophoretic separation of a free RNA or DNA from complexed RNA or DNA via a native polyacrylamide or agarose gel for a short period (about 1.5-2 hr for a 15- to 20-cm gel).[89] The rate at which different molecules or complexes migrate through the gel is determined by their size and charge and, to a lesser extent, their shape. The smaller and/or more negatively charged the molecule, the faster it migrates as a result of the applied current. In this experiment, multiple samples are made where the RNA concentration is held constant where increasing concentrations of ligand are added. Samples are then incubated to allow any binding interaction to occur, and subsequently run in parallel on a native PAGE gel. Under the correct experimental conditions, any binding interaction between the RNA target and protein is stabilized, and the ratio of bound to unbound nucleic acid on the gel reflects the fraction of free and bound RNA molecules in solution at equilibrium. After electroporation, the control lane will contain a single band corresponding to the unbound DNA or RNA fragment. However, assuming that the protein is capable of binding to the fragment, the lanes with protein present will contain another band that represents the larger, less mobile complex of the RNA target bound to protein which is 'shifted' up on the gel.

There are multiple ways in which to visualize the resulting banding pattern. The nucleic acid fragment is usually labeled with a radioactive, fluorescent or biotin label. Standard ethidium bromide staining is less sensitive than these methods and can lack the sensitivity to detect the nucleic acid if small amounts are used in these experiments. Limiting the visualization technique to include only the DNA or RNA target allows a clear and concise way to evaluate the bound / unbound state of the target without the visual clutter of the protein. The affinity of the protein for the nucleic acid sequence may subsequently be determined by evaluating the ratio of bound to unbound target if the concentrations of protein and RNA target are known.[89] The use of EMSA to characterize bTAR RNA binding interactions is well documented.[69, 90, 91]

UV Thermal Denaturation Analysis

A thermal denaturation experiment is often used to determine the stability of RNA and DNA secondary structures by means of determining the T_m, the temperature of melting or more accurately the temperature of midtransition.[92] RNA and DNA complex secondary structures are stabilized by base-base hydrogen bonding. The amount of energy or heat needed to disrupt these interactions is directly proportional to the stability of the complex. As the complex is heated and “melts”, the resulting conformational changes of the molecule in solution lead to changes in the absorbance properties. By coupling a thermoregulator cuff to a Circular Dichrosim or UV-visible spectrophotometer, it is possible to monitor the change in absorbance at a given wavelength as a function of temperature and determine the T_m of a sample.

In most cases, RNA thermal denaturation experiments are performed using a UV-visible spectrophotometer by recording the absorbance at 260 nm as a function of temperature. This analytical technique was first reported over 50 years ago,[92] and has been used extensively to study bTAR and TAR hairpin structure and the stabilization of the hairpin structure via Tat protein and other ligand binding.[69, 93-95]

Isothermal Titration Calorimetry

One biophysical technique that is used to probe the thermodynamics of RNA-protein binding interactions that is independent of both RNA sequence and peptide structure is isothermal titration calorimetry (ITC).[71] ITC is a powerful quantitative technique that can directly measure the binding affinity (K_a), enthalpy changes (ΔH), and binding stoichiometry (n) of the interaction between two or more molecules in solution. From initial measurements, Gibbs energy changes (ΔG) and entropy changes (ΔS) can be determined using the following relationship:

$$\Delta G = -RT\ln K = \Delta H - T\Delta S,$$

R = Gas constant = 8.314 J mol^{-1} K^{-1}, and T = absolute temperature in Kelvin.

This technique employs the use of sample and reference cells which are maintained at a common temperature. A feedback loop controls the heating of the cells and the instrument monitors the energy required to maintain the temperature as a function of time. During an experiment, the sample cell containing a known concentration of peptide sample is monitored as a known concentration of potential ligand, RNA, is titrated in. The temperature of the peptide sample and RNA sample are previously equilibrated along with their buffers, which means that any change in sample cell temperature is due to the amount of energy absorbed or released as a result of a binding event. Each data point represents a deflection in the relative power versus time curve as the instrument compensates for the heat (*qi)* absorbed or released by a given injection to the subsequent binding event. The peaks are integrated to yield the injection heat q_i for a given injection, which is a function of the fractional saturation of the binding reaction, the stoichiometry of the binding reaction, the total concentration of the ligand titrant, the binding enthalpy, and the total cell volume. So long as one knows the initial concentration of the RNA in the cell, it is possible to obtain the ΔH, dissociation constant, and stoichiometric ratio of RNA to ligand from this data.[96]

ITC has been applied to the study of proteins for many years. Its use in the biophysical analysis of RNA has lagged significantly behind its use in protein biochemistry mainly due to the relatively large sample volume required because of limitations in sensitivity. As the instrumentation has become more sensitive, the ability to obtain high quality data on RNA folding and RNA ligand interactions has improved dramatically.[96] ITC has been intstrumental in the area of RNA biochemistry in elucidating small molecule binding,[97-99] RNA-protein interactions,[100] and fundamental RNA folding studies.[101]

Fluorescence Quenching

Fluorescence quenching is widely used to study protein-ligand interactions because of its simplicity and its sensitivity in the high μM to low nM range, where many protein–nucleic acid dissociation constants fall.[83, 102-105] In general, fluorescence quenching assays measure the decrease in fluorescence emission of a fluorophore as it binds to a macromolecular target. The amount of quenching is directly proportional to the amount of bound fluorophore complex, allowing for rapid assessment of dissociation constants (K_d).

Except in a few specific cases, nucleic acids do not contain any intrinsic fluorescence. This enables protein / RNA interactions to be studied by monitoring the fluorescence of the tryptophan or tyrosine residues in a peptide or protein when present.[87] Tryptophan residues undergo excitation when irradiated, with a peak in the absorption profile at 280-290 nm, and have a characteristic emission profile with a peak between 350-355 nm. These amino acids have a much higher extinction coefficient than tyrosine residues and therefore contribute more to the native fluorescence of the peptide or protein. It is important to have at least one tryptophan residue present in the peptide or protein to monitor binding in this way. Alternatively, the RNA can be either 5' or 3' labeled with a fluorophore if the peptide does not contain any fluorescent amino acids.

II. Results and Discussion

2.1 Gel shift: bTat and bTAR

Since the scaffolds that are selected need to function as discrete entities, the synthetic cysteine constrained cyclic peptide scaffolds also need to be analyzed for their ability to bind target RNA. *In vitro* analysis of the relative binding affinities can be accessed by gel shift experiments. K_d values can be obtained by analyzing the relative intensities of the bands by quantitative image analysis software. This technique also provides an *in vitro* method for analyzing whether the cyclic peptide scaffolds identified by selection have the capability of displacing the endogenous bTat-bTAR interaction.

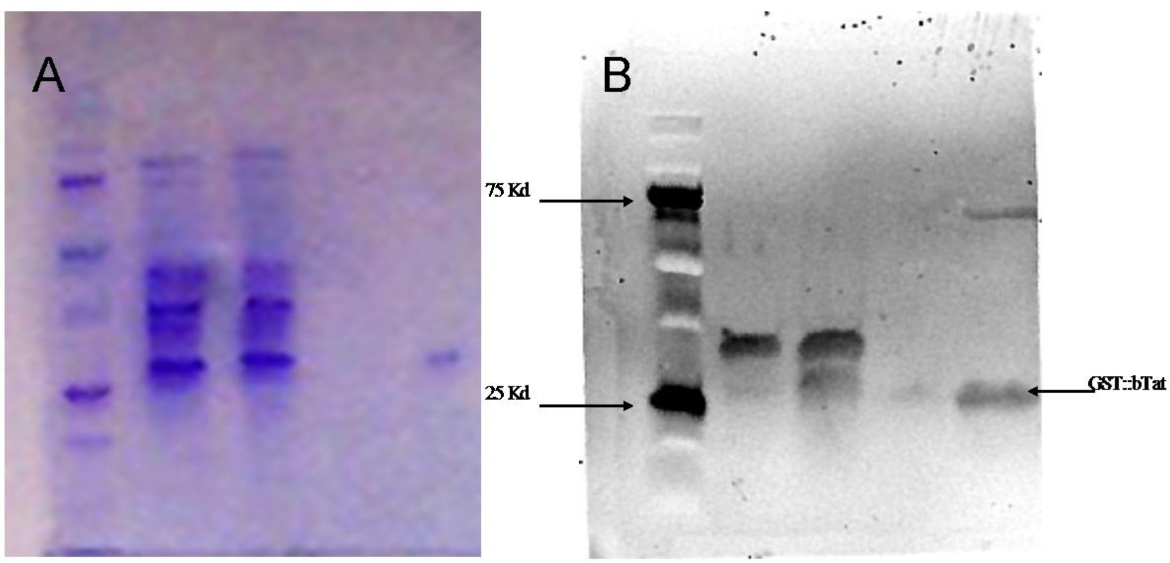

'igure 3.2. Results of GST::bTat expression and purification. Samples were loaded and run in duplicate on a 0% PAGE gel. (*A*) total protein stained with Coomassie Blue. (*B*) results of Elisa performed with anti-GST-IRP conjugated antibody From left to right, Lane 1: MW ladder, Lane 2: uninduced total lysate, Lane 3: ıduced total lysate, Lane 4: blank, Lane 5: eluted GST::bTat protein

Due to the small size of our cyclic peptide scaffold, the differential migration of free bTAR RNA vs. bound bTAR-cyclic peptide RNA could be potentially difficult to discriminate. My original approach to overcome this issue was to move directly to competitive gel shift analysis with bTat protein. In order to proceed with these experiments, non-biotinylated bTAR RNA was radioactively labeled at the 5'-terminus to allow for very low concentrations to be analyzed, and GST::bTAT was expressed and purified from a plasmid provided by Professor Bryan Cullen's Lab at Duke University.

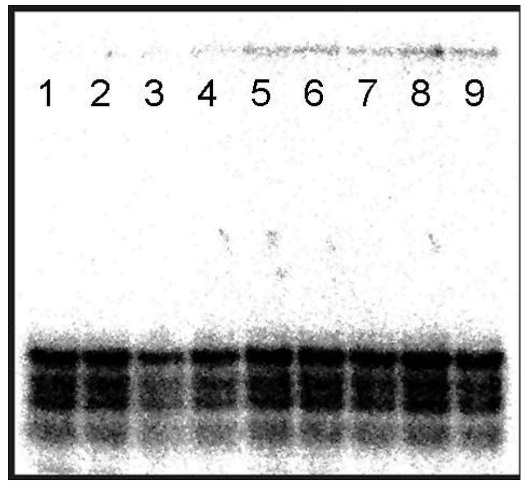

Figure 3.3. Gel shift analysis of bTAR RNA with GST::bTAT protein. 0.2 pmol of labeled bTAR RNA was incubated with varying concentrations of protein in 15 µL binding reactions (TK buffer) at 4 ºC for 30 minutes. Samples were then loaded on a 10% native PAGE gel. GST::bTAT content (pmol) from lane 1 to lane 9: 0, 0.02, 0.1, 0.2, 0.4, 1, 2, 4, 10.

The GST::bTat fusion protein expression vector was transformed into BL21 cells and plated on LB-Amp to evaluate transformation efficiency. Six colonies were picked at random for testing of GST::bTAT expression under IPTG control. Levels of the 36 kDa GST::bTAT were ascertained by ELISA using a commercially available anti-GST-HRP conjugated antibody and subsequent chemiluminescence detection. The clone displaying the highest levels of protein production was carried forward for scaled up production (3 liters) of GST::bTat. The GST::bTat fusion protein was purified using the B-PER GST Spin Purification Kit^{TM} from Pierce. ELISA was again used for evaluation of the purity of the GST::bTat purified sample, and Bradford analysis was used to quantitate the sample with final yields of 80 μL, 1.6 pmol/μL (**Figure 3.2**).

Preliminary gel shift experiments to establish GST::bTat / bTAR binding conditions and relative concentrations to be used in later competitive analysis with potential cyclic peptide scaffolds were unsuccessful (**Figure 3.3**). Various buffer and binding conditions were investigate; however, I was never able to elicit a gel shift even when increasing the GST::bTat concentration above previously reported values required for gel shift visualization.

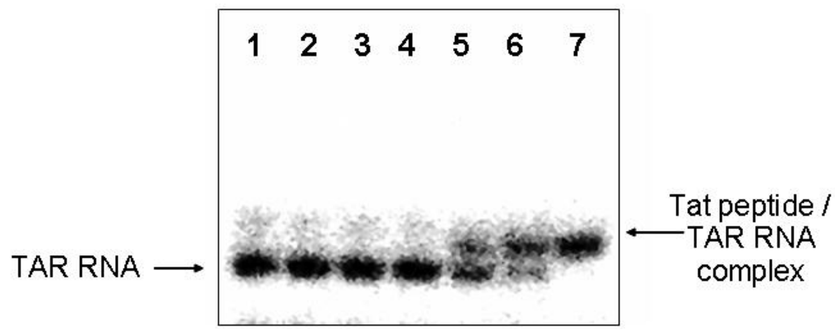

Figure 3.4. The binding of bTat peptide to bTAR RNA *in vitro*. 0.1 nM labeled bTAR was incubated with bTat peptide of increasing concentrations at 4 ºC for 30 minutes. Binding interactions were visualized by 13.3% native PAGE, 0.5X TBE. bTat peptide concentrations (nM) from lane 1 to 7: 0, 0.0025, 0.025, 0.25, 2.5, 25, 250.

My next attempt was to use the 17-mer bTat minimal recognition motif that was used during selection experiments. After numerous trials, I determined that I could elicit a full gel shift using the bTat peptide with ratios on the order of those previously reported for bTat protein (**Figure 3.4**). Results indicate that 2 fmol of bTAR RNA incubated with 5 pmol of bTat peptide at 4 ºC for 30 minutes in a 20 μL reaction volume (TK buffer) elicits a full shift of the labeled RNA. These are the conditions that were used for subsequent competitive analysis of cyclic peptide scaffolds. Various concentrations of cyclic peptide were tested for the **P1**, **P2**, and **P3** competitive gel shifts with values up to 1000 fold excess of peptide compared to that of bTat; however, the results did not indicate any change in the banding pattern when compared to the bTat / bTAR complex. These results indicate that either the size of the bTat/ bTAR and peptide / bTAR complexes were too similar to yield a distinguishable banding pattern, the peptide is not binding under the assay conditions, or that the peptide is binding in a way that is not competitive with the bTat peptide.

2.2 UV Thermal Denaturation Analysis

The UV Thermal Denaturation Analysis was completed by our collaborator Darnell Graham of Dr. Paul Agris's Lab, Biochemistry Department at NCSU.

Experiment	ΔH (kcal/mol)	ΔS (cal/K*mol)	ΔG (kcal/mol, 37°)	Tm (°C)
bTAR	-21.95 ± 2.56	-66.95 ± 8.1	-1.19 ± 1.18	54.83 ± 2.91
bTAR / P1	-37.98 ± 16.89	-115.08 ± 50.82	-2.20 ± 1.27	56.74 ± 2.58
bTAR / P2	-45.20 ± 17.90	-137.11 ± 54.82	-2.67 ± 0.91	56.79 ± 1.31
bTAR / P3	-33.59 ± 16.49	-97.89 ± 54.08	-1.09 ± 0.87	56.06 ± 2.50

Table 3.1. UV-Vis denaturation data completed in collaboration with the Agris Lab, NCSU Biochemistry Department

Specific peptide binding to the bTAR RNA has previously been shown to significantly enhance the thermostability of the hairpin structure.[69] By using UV thermal denaturation analysis to analyze the conformational stability of the bTAR hairpin with and without the cyclic peptide scaffolds, it is possible to evaluate cyclic peptide / bTAR RNA interactions. These experiments were performed with low μM concentrations of bTAR RNA and a 1:15 ratio of bTAR RNA to cyclic peptide in TK buffer (**Appendix A.2**). The UV absorbance at

260 nM was measured as a function of temperature as samples were heated from 4 to 95 ºC. A total of 6 cycles were completed and averaged for each test sample. The resulting data is summarized in **Table 3.1.**

Overall, the data is inconclusive as to the elucidation of a binding scenario. The data obtained from the UV thermal denaturation analysis possibly indicates a binding interaction by the 3 cyclic peptides tested resulting in the slight stabilization of the bTAR hairpin (T_m increase of approximately 2 ºC). However, it should be noted that previous reports of the stabilization of the bTAR hairpin by the specific binding of peptides are on the order of 6-14 ºC.[69, 94, 95] One possible reason that the thermostabilization was less than that observed in previous experiments investigating bTAR binding to bTat could center around the experimental conditions. It is important to the experimental design of this technique that concentrations of target RNA and peptide ligand be such that the RNA is found primarily in the complexed (bound) form. Although the bTAR / cyclic peptide concentrations used for analysis were analogous to previously reported conditions, those were developed based on the assumption that the ligand affinity for the target RNA being investigated was in the low nanomolar range. Upon evaluating the data that was provided from these studies, I noticed that if the affinity was in the low micromolar range instead of low nanomolar range, the experimental conditions would yield only 75% of the RNA target being found in the bound state (as compared to over 99.99% for nanomolar binders). Given this evaluation of the experimental conditions, it is possible that the observed differences in the measured T_m for free bTAR RNA as compared to cyclic peptide bound bTAR could be an underestimation of the thermal stabilization of the complex by cyclic peptide binding interactions. Further *in vitro* analysis needs to be conducted to characterize the binding interactions.

2.3 ITC

ITC provides some significant benefits over those of EMSA for studying protein / nucleic acid binding. The flexibility and control with respect to condition space is a significant advantage as is the ability to obtain directly ΔH, ΔS and stoichiometric information in addition to the K_d.[96] All Isothermal Calorimetry data presented here was completed in collaboration with Darnell Graham of Dr. Paul Agris's Lab, Biochemistry Department at NCSU.

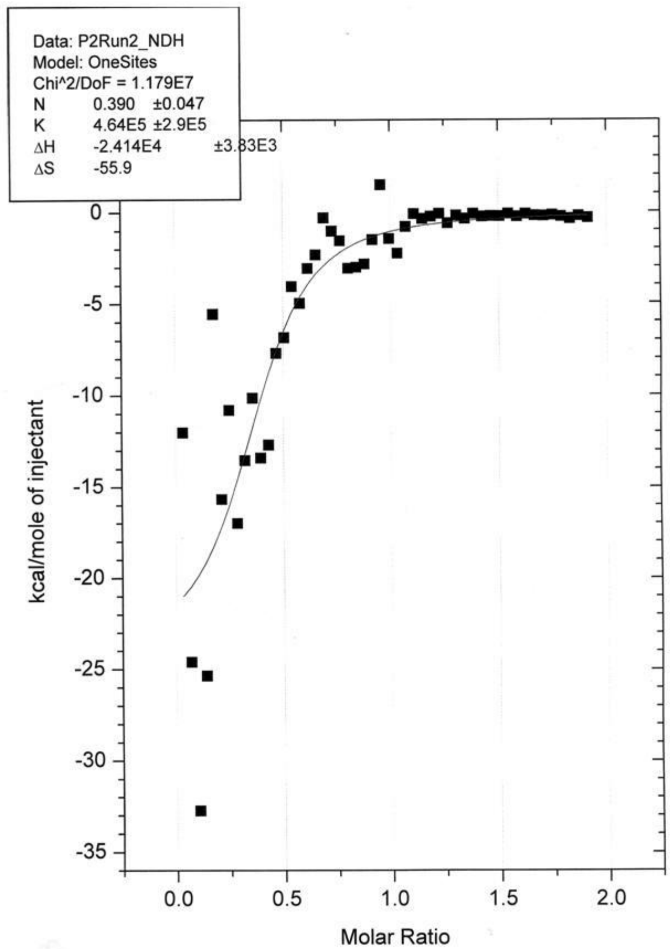

Figure 3.5. Preliminary ITC data for the binding of **P2** to bTAR RNA.

The initial result for the titration of **P2** and bTAR is shown in **Figure 3.5.** Experiments were performed by monitoring the temperature of 1.4 mL of 40 μM bTAR RNA as cyclic peptide was titrated in a series of 5 μL injections of 400 μM cyclic peptide stock. A total of 40 injections were performed which allowed for a peptide concentration range from 0 – 1.25X that of bTAR. Problems with reproducibility plagued our collaborators and reliable data was difficult to ascertain even though the initial results looked promising. Analogous to the UV thermal denaturation experiments, this technique also relies on the experimental concentration of the bTAR target molecule being such that it favors the bound state of the titrated peptide at each injection point. This is accomplished by making sure that the target RNA concentration is at least 5 times higher than the expected K_d. Evaluation of the experimental conditions for the data provided (40 μM RNA) suggests that some of the issues observed with reproducibility could be due to inappropriate experimental conditions if the affinity of the cyclic peptides for the bTAR target is above 8 μM. This incurred variability in the experimental results combined with the large quantities, and therefore large cost, of bTAR RNA associated with this technique prompted the exploration of alternative forms of *in vitro* analysis.

2.4 Fluorescence Quenching

In the case of cyclic peptides P1 and P2, the intrinsic fluorescence emission of the tryptophan residue was used to monitor binding as cyclic peptides P1 and P2 bound bTAR RNA. Since N1 and P3 did not serendipitously contain a tryptophan residue, initial binding experiments focused on scaffolds P1 and P2 for evaluation of this approach for biophysical characterization of binding.

Tryptophan residues undergo excitation when irradiated, with a peak in the absorption profile at 280 nm, and have a characteristic emission profile with a peak between 350-355 nm. For fluorescence quenching experiments performed with **P1** and **P2** (**Figure 3.6**), the peptide concentration was held constant and RNA ligand was titrated in. The fluorescence was monitored with an excitation of 290 nm to minimize the overlap of the peptide and RNA UV-visible absorption spectra thereby minimizing any inner filter effect. The change in emission intensity at 350 nm was monitored. The observed fluorescence emission ratio (F_{obs}/F_0, F_0= Em_{max}) was then plotted as a function of RNA concentration and fit to **Eq. (1)**[102] where F_{ratio} is the observed fluorescent ratio, Φ is the fluorescent ratio change amplitude (= 1 - F^{∞}_{ratio}), P_0 is the protein concentration, K_d is the dissociation constant, n is the stoichiometry, and L_T is the total ligand concentration (**Appendix A.3**).

$$F_{ratio} = 1 - \Phi \left[\frac{(K_d + nP_0 + L_T) - \sqrt{(K_d + nP_0 + L_T)^2 - (4nP_0 \cdot L_T)}}{2nP_0} \right] \quad (1)$$

The accuracy of the calculated K_d depends on exact quantitation of peptide and RNA concentration and on correcting for inner filter effects and dilution effects for the observed fluorescence ratio. UV absorption was employed to determine concentrations of both **P1** and **P2** peptides along with RNA ligand concentrations. Corrections were also made for the reduction in P2 fluorescence signal due to photobleaching and dilution of the sample (**Appendices A.4 – A.5**). Corrected values of F_0 (Em_{max}) could then be obtained for each titration point based on the exact peptide concentration of the sample. Corrected values of F_0 were used to determine the observed fluorescence emission ratio.

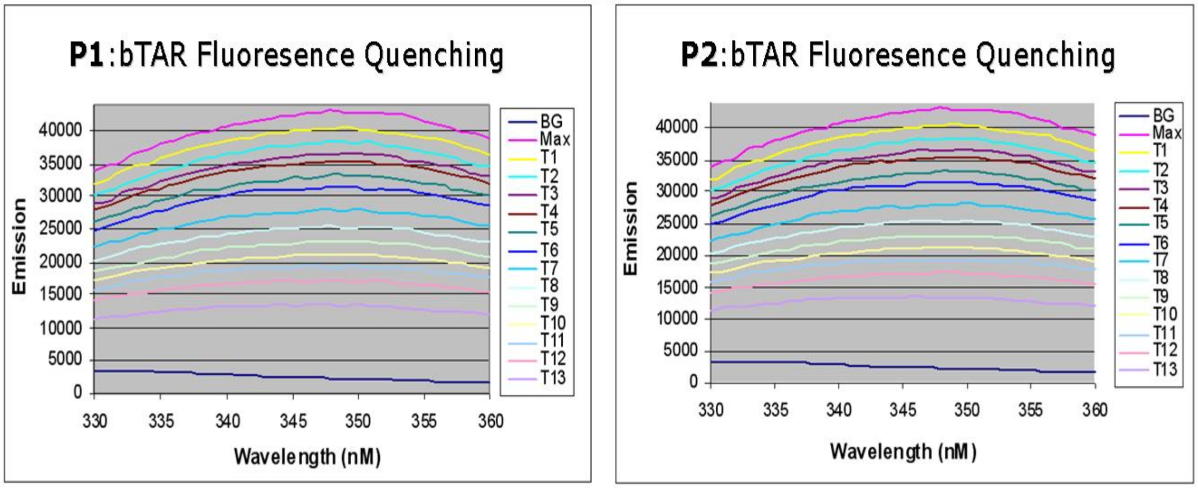

Figure 3.6. Fluorescence quenching profiles of bTAR RNA with **P1** and **P2**.

The resulting fluorescence quenching curves are depicted in **Figure 3.7**. **P1** bound with a K_d of 7.9 ± 0.5 μM to bTAR, while **P2** bound with a K_d of 9.1 ± 1.2 μM to bTAR. These affinities are similar to longer, linear peptides that have been selected using phage display techniques to bind to other, un-related RNA sequences.[106, 107] It is also noteworthy that the binding affinities determined by fluorescence quenching experiments support that the

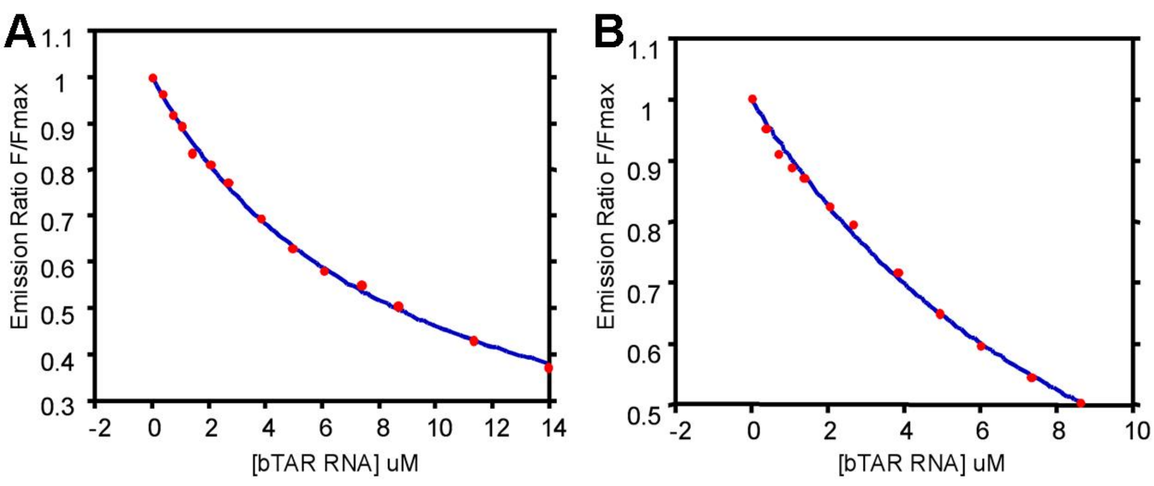

Figure 3.7. Fluorescence quenching of (*A*) **P1** with bTAR RNA, and (*B*) **P2** with bTAR RNA fit to equation

experimental conditions used for the previous ITC experiments were inappropriate.

Allthough we did not do iterative rounds of negative selection, we wanted to see what natural selectivity the cyclic scaffold have against other RNA. I designed and tested 2 RNA oligos (**Figure 3.8**): **N1-RNA** being the randomer sequence that we used during our negative selection round, **N2-RNA** being a hairpin oligonucleotide designed to closely mimic the bTAR secondary structure with a different primary sequence. Exploration of binding capabilities of the cyclic peptide constructs **P1** and **P2** for **N1-RNA** and **N2-RNA** provided insight into the scaffolds' ability to distinguish between different primary sequences given conserved secondary and tertiary structures.

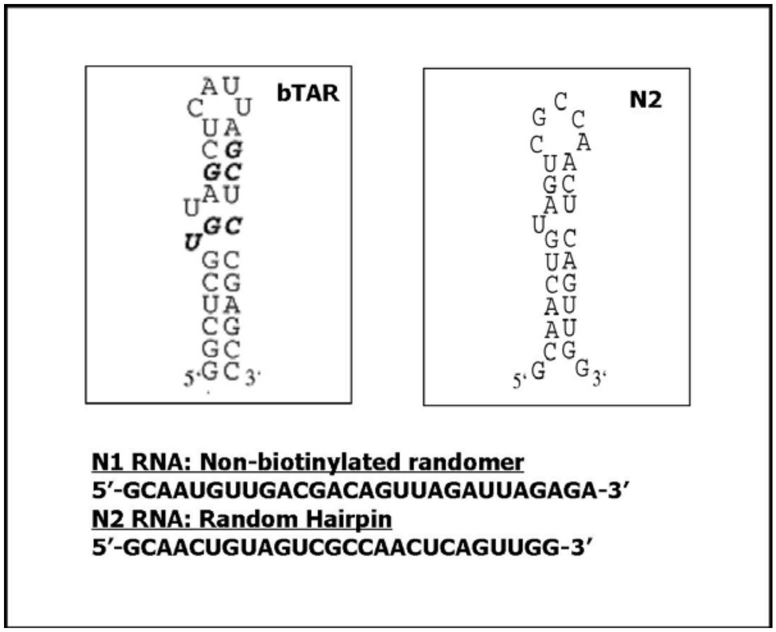

Figure 3.8. Negative RNA controls used for the determination of sequence specific recognition of cyclic peptide scaffolds. The bTAR sequence is also shown for comparison of secondary and tertiary structure.

Fluorescence quenching was performed in the same manner as previously stated. **Figure 3.9a and 3.9b** depict binding of the two cyclic peptide constructs with **N1-RNA.** Although **N1-RNA** is comparable in length to the bTAR target, it is devoid of any secondary structure. **P1**

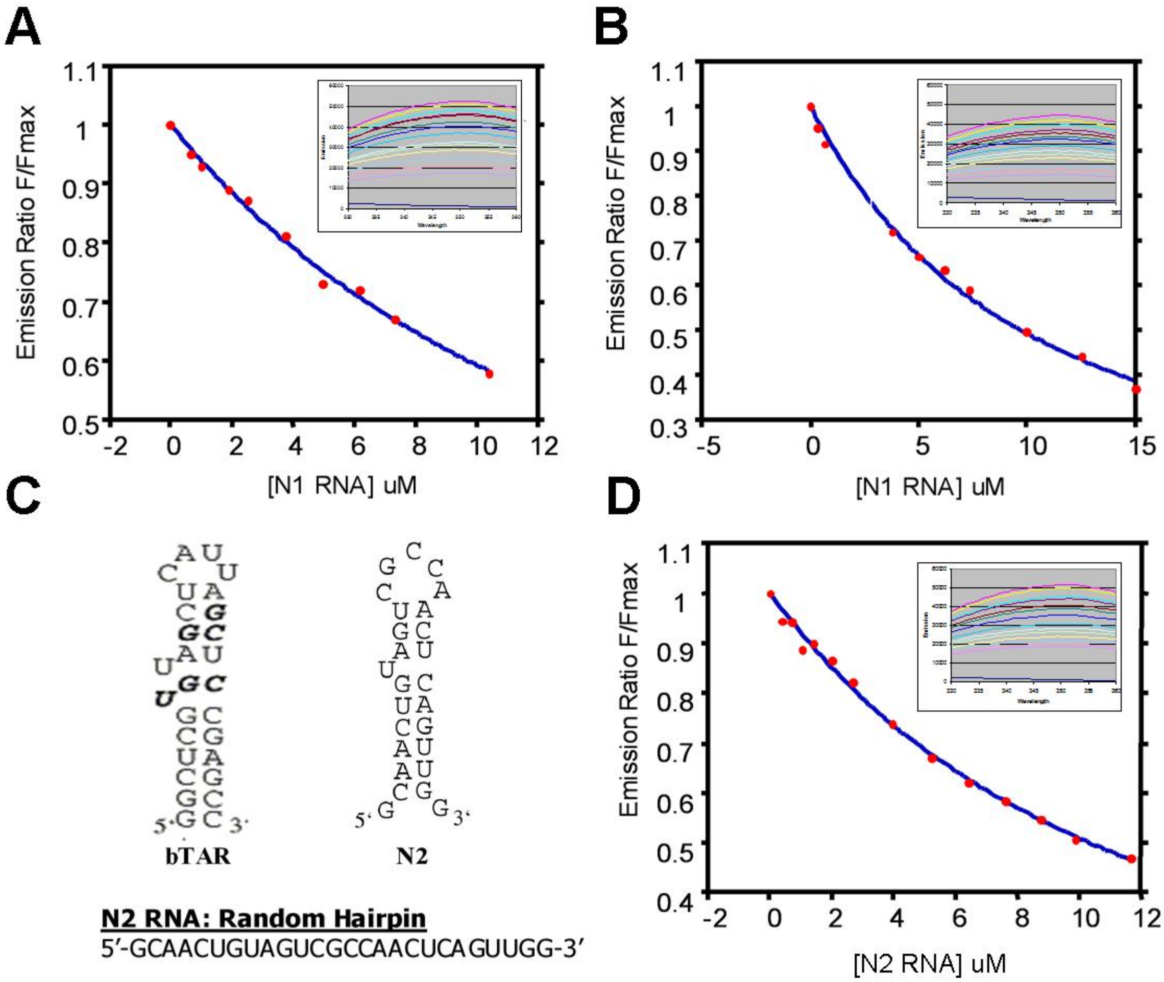

Figure 3.9. Fluorescence quenching profiles (QPs) for **P1**and **P2** with negative RNA controls. (A) **P1** with N1-RNA; (B) peptide 2 with N1-RNA; (C) bTAR sequence (bTat binding indicated in bold) compared to the N2 sequence, secondary structure, and (D) is **P1** QPs profile with N2-RNA.

displayed a slight selectivity with a K_d of 15.9 ± 3.2 μM compared to binding bTAR with a K_d of 7.9 ± 0.5 μM, however **P2** bound **N1-RNA** with a K_d analogous to bTAR, at 9.1 ± 1.2 μM displaying no specificity for the target oligo. **P1,** showing modest signs of selective binding to target RNA over randomer RNA, was subsequently tested with the second negative RNA control, **N2-RNA**, to determine its ability to distinguish between secondary structure analogues. The results are shown in **Figure 3.9c**. Fluorescence quenching indicates that although **P1** has higher affinity for **N2-RNA** than **N1-RNA** with a K_d of 11.8 ± 0.5 μM, **P1** has limited capabilities of differentiating between secondary structure analogues and binding in a sequence specific manner.

These initial results indicate that the **P1** scaffold binds bTAR with a slightly higher affinity than the P2 scaffold. This is not surprising knowing the **P1** scaffold was represented in ther sequencing pool (**Figure 2.14**) a total of 11 times where as the **P2** scaffold was represented only 2 times. The fluorescence data also indicates that the specificity of **P2** is less than that of **P1.** Analysis revealed that the cysteine constrained **P1** scaffold is a low micromolar binder of the target bTAR RNA with the capability, although limited, to discriminate between bTAR and other RNA sequences. General specificity of **P1** for the bTAR target, defined as the binding affinity of **P1** for bTAR RNA site divided by its average affinity to negative control RNAs, was calculated to be 1.7. It should be noted that when there was no conserved secondary and tertiary structure between the target RNA bTAR and negative contol RNA, as with **N1-RNA**, the specificity was much greater with a calculated value of 2.0.

2.5 In Silico Modeling of bTAR / P1 and bTAR / P2 Interactions

Computer modeling experiments of the **P2**-bTAR interactions have been performed by Ben Bobay of Dr. Cavanagh's group, NCSU Biochemistry Department. Models were generated using the HADDOCK docking protocol which has had previous success in protein/ligand docking studies.[53, 67] Results from the **P2**-bTAR modeling studies are shown in **Figure 3.10**.

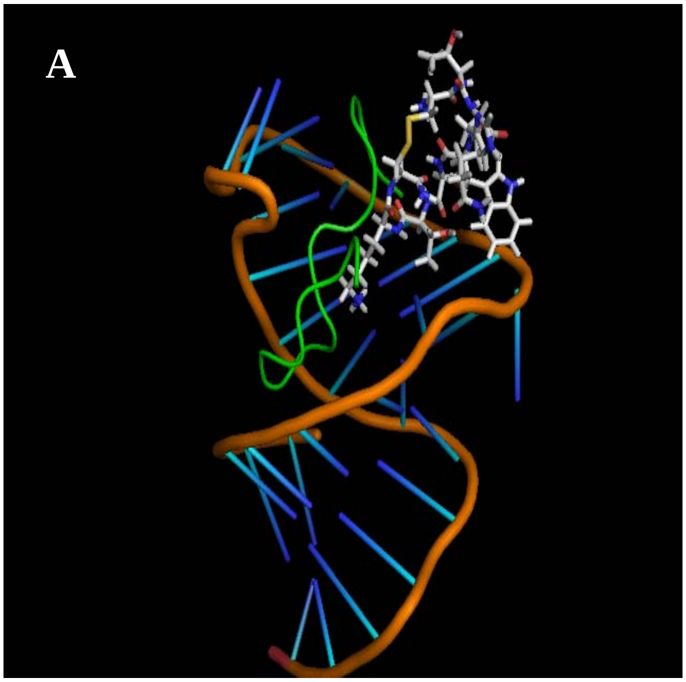

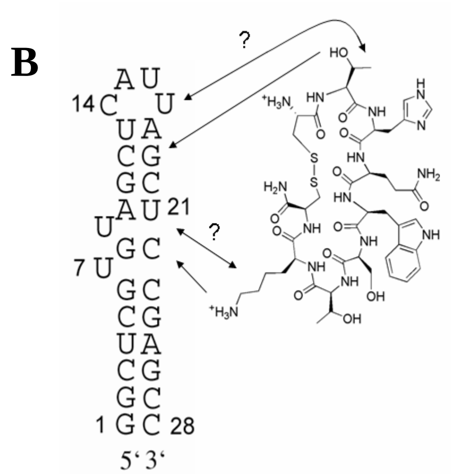

Figure 3.10. P2/bTAR complex. Single headed arrows indicate H-bonds predicted by HADDOCK modeling, double headed arrows indicate sites for introduction of H-bonds.

Results support the data that we have accumulated from other biophysical characterization experiments, and the modeling of the **P2**-bTAR interaction has provided insight into options for implementation of structure-based design.

III. Summary and Conclusions

In conclusion, we have demonstrated that it is possible to generate novel cyclic peptide motifs that bind with relatively high affinity to a predetermined RNA target by use of cysteine-constrained phage libraries. In this phase of the methodological study, we showed that the evolved cysteine constrained cyclic peptide scaffolds identified by phage display are capable of binding their target RNA as discrete entities with desirable affinities. The two cyclic peptide scaffolds studied most extensively, **P1** and **P2,** were determined by fluorescence quenching experiments to have dissociation constants for binding the bTAR

RNA target in the low micromolar range (7.9 ± 0.5 μM and 9.1 ± 1.2 μM, respectively). This data was supported by the preliminary results of the UV thermal denaturation and ITC experiments (**P2** / bTAR binding K_d estimated at 2.2 μM with ITC). *In silico* modeling provides useful information as to the nature of the RNA / peptide interactions and this technique may be exploitable for future structure-based design efforts. Given the flexibility of phage methodology, it should be possible to use this approach to generate novel, cyclic peptide scaffolds for any predetermined RNA motif.

CHAPTER 4: DEVELOPMENT, SYNTHESIS, AND TESTING OF DICARBON CONSTRAINED ANALOGUES

I. Introduction

The limiting factor for the use of cysteine constrained phage libraries to develop ligands to target RNA for *in vivo* applications is that the resulting scaffold's macrocyclic linkage is a di-sulfide bond. The cysteine constrained molecular scaffold would most likely be cleaved when subjected to reducing conditions, such as those present in cellular environments, rendering the peptide in a linear conformation. Linearization due to reduction would have major drawbacks including negative affects on biostability and bioavailability and also could result in lowered binding affinity and specificity for the target RNA. Linearization of the scaffold opens the door to protease based degradation. Also, by unlocking the cyclic structure, the resulting peptide is able to adopt a multitude of conformations due to the introduction of additional degrees of freedom.

The metabolic stability of RNA-binding cyclic peptides derived from cysteine-constrained phage libraries can be significantly increased through the installation of an alternative redox stable macrocyclic linker, resulting in stabilized surrogate analogues to be used for *in vivo* applications. Based on previous *in silico* modeling data (**Figure 3.10**), the disulfide linker should be amenable to substitution. It is believed to only provide the necessary covalent linkage to generate the cyclic molecular architecture rather than providing H-bond donor / receptor interactions with the oligonucleotide. Investigational studies of alternative, non-cleavable macrocyclic linkages using Spartan software have indicated a dicarbon based linker will sufficiently mimic the disulfide linker without distorting the evolved scaffold resulting in little to no loss in affinity for the RNA target. This surrogate for the disulfide linkage also has the added benefit of being synthetically feasible. A facile way to replace the disulfide bridge is through the well-known ring closing metathesis (RCM) of an olefin flanked linear peptide to generate the dicarba analogues of **P1** and **P2**. All the synthetic work was completed by my colleague, Anne Basso.

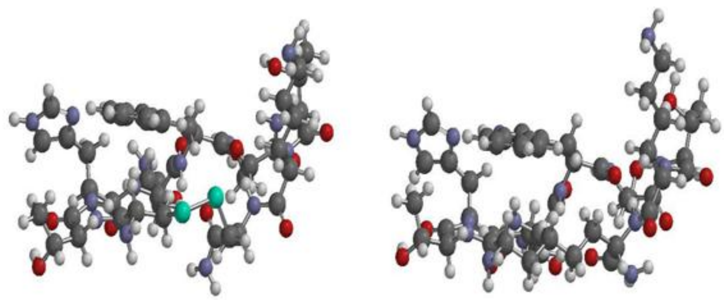

Figure 4.1. Spartan modeling of disulfide constrained cyclic peptide **P2** (left) and ethene constrained cyclic peptide **P2$_1$** (right).

Using this approach, the disulfide bond of the cysteine scaffold was replaced with a carbon-carbon double bond resulting in 1st generation alkene constrained analogues **P1$_1$** and **P2$_1$**. Analysis of the two models by Spartan reveals that this change elicits very little structural change in the scaffold (**Figure 4.1**) and the relative length of the macrocyclic linkage changes from 8.97 angstroms to 7.57 angstroms (**Figure 4.2**).

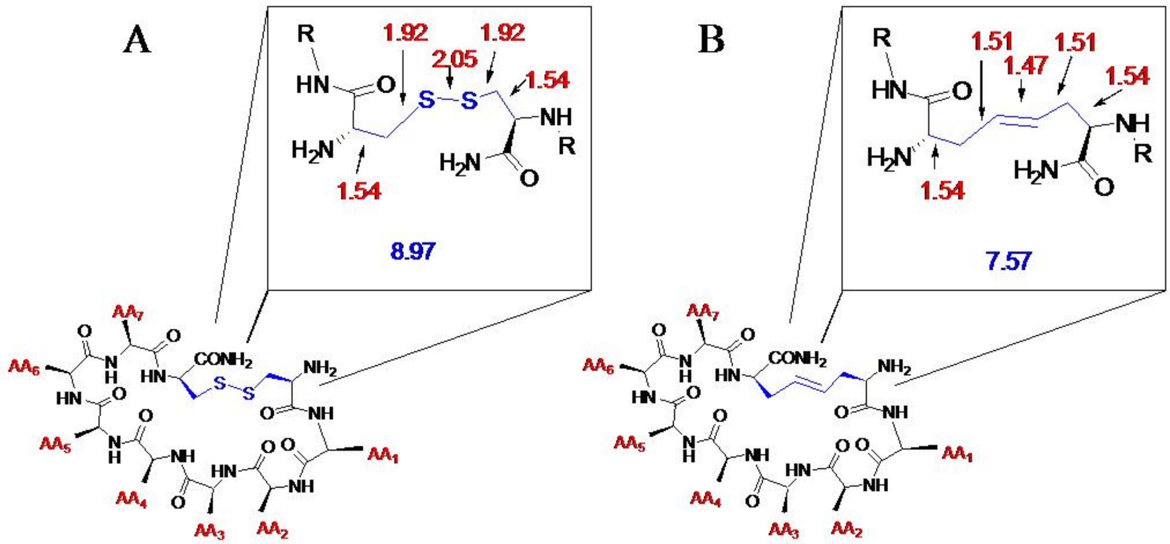

Figure 4.2. Comparison of macrocyclic linkers. (A) Disulfide constrained cyclic peptide scaffold. (B) Dicarbon constrained cyclic peptide scaffold. All bond lengths are indicated in red and reported in Angstroms.

Hydrogenation of the unsaturated alkene anologues allows for a direct and easy way to generate a 2nd generation of macrocyclic linkers (**P1$_2$** and **P2$_2$**). Further reduction of the alkene linker to an alkane based model allows for a slight increase in the linker length to better mimic the disulfide constrained scaffold (**Figure 4.3**).

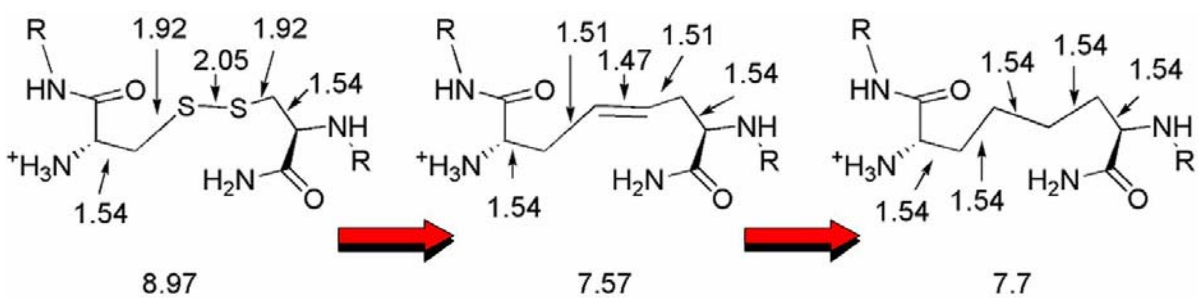

Figure 4.3. Comparitive analysis of macrocyclic linker lengths between the disulfide constrained scaffold (left), the alkene constrained 1st generation analogues (middle), and reduced, alkane constrained 2nd generation analogues (right).

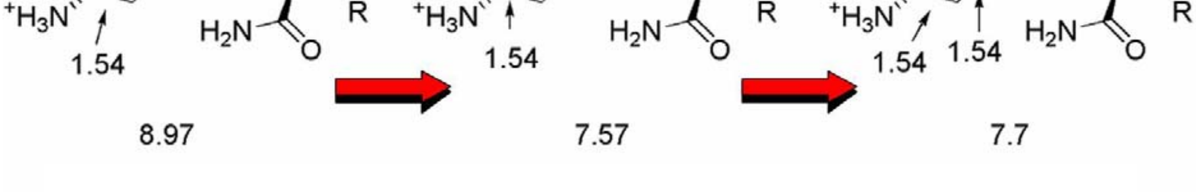

The following synthetic scheme was developed by my colleague, Anne Basso: The general approach involved the synthesis of linear peptides using standard Fmoc-chemistry on Rink-amide-MBHA resin. This resin was chosen for its ability to generate the C-terminus amide functionality upon cleavage. This enabled easy installation of the necessary flanking olefin residues using Fmoc-chemistry along with Fmoc-L-allylglycine residues under standard coupling procedures. RCM via Grubbs catalyst was subsequently performed while the peptide was still tethered to the resin. Proceeding along this route allowed for cyclization followed by cleavage and deprotection of side chains to be performed in one step. Purification of the cyclic peptide was achieved using reverse phase HPLC with the addition of DMSO which facilitated purification to yield the desired unsaturated $\mathbf{P1_1}$ and $\mathbf{P2_1}$ as a mixture of cis and trans isomers. Hydrogenation of the alkene constrained 1st generation analogues to yield the alkane constrained 2nd generation analogues was performed under standard conditions using a palladium catalyst. Purification of the 2nd generation analogues was also done by reverse phase HPLC.

After successful synthesis of the saturated and unsaturated analogues, it was essential to test for retention of binding properties as compared to the evolved cysteine constrained scaffold. Thus, binding affinities were assessed using fluorescence quenching as previously reported. Furthermore, competitive fluorescence quenching experiments were performed to investigate the ability of the cyclic peptides to displace or compete for binding with the endogenous bTat protein. Circular dichroism was also employed for *in vitro* analysis of the bTAR RNA recognition site for cyclic peptide binding.

II. Results and Discussion

2.1 Fluorescence Quenching

For the alkene constrained cyclic peptide analogues **P1**$_1$ and **P2**$_1$, fluorescence quenching experiments were performed analogous to those performed for disulfide constrained **P1** and **P2** scaffolds. The emission of the tryptophan residue was monitored as the bTAR RNA ligand was titrated into the sample and fluorescence quenching ratios (F/ F_{max}) were plotted as a function of RNA concentration. The initial peptide concentration was 0.63 μM for **P1** and 0.8 μM for **P2**. RNA concentrations at the final titration point were such that the ratio of RNA to cyclic peptide was approximately 45:1. Assuming that the alkene constrained analogues displayed binding affinities on the same order as the disulfide constrained ones (around 10 μM), these experimental conditions should elicit around a 75-80% quenching of the peptide fluorescence at the highest titration point. The resulting data was corrected for

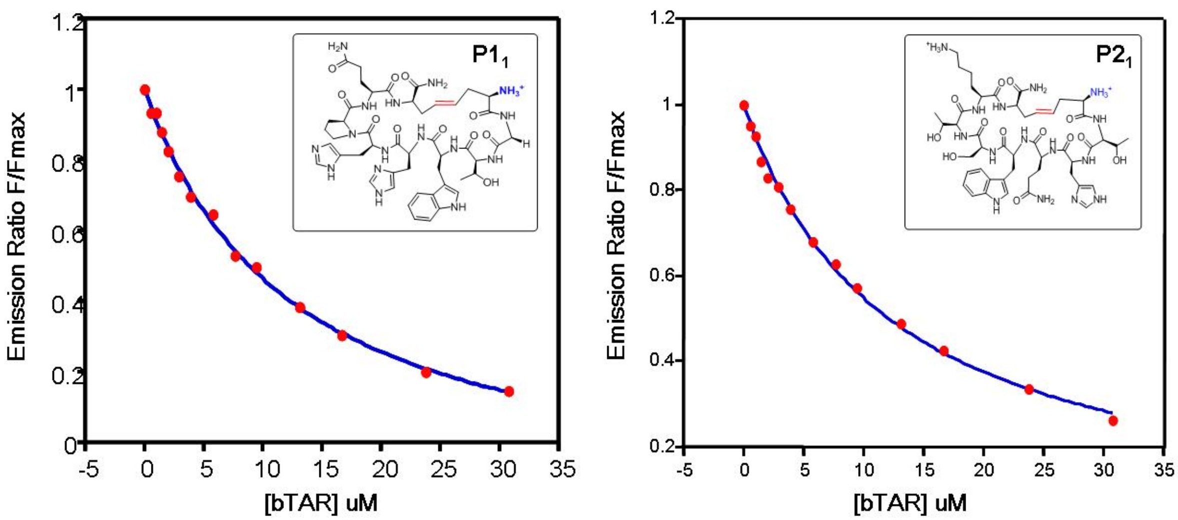

Figure 4.4. Fluorescence quenching profiles of 1st generation alkene analogues with bTAR RNA. (left) **P1**$_1$ with bTAR RNA, (right) **P2**$_1$ with bTAR RNA

dilution and photobleaching and subsequently fit to **Eq. 1**.

The resulting data, shown in **Figure 4.4**, indicates that although there was a slight loss in binding affinity from the installation of the alkene based macrocyclic linker as compared to the disulfide cysteine constrained scaffold, the first generation analogues roughly retained their binding properties. **P1$_1$** was shown to have a K_d of 10.6 ± 0.7 μM (compared to 7.9 ± 0.5 μM for **P1** scaffold) and the results for **P2$_1$** were analogous to those of **P1$_1$** with K_d measurement of 11.8 ± 0.8μM (compared to 9.1 ± 1.2 μM for **P2** scaffold).

Given that there is no rotational freedom in the unsaturated sp^2 hybridized dicarbon linker, the 1st generation alkene analogue is even more constrained than its cysteine counterpart. This increased rigidity of the 1st generation cyclic peptide analogue can potentially have two affects on binding, a decrease in binding affinity and an increase in binding specificity. The data indicate that although there is a decrease in affinity for the 1st generation scaffold to the bTAR target, the decrease is in an acceptable range to carry these studies forward and the cost (decrease in affinity) does not outweigh the benefit (increase in stability) of installing the redox stable linker. Loss in affinity can later be mitigated and potentially overcome through future structure based design to modify the scaffold.

Increases in specificity stem from the same basic concepts addressed for the argument of decreased affinity. By increasing the rigidity of the cyclic peptide backbone, there is a decrease in the ability for the peptide to adopt alternative binding conformations (less "wiggle" room) resulting in an increase in binding specificity assuming that nonspecific interactions are not electrostatic interactions. To further explore the affects of the alkene constrained analogue on specificity, we tested the **P2$_1$** scaffold for relative affinities to bTAR RNA and N1-RNA (randomer RNA designed for previous experiments). The fluorescence quenching experiments were performed as described above. The results are shown in **Figure 4.5.**

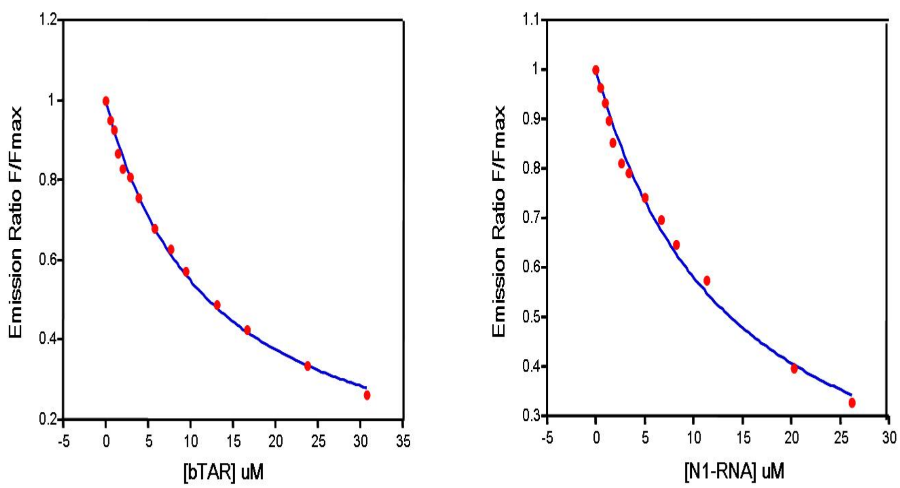

Figure 4.5. Comparitive fluorescence quenching profiles of 1st generation alkene **P2$_1$**. (left) bTAR RNA, (right) N1-RNA

Fluorescence quenching experiments performed with the **P2** cysteine constrained scaffold indicated no discernable difference in binding affinities for the target bTAR RNA as compared to randomer N1-RNA. To test whether installation of the alkene macrocyclic linkage could impart specificity into the model system, the **P2$_1$** analogue was tested. Results indicate a slight increase in specificity, with the K_d measurements for the **P2$_1$** analogue for bTAR and N1-RNA being 11.8 ± 0.8 μM and 13.4 ± 1.6 μM, respectively. The increase in specificity for the bTAR target as compared to the N1-RNA showed a very modest improvement from 1 to 1.14 indicating that the additional conformational constraints imparted by the alkene macrocyclic linker may increase relative specificity of the scaffold for its predetermined target.

To determine whether the aforementioned decrease in affinity and slight increase in specificity was due to the additional conformation constraints imparted by the alkene macrocyclic linker, we performed the same fluorescence quenching experiments using the 2nd generation alkane constrained analogue **P2$_2$**. Hydrogenation of the sp^2 hybridized alkene to the sp^3 hybridized alkane reinstates the flexibility of the peptide backbone as seen in the disulfide constrained scaffold. In this scenario, the loss of the stereochemistry around the sp^2 hybridized carbons would decrease the specificity, but the increase in rotational freedom of

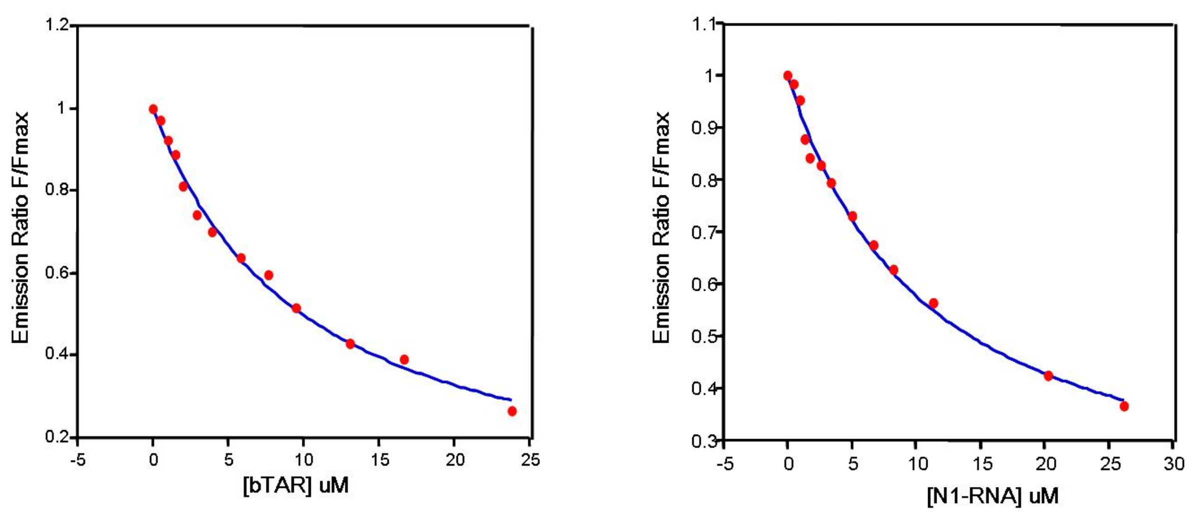

Figure 4.6. Comparitive fluorescence quenching profiles of 2nd generation alkane **P2$_2$**. (left) bTAR RNA, (right) N1-RNA

the cyclic peptide backbone along with a slight elongation of the overall linker length would lead to an increase in affinity. The results of the fluorescence quenching experiments are shown in **Figure 4.6**.

As expected, although the binding affinities were increased and closer to that of the disulfide linked scaffold, the specificity of **P2$_2$** for bTAR over that of randomer N1-RNA was decreased. The K_d of **P2$_2$** for bTAR was determined to be 9.5 ± 1.0 μM (**P2** = 9.1 ± 1.2 μM, **P2$_1$** = 11.8 ± 0.8 μM) which is comparable to the cysteine constrained scaffold. The K_d of **P2$_2$** for randomer N1-RNA was determined to be 10.1 ± 1.0 μM (**P2** = 9.1 ± 1.2 μM, **P2$_1$** = 13.4 ± 1.6 μM) .This represents a reduction of any specificity gained from the **P2$_1$** analogue.

2.2 CD Spectroscopy

Circular dichroism spectroscopy is a well established tool for monitoring bTAR structural changes upon bTat binding.[69, 94, 95, 108, 109] CD spectra of A-form bTAR RNA contain a characteristic peak around 265 nm and a relatively large negative band at 210 nm. Previous studies have shown that binding of the hairpin bulge region by bTat protein, bTat peptide and numerous other arginine rich ligands all result in a decrease in the 265 nm peak in the CD spectra. Base stacking interaction contribute to the characteristic CD spectra associated with various secondary nucleic acid structures, and it is widely believed that the decrease in the 265 nm peak of bTAR RNA is due to perturbations in base stacking upon binding of the ligand. bTat is known to bind the bulge region of the hairpin structure by specifically interacting with one of the uridine bases of the bulge and the G-C and A-U base pairs located adjacent to the bulge site.[109] In the unbound state, nucleotides in the bulge appear to be at least partially stacked between two A-form helices. When the bound complex is formed, the bases in the bulge become unstacked and the two double stranded helices become coaxially stacked. The net loss of base stacking in the bTAR RNA bound hairpin results in the observed decrease in the signal at 265 nm.

We employed CD spectroscopy to investigate the binding of the 1st and 2nd generation cyclic peptide analogues by monitoring their ability to elicit structural changes in the bTAR hairpin. All samples were prepared with final bTAR RNA concentrations of 20 μM and final cyclic peptide concentrations (where relevant) of 80 μM in TK buffer. Spectra were acquired from 200 – 300 nm at a 1nm interval, 0.8 seconds per point. A total of 10 scans were taken for each sample condition and averaged then smoothed over 5 points (**Appendix A.9).** For each ligand tested, a background scan using test parameters was performed for correction of the CD spectra (**Figure 4.7**).

Five total samples were investigated: free bTAR RNA, bTAR + bTat peptide, bTAR + **P1$_1$**, bTAR + **P2$_1$**, and bTAR + **P2$_2$ (Appendix A.9**). **Figure 4.7f** summarizes the results of the CD binding study. Although we observed the previously reported affects of bTat-bTAR

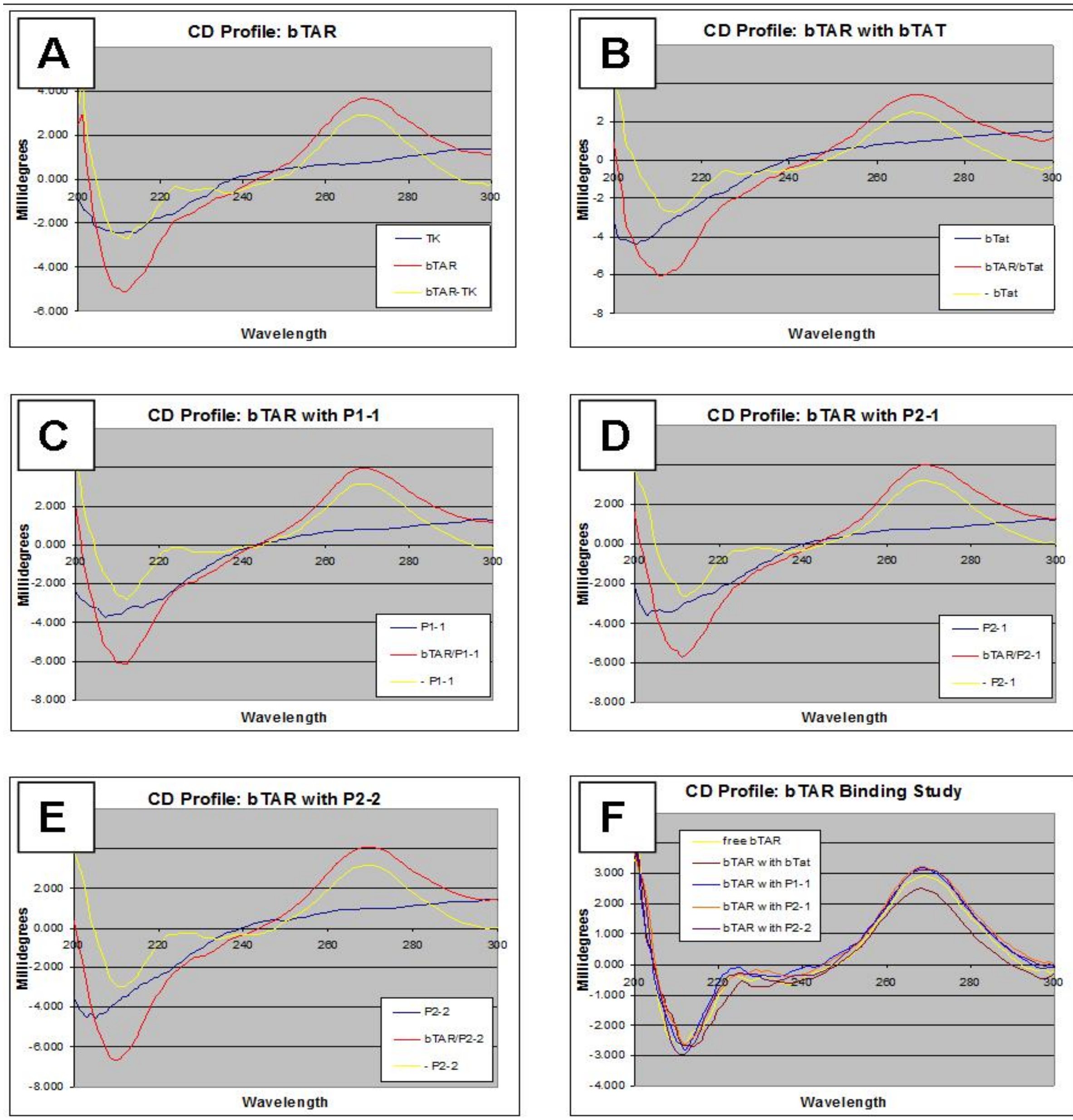

Figure 4.7. CD Analysis of bTAR hairpin structure upon binding of cyclic peptide analogues.

binding by the characteristic decrease in the peak at 265 nm, none of the cyclic peptide analogues elicited this same affect. The spectra of the cyclic peptide analogues actually had the opposite trend, a slight increase in the peak at 265 nm. This might provide evidence that upon binding, they actually serve to increase the base stacking character of the bTAR hairpin. If true, this could possibly be through distortion of the helical structure that allows for an increase in the cooperative base stacking between the two alpha helices or by partial intercalation of one of the aromatic peptide side chains (such as tryptophan) therefore increasing the overall base stacking character.

2.3 Competitive Fluorescence Quenching

Competitive fluorescence quenching assays were performed in order to further characterize the binding of the cyclic peptide analogues to the target bTAR RNA. The bTat peptide was used as the competitor ligand due to the fact that (a) the 17-mer minimal recognition motif serendipitously does not yield any measurable fluorescence at the experimental conditions and (b) the binding is extremely well characterized. Given the CD spectral data indicating that the cyclic peptide analogues might bind in an alternative fashion to that of bTat, it will also allow us to probe if the cyclic peptide analogues compete for binding with the endogenous bTat ligand. Competitive fluorescence experiments were designed to monitor the fluorescence quenching of the cyclic peptide analogues due to the binding of the bTAR RNA with and without the presence of the bTat peptide. In a noncompetitive binding scenario, the measured quenching upon binding of the cyclic peptide analogue to the target bTAR RNA (defined here as $F_{max} / F_{quenched}$) would not be reduced in the presence of bTat

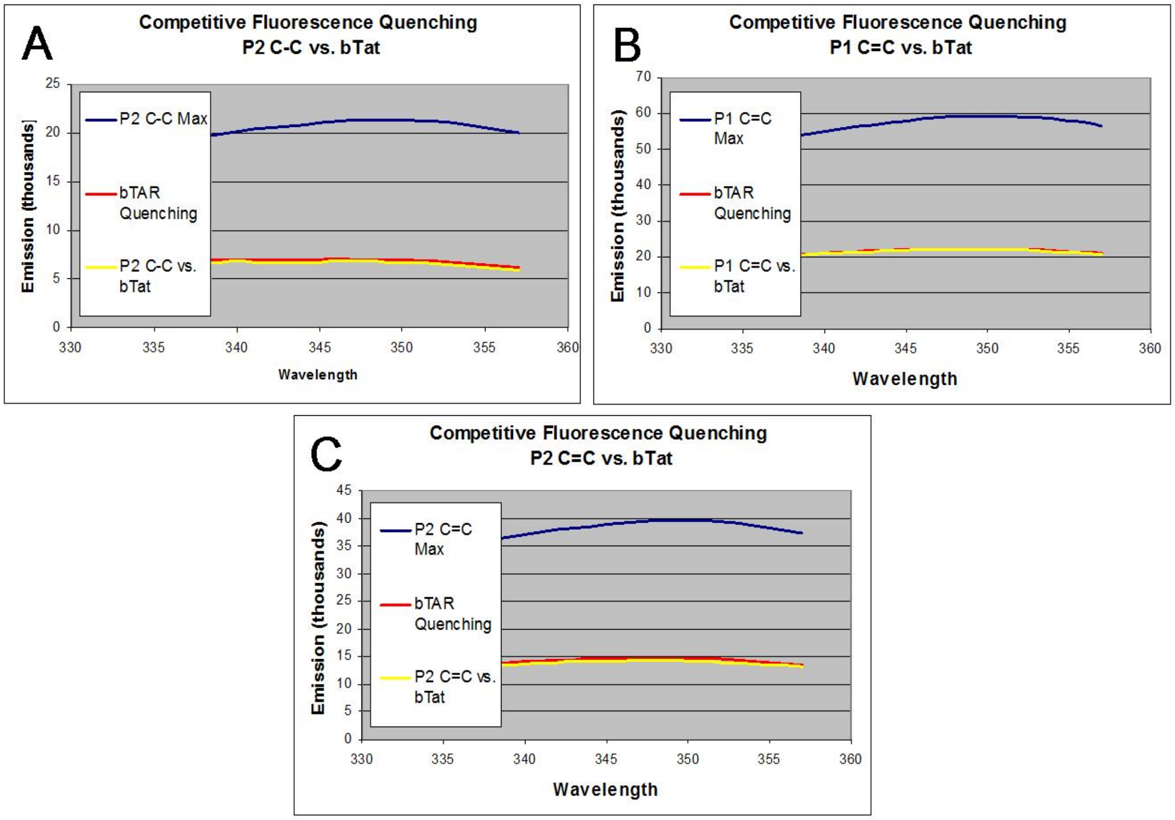

Figure 4.8. Competitive fluorescence quenching results. (A) competitive quenching profile of **P2$_2$**, (B) competitive quenching profile of **P1$_1$**, and (C) competitive quenching profile of **P2$_1$**.

peptide. In a competitive binding scenario, the presence of bTat peptide would diminish the binding capabilities of the cyclic peptide analoguee and therefore result in a reduction in the measured quenching capabilities at a given concentration.

All three analogues were tested (**P1$_1$**, **P2$_1$**, and **P2$_2$**) by adding 30 µL of 20 µM stock (0.6 nmol) to 670 µL of TK buffer. This yielded cyclic peptide analogue concentrations analogous to those used with fluorescence quenching experiments (0.86 µM). Fluorescence measurements were then taken to establish the maximum fluorescence for each sample. 20 µL 1.17 mM bTAR RNA stock was then added and the quenched fluorescence profiles were measured. The bTat peptide was subsequently added to the sample in a 1:1 ratio with the cyclic peptide analogue (0.6 nmol). Given that the bTat peptide's affinity for the bTAR target is known to be in the low nanomolar range (at least 1000X that of the cyclic peptide analogues), the experimental conditions should (a) yield bTat in an almost 100% bound state and (b) displace any cyclic peptide analogue if there is overlap in recognition sites. Following the addition of bTat to the cyclic peptide analogue / bTAR samples, competitive fluorescence measurements were taken. All experimental measurements were completed in triplicate and subsequently averaged and smoothed over 5 points (**Appendices A.6 – A.8**). The data is shown in **Figure 4.8**.

Results from the fluorescence quenching experiments support the CD spectral results and indicate that the bTAR recognition site of all three of the cyclic peptide analogues does not overlap with that of the bTat peptide. No decrease in the fluorescence quenching was observed in the presence of bTat. The combined results shed valuable light on earlier work regarding competitive EMSA assays completed with the cysteine constrained analogues. Now, knowing that the bTat peptide does not compete for binding with the evolved cyclic peptide scaffolds, it is clear why we were never able to elicit a competitive gel shift using the bTat peptide.

III. Summary and Conclusions

The *in vitro* analytical techniques employed here validated the use of the dicarbon based macrocyclic linker as an alternative method of cyclization for the cysteine constrained cyclic peptide binding scaffolds discovered through the use of phage display. Thus, the replacement of the disulfide bond of RNA-binding peptides derived from cysteine-constrained phage libraries with dicarbon analogues may represent a general approach to the rapid generation of RNA-targeting ligands. This achievement signifies the culmination of a multistep process embarked upon to develop a direct and efficient approach to targeting nucleic acids for *in vivo* applications.

CHAPTER 5: APPLICATION - TARGETING HTELO G-QUADRUPLEX DNA

I. Introduction

It has been shown that using our proposed methodology, novel cyclic peptide scaffolds could be identified as RNA binders. One of the overall strengths of our approach is that this methodology can potentially be applied to any predetermined oligonucleotide to generate cysteine-constrained peptide binders regardless of sequence, secondary or tertiary structure. Investigations are underway to apply this approach to generate cyclic peptide library against a biotinylated analog of poly-$(CUG)_{54}$ RNA oligonucleotide. Analogous to the bTAR RNA, this target has a helical hairpin secondary structure. Results from these studies show that this approach can be applied successfully to the poly-$(CUG)_{54}$ RNA target, and has yielded novel cyclic peptide scaffolds for potential therapeutic applications.

Given the success of this approach with identification of cyclic peptide scaffolds to target bTAR RNA and poly-$(CUG)_{54}$ RNA hairpins, it is reasonable to assume that selections for double stranded DNA helices would yield similar positive results. In order to really test the limits of this application, we have chosen to investigate the G-quadruplex DNA structure as a potential target.[3, 5, 8, 10, 12, 15, 110-130] These complex guanine tetrad structures are stabilized by Hoogsteen hydrogen bonding interactions between guanine bases. Each base serves as the donor and acceptor of two hydrogen bonds with its neighbor. The resulting planar cyclic guanine arrangement is stabilized by association with a cation at its core. Given the large architecture and limited opportunities for ligand hydrogen bonding interactions, G-quadruplex DNA provides a theoretically interesting target for cyclic peptide phage display.

Specifically, the human telomerase binding (Htelo) G-quadruplex oligo will be targeted for selection.[10, 111, 113-115, 122, 125, 130] This sequence has been well studied and shown to form a relatively stable intramolecular quadruplex in the presence of sodium and potassium ions [114] under *in vitro* conditions.

II. Results and Discussion

2.1 Preparations for Selection

As with the development of the protocol for targeting bTAR RNA, there are many points of modification within the procedure to consider. The choice of buffer system is of particular importance for this scenario given that the secondary G-quadruplex structure is less stable than the bTAR RNA hairpin structure and is susceptible to unfolding under low salt conditions.[GN1] Previous experiments have reported the formation of Htelo, G-quadruplex structures in Tris based buffer systems with greater than 100 mM NaCl or KCl. The NEB Phage Display C7C Ph.D. kit protocol suggests using a TBS buffer (50 mM Tris HCl, pH 7.5, 150 mM NaCl) for binding and washing steps. Since the TBS buffer should be amenable to G-quadruplex formation, it was used for all assay and selection conditions.

To test the purity of the biotinylated (B-Htelo) and nonbiotinylated (Htelo) stocks before starting any selection assays, the lyophilized samples were resuspended in TBS buffer, quantitated using UV-Visible spectroscopy and analyzed via native polyacrylamide gel electrophoresis (native PAGE). My first attempt at visualizing the DNA stocks by staining with ethidium bromide (EtBr) was unsuccessful even though I loaded up to 500 times the reported detection limit (0.1 pmol DNA). After multiple attempt and retesting stock concentrations by absoption spectroscopy, it was determined that the EtBr could be the culprit. Ethidium bromide stains DNA and RNA by intercalation along the double stranded backbone. EtBr is quenched in solution due to the association of H_2O molecules; however, insertion of the ethidium cation heterocyclic core into the hydrophobic environment of the RNA or DNA duplex causes the dissociation of H_2O molecules, thereby allowing the molecules to fluoresce. Due to the fact that the G-quadruplex structure is structurally very different than an RNA or DNA duplex, it might not offer the same hydrophobic environment required for EtBr fluorescence.

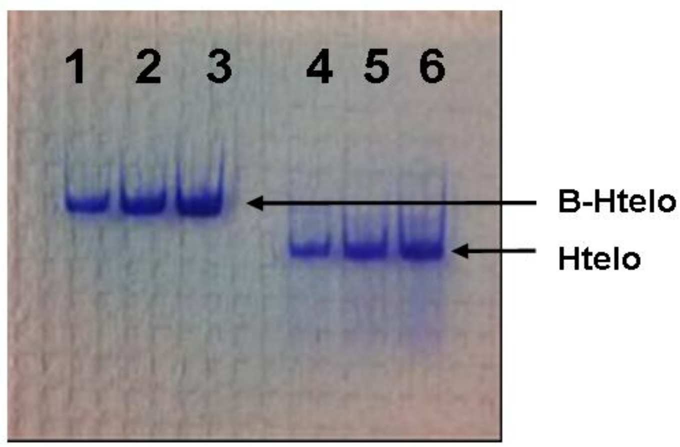

Figure 5.1. Analysis of B-Htelo and Htelo DNA stocks via native PAGE. Samples were prepare in TBS buffer and then heated and cooled to induce folding of the G-quadruplex. Lanes 1-3 contain B-Htelo samples of 250 pmol, 500 pmol and 750 pmol from left to right. Lanes 4-6 contain Htelo samples of 250 pmol, 500 pmol, and 750 pmol from left to right.

An alternative method of staining RNA and DNA is the use of Methylene Blue. This dye does not intercalate and therefore is not reliant upon base stacking interactions or hydrophobic environments for detection. The limitations of using methylene blue as a substitute for EtBr staining is a decrease in sensitivity, with the detection limits on the order of 20X lower than that of EtBr. Three samples from both the B-Htelo and Htelo stocks were prepared and analyzed by 15% native PAGE. The gel was subsequently stained using methylene blue. The results, shown in **Figure 5.1**, indicate that the samples are pure and free of degradation. They also indicate that the installation of the biotin linker was successful.

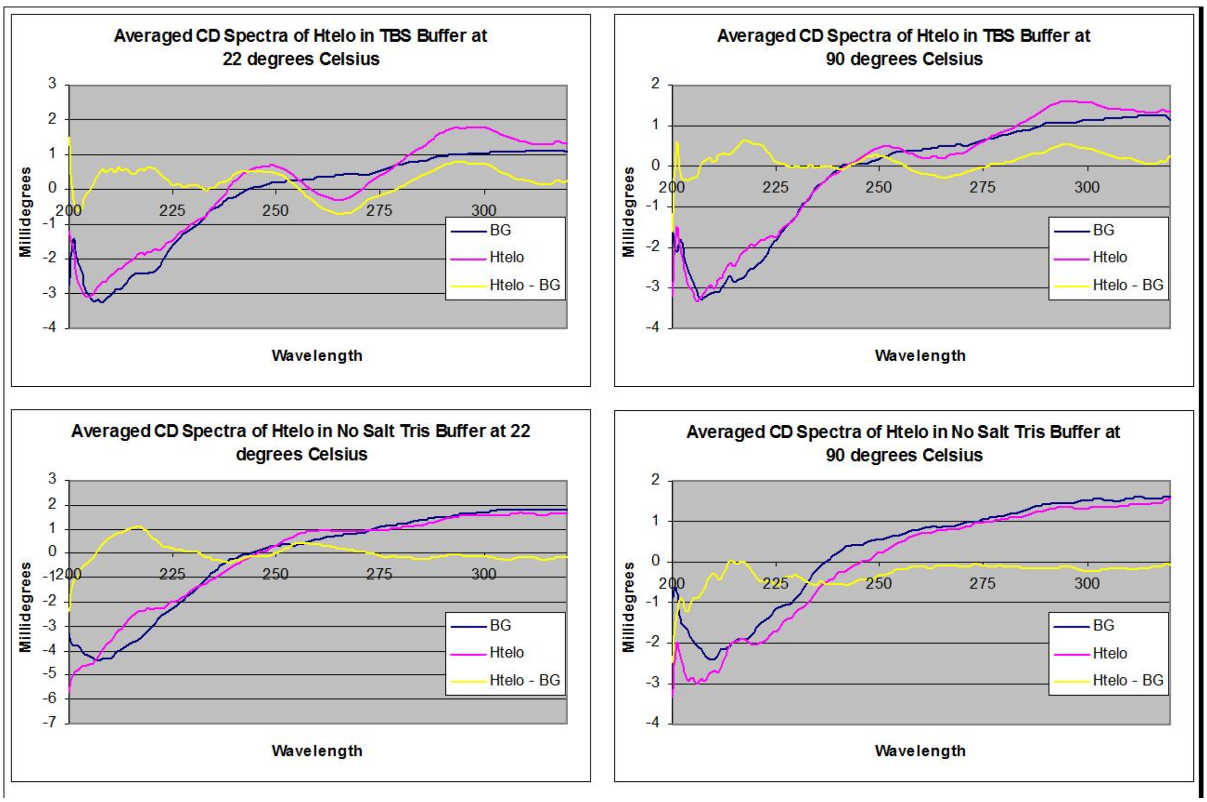

Figure 5.2. Folding study of Htelo by Circular Dichroism Spectroscopy.

Circular Dichroism was also used to assess the formation of the G-quadruplex structure under selection conditions. CD analysis of G-quadruplex structures has been extensively used to analyze the specific nature of G-quadruplex formation. CD spectra are extremely sensitive to base stacking geometries; hence, the different types of G-quadruplex structures elicit specific spectral characteristics.[114, 130] For these experiments, nonbiotinylated Htelo stock was analyzed in two different buffer solutions (with and without salt) each at two different temperatures (22 and 90 ºC). CD spectra of the two test buffers were also acquired at both test temperatures for background correction of the data (**Figure 5.2**).

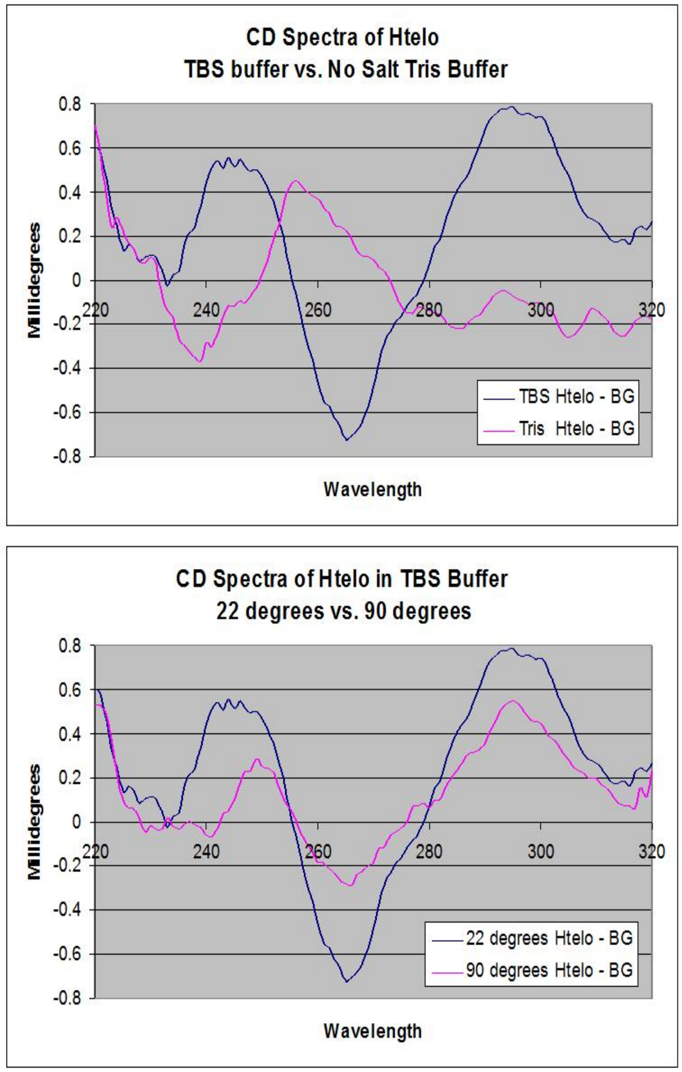

Figure 5.3. Overlay of CD spectra from Htelo folding study

Overlaid spectra for comparison of buffer conditions are depicted in **Figure 5.3** (**Appendices A.10 – A.13).**

Results from the CD folding study indicate that the G-quadruplex is forming in the TBS buffer and that it is stable at ambient temperatures. The strong peak at 295 nm and strong minimum at 260 nm in the TBS Htelo sample are indicative of antiparallel G-quadruplex formation. The spectra resulting from Htelo in no salt Tris buffer are analogous to the spectra previously reported for non quadruplexed Htelo sequences.[112, 114] Temperature studies of Htelo in TBS buffer also indicate that the G-quadruplex is stable at ambient temperatures and retains some of its structural characteristics even when heated to 90 ºC in the presence of salt.

In the bead binding scenario that I have chosen to use for the B-Htelo selection process, target loading can greatly influence the selection process. A low target population can apply excess stringency to the selection at early stages, and the resulting low packing density of the target on the bead surface can create an opportunity for the evolution of phage that are potentially interacting with the streptavidin coated bead. If the target is loaded at too high a density, then the surface can be crowded to the point that it limits the access of the phage for potential target recognition. Optimum loading concentrations would be the result of the balance of these two opposing forces. Given that each target is comprised of a unique architecture based on its secondary structure, it reasons to think that the optimal loading density would be defined on a per target basis.

In the proof of concept experiment using bTAR RNA, target concentrations were in accordance with the “Alternate Epitope Mapping Procedure” listed as an addendum in the NEB protocol booklet. This loading of 2 pmol of target is only 2% of the binding capacitiy of the beads according to the product literature. For the B-Htelo experiment I wanted to explore alternative loading densities. The large, squat architecture of the B-Htelo g-quadruplex as compared to that of the bTAR hairpin should have a greater impact / molecule in terms of space filling attributes (higher coverage of the SA bead surface / molecule). The binding capacity of the beads is based on the size of the molecule that is being loaded. The relative height by which the molecules extend radially from the surface is also low compared to the of other DNA or RNA targets. This further limits access to the target molecule for phage recognition.

Protocols have been developed to determine the amount of target loading on SA coated beads, however these procedures are either target specific or require the use of specialized equipment. A general approach to evaluate bead binding (bead loading) that employs the use of common benchtop equipment and is universally applicable to all SA coated surfaces was developed throughout the course of these experiments. Although selection experiments never bore fruit by elucidating cyclic peptide scaffolds for targeting purposes, the troubleshooting engaged along the way led to the development of two broad reaching assays.

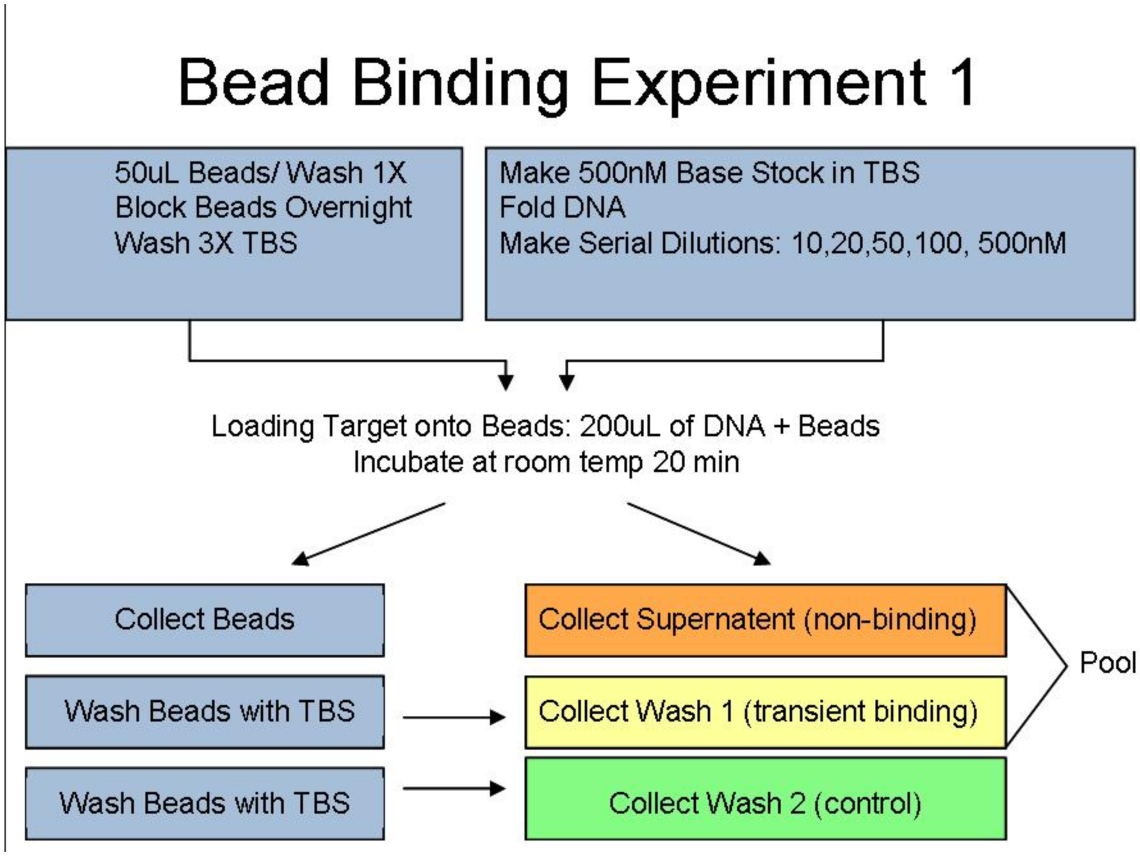

Figure 5.4. Initial Bead Binding Scheme. According to this scheme the pooled samples comprising the non-binding and transient binding biotinylated target would be visualized through gel electrophoresis

From the beginning of this endeavor, there was thought given to the potential ways to probe target loading through developing a bead binding assay. Initial thought on how to accomplish this were based on the incubation of varying concentrations of the biotinylated target with the SA coated beads under binding according to the selection protocol and subsequent separation and quantitation of the non-binding target through by native PAGE (**Scheme 5.1**). This method allows for direct calculation of the amount of target sequestered by the SA coated bead if the initial loading concentrations of target are known. This approach was later abandoned upon realization that the quantities of biotinylated target used in a selection protocol were well below the detection limits of methylene blue staining. Bead binding experiments were designed to test a range of DNA loading concentrations which started at the suggested loading of 10 nM DNA (2 pmol) to the maximum binding capacity reported by the suppliers of 500 nM DNA (100 pmol). The detection limit of methylene blue for B-Htelo target is about 100 pmol based on previous PAGE experiments (**Figure 5.1)** Given that the total loaded B-Htelo at the highest experimental concentration is equal to the detection limit and that the assay actually requires for the visualization of the nonbinding phage (which would be a small fraction of the total loaded until approaching the binding capacity), this approach is not feasible to quantitate bead loading of the biotinylated target. Even if the general approach was modified such that the binding target was eluted and quantitated directly, the total loading is still well below the detection limit except potentially at the highest experimental condition.

2.2 Selection: Experiment 1

Since we were not able to quantitate loading of the SA coated bead, the suggested loading of 2 pmol in 200 μL of TBS buffer was used for the first selection experiment. The same general selection procedure that was developed for bTAR RNA was employed for B-Htelo selection with the exception of (1) the change in buffer system (2) introduction of negative selection preceeding each positive selection for rounds 2-4. The evolved pool showed clear signs of convergence upon evaluation of the round 4 unamplified phage titers, therefore clones were picked for sequencing. A total of 12 negative clones and 84 positive clones were picked. Of the 96 total clones sequenced, 93 sequences were readable with only 2 wildtype phage present in the sequencing pool. 88 of the 91 remaining sequenced phage were determined to contain the known SA binding motif. These results indicate that we evolved a pool of SA phage binders, not B-Htelo binders.

These results clearly elucidate the importance of bead binding assays to determine loading density. There are two possible reasons for the observed evolution of SA binding phage, both of which emanate from the ability of SA binding phage present in the original library to access and recognize uncoordinated SA sites on the bead surface. Experiments had to be developed to ensure that the B-Htelo was capable of binding the SA bead and to determine the extent of coverage for a given a sample loading concentration.

2.3 Development of Bead Binding Assay

The first experiment was designed to ensure that the biotin functionality of the B-Htelo molecule was "active" and capable of binding free SA in solution. This was accomplished by incubating Htelo and B-Htelo with and without free SA in TBS buffer followed by visualization on a 15% native PAGE gel. Differentiation of unbound B-Htelo compared to Htelo – SA complex via PAGE is possible

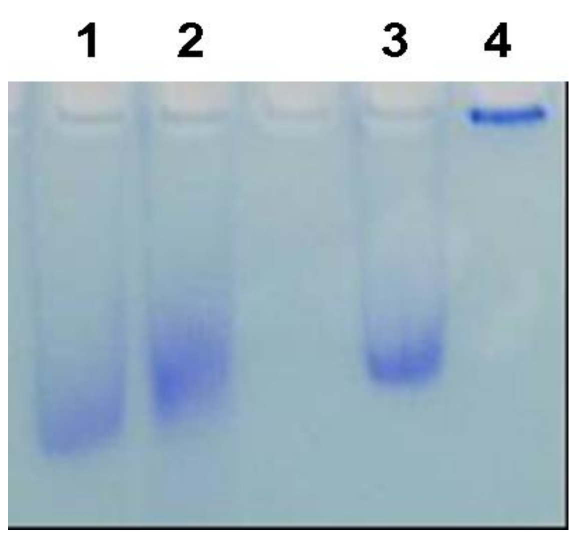

Figure 5.5. B-Htelo / free SA binding experiment. Lane 1: Htelo, Lane 2: Htelo + SA, Lane 3: B-Htelo, Lane 4: B-Htelo + SA.

due to the fact that each SA molecule contains 4 biotin coordination sites. If the B-Htelo is capable of binding the free SA, then the 1SA : 4B-Htelo complex will migrate much slower than free B-Htelo. The results clearly indicate that the B-Htelo is recognizing and binding free SA in solution (**Figure 5.5**).

Although this experiment indicates that the 5'-biotin linker is capable of binding free SA molecules in solution, it does not necessarily follow that B-Htelo can bind SA when conjugated to the magnetic bead where a higher degree of sterics is involved. The development of additional bead based binding assays was still critical to address concerns of biotinylated target loading. More information needed to be ascertained that correlated loading sample concentrations to the resulting packing density of the target on the bead surface. This information could then be used to systematically proceed with phage selection experiments by determining the loading concentrations that sufficiently coat the bead surface (masking any uncoordinated SA sights) thereby minimizing selective pressures for the evolution of SA binding phage. It was by thinking of the dilemma in terms of determining phage access to uncoordinated SA sites that I arrived at the second bead binding approach.

The total binding capacity of the SA coated beads is reported to be approximately 100 pmol of biotinylated target (based on 20 bp biotinylated oligonucleotide). After loading of the target onto the beads, all SA binding sites are either (1) bound to target or (2) free (unbound). Mathematically this is expressed as **Eq 2.** Previous attempts at studying target loading were geared towards direct quantitation of the bound or unbound sites. An alternative way to think about target loading is in terms of "blocked" and "open" sites. In this vein, following target loading, all of the SA sights are either blocked or open to phage (**Eq. 3**).

$$SA_{total} = SA_{bound} + SA_{unbound} \qquad \textbf{(2)}$$

$$SA_{total} = SA_{blocked} + SA_{open} \qquad \textbf{(3)}$$

$$SA_{blocked} = f(SA_{bound}) \qquad \textbf{(4)}$$

The number of blocked sites ($SA_{blocked}$) is a function of the number of bound sites (SA_{bound}) and the ratio of blocked vs. bound is theoretically partly determined by the architecture of the biotinylated target molecule. In other words, the larger the biotinylated target, the more SA sites it blocks upon binding (In a single site) to the bead. The relationship between $SA_{blocked}$ and SA_{bound} can be summarized by **Eq. 4**. The key for using this thought process in the development of a bead binding assay is to note that by probing the fraction of SA sites that are open to SA binding phage, it is possible to determine the number of sites that are blocked and therefore gain information as to the packing density of the target on the surface of the bead. Furthermore, the number of blocked sites is directly related to the number of bound sites and can be used to evaluate bead loading. The binding capacity, and therefore the value of f in **Eq. 4,** could be established by testing varying concentrations of target loading for a given biotinylated target.

This approach exploits the use of SA binding phage to probe target loaded beads to determine the number of SA_{open} sites. SA binding phage stock can be easily produced by completing a selection experiment against non-target coated beads. The SA binding phage stock used for these experiments was obtained from pooling the samples leftover from the first selection experiment with B-Htelo that were determined through sequencing to be SA binding phage. The target is loaded according to selection protocols following a brief wash step, SA phage stock is incubated with the target coated beads. Beads are then gently washed to remove non-bound SA phage. Attempts were made to quantitate the remaining SA binding phage directly on the bead surface by using anti-M13phage-HRP-antibody and chemiluminescence. Results indicated that the phage concentration was below the detection limits of this technique.

Four different samples
Control = Binding buffer
B-Htelo = Biotinylated Htelo sequence
Htelo = non-Biotinylate Htelo sequence
Free Biotin = free Biotin

3 Different Concentrations
10nM = Suggested loading
100nM = 10X suggested loading
500nM = estimated binding capacity

	10 e0	10 e1	10 e2	10 e3
Control (TBS)	——	——	——	416
B-Htelo 10nM	——	——	TMTC	256
B-Htelo 100nM	——	300	18	——
B-Htelo 500nM	53	8	——	——
Htelo 100nM	——	——	——	392
Htelo 500nM	——	——	——	440
free Biotin 10nM	——	——	TMTC	208
free Biotin 100nM	——	TMTC	TMTC	——
free Biotin 500nM	TMTC	TMTC	——	——

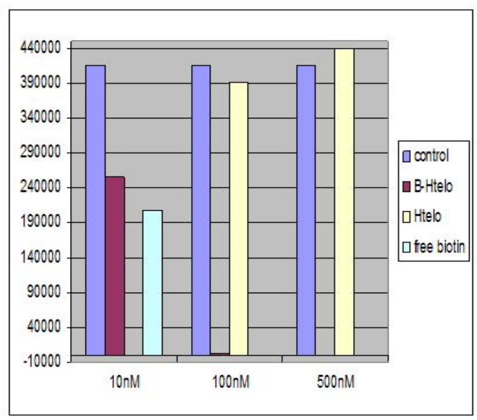

Figure 5.6 Results of the bead binding study. The chart (bottom left) shows results for the phage titer with the column headings indicating the dilution factor for the samples. The bar graph (bottom right) shows relative quantities of SA binding phage for the different samples.

The experiment was performed a second time under the same procedure except that following the removal of non-binding SA phage, the binding phage were eluted using nonspecific glycine buffer and neutralized according to selection assay protocols. Phage were then quantitated using the same titering technique that was used during the selection. This approach has the benefit of quantitating very low concentrations of phage with virtually no limit to sensitivity. The drawback is that it is labor and time intensive, requiring the overnight incubation of plates. Since sensitivity was not a concern, multiple different loading concentrations were tested. The results are shown in **Figure 5.6**.

The results indicated that this is a valid approach for exploring loading density of biotinylated targets. The control (no target) indicates that the maximum SA binding phage recognition for 50 μL of beads is approximately 4.16×10^5. These levels were analogous to those seen for non-biotinylated target incubations. This indicates that the binding event observed with the B-Htelo samples is due to a specific biotin / streptavidin interaction. It is also clear that the B-Htelo is capable of recognizing the SA on the bead surface. It is noteworthy that there is a non-linear relationship between the increase in loading and the resulting blocking of SA phage. Titers indicate that under the suggested loading conditions (2 pmol biotinylated target) only 38% of the SA binding sites are blocked. This leads to a large selective pressure for the evolution of SA binders. If the target loading is increased to 20 pmol (100 nM) then 99.3% of the SA sites are blocked. The increased ability for the G-quadruplex to block SA sites is most likely due to its large architecture. This is also evidenced by the fact that free biotin of equal concentration to biotinylated target does not block the SA binding phage as efficiently.

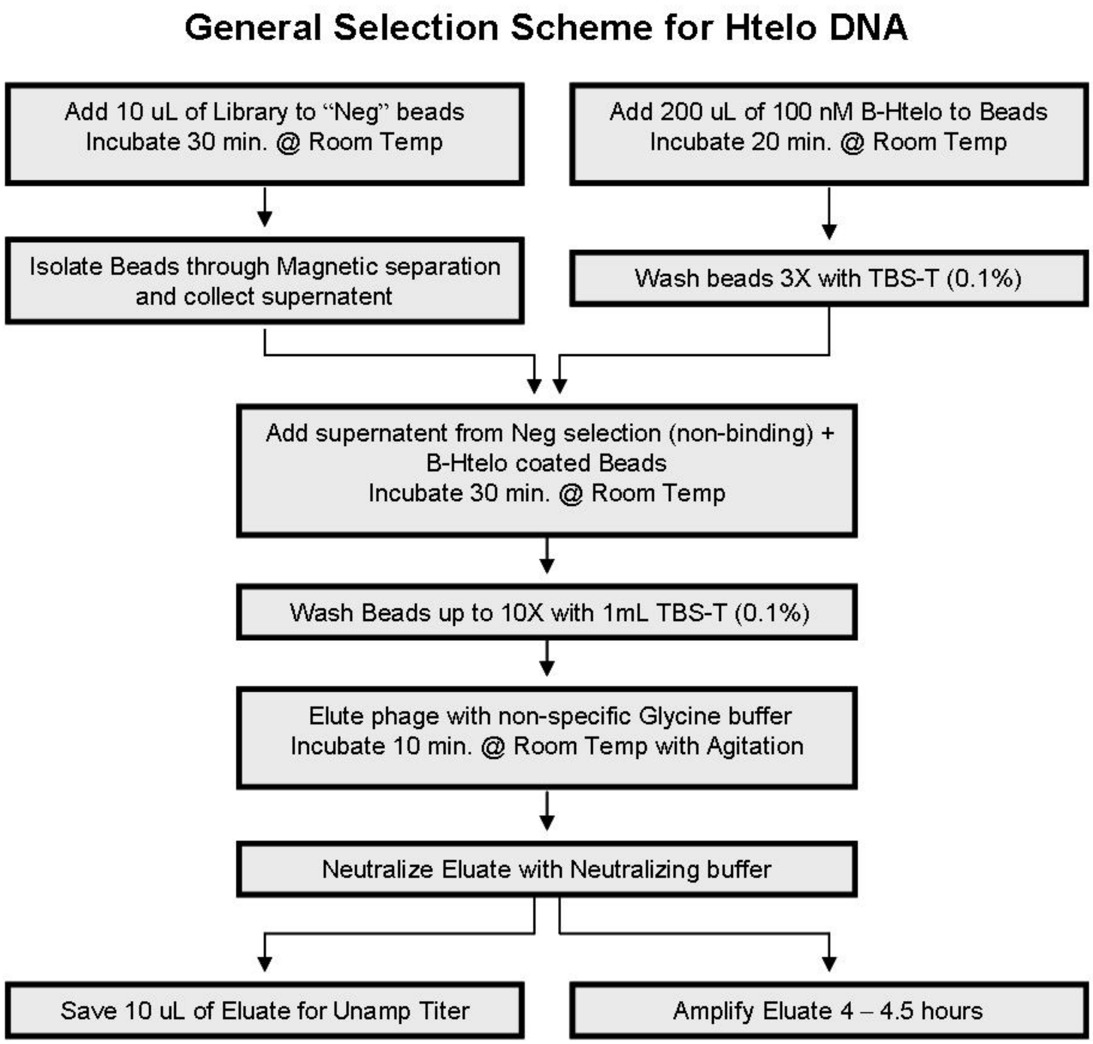

Figure 5.7 General Selection Scheme for Htelo DNA

2.4 Selection: Experiment 2

Applying the knowledge gained from the first selection experiment and the bead binding assay, we developed the selection scheme for our second attempt at targeting Htelo. Two main modifications were made to the protocol to minimize selective pressures towards the evolution of SA binding phage. The first modification was that the B-Htelo target concentration was increased to 100 nM (20 pmol in 200 μL). The second modification was to include a negative round of selection preceding the first round of positive selection. Incubation of the original library with non-coated beads should sequester any streptavidin binding phage from phage pool while the relative copy number is low (average of 10 copies). The resulting selection scheme is depicted in **Figure 5.7**.

	Unamplified	Amplified	% Recovered
Rd. 1	N/A	1.25E+11	N/A
Rd. 2	770	3.00E+11	6.16E-09
Rd. 3	1700	1.50E+12	5.67E-09

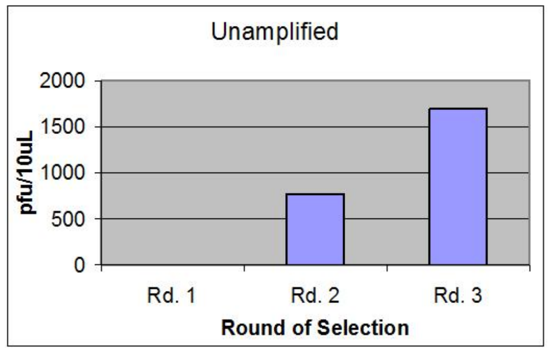

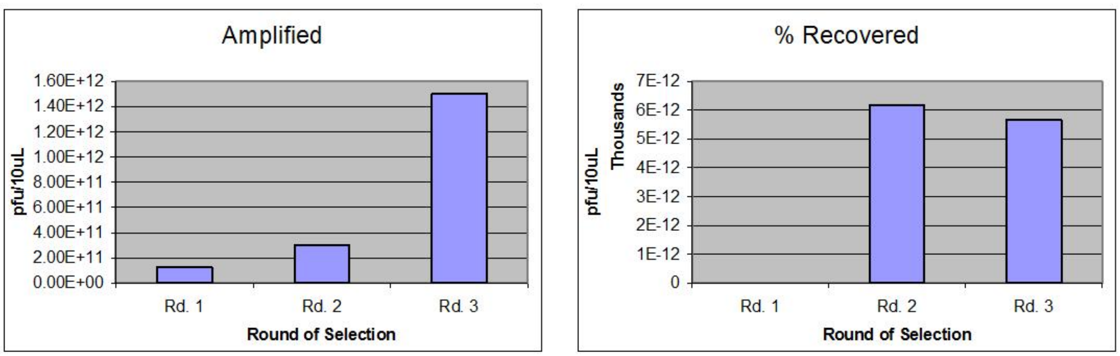

Figure 5.8. Results from phage titers for Selection Experiment 2 with B-Htelo. % Recovered is defined as the (pfu/10μL loaded) / (pfu /10μL recovered).

During the second selection experiment, there was a notable difference in the amplification rate as compared to all previous selection attempts. Following the 3rd round of selection, the amplified phage stocks were at 1.5 x 10^{12} pfu/10 μL. Faster replication time can signify wildtype contamination. Cloning of the cyclic peptide into the coat protein slightly attenuates the infectivity of the virus therefore wildtype virii have faster replication times as compared to those that are cloned to express the cyclic peptide coat protein. Evalutaion of the phage titers for rounds 1-3 are listed in **Figure 5.8.**

2.5 Development of Progress Report Assay

Concerns about wildtype contamination in the phage stock prompted the development of a second assay, the "Progress Report Assay". The concept was to develop an assay that would allow a researcher an alternative avenue to monitor the progress of the phage selection as frequently as desired instead of solely relying upon phage titer counts. The hopes were that the assay would specifically aid in the identification of wildtype contamination or SA binding phage evolution before the expense and time of preparing individual clones for sequencing. The fundamental principles on which this assay was built are the same that were used for developing the bead binding assay previously described.

From previous data, we know that we can load the target onto the beads at a density that eliminates over 99% of SA binding phage recognition of the target coated bead as compared to that of non-coated beads. A pool of phage can be evaluated for populations of SA binding phage and wildtype phage by comparing their binding capabilities for target coated beads vs. non-coated beads. The general assay protocol involves the incubation of an evolved pool with non-coated beads (free SA) and beads loaded with 100 nM target. After non-binding phage are removed using a TBS-T (0.1%) wash, binding phage are eluted with nonspecific

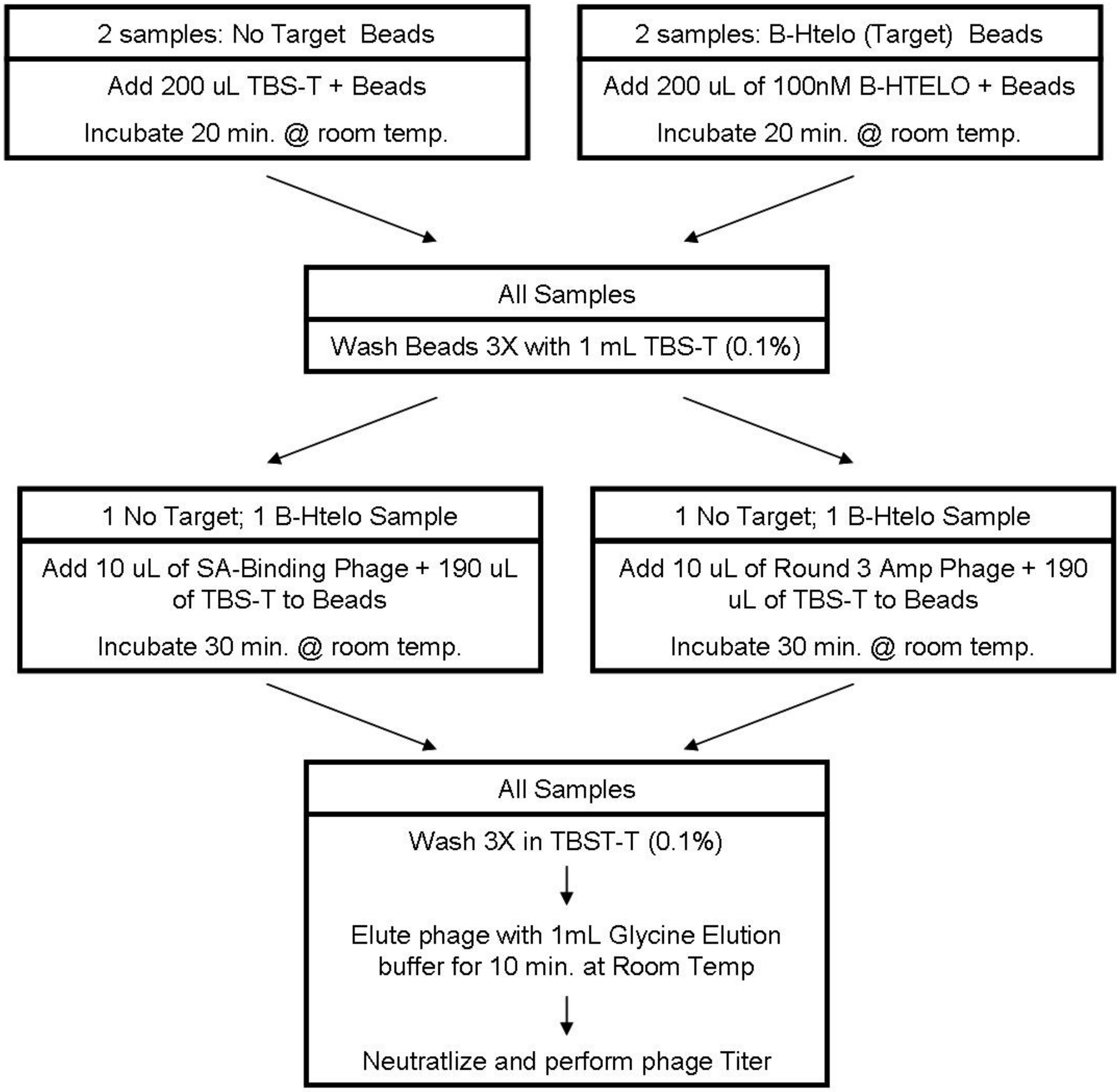

Figure 5.9. Progress Report Assay Protocol

glycine elution buffer and subsequently neutralized according to selection protocols. A phage titer is performed to determine the relative binding capabilities of the pool for both the SA beads and target loaded beads. The same process can be performed with the SA binding phage pool for control purposes. For this trial experiment, the SA binding phage and the round 3 amplified stock from the second selection were each tested for differential binding capabilities to the non coated beads and target coated beads. A total of four samples of beads were blocked and washed according to selection protocol for use in the assay (**Figure 5.9**).

Information can be easily obtained by thoughtful evaluation of the relative phage titers from the 4 samples. Control samples (SA binding phage samples) provide reference titer levels for the assay. SA binding phage incubated with beads that were not loaded with target provided the expected pfu / 10µL for a completely converged pool of binders when incubated with their target. SA binding phage incubated with the B-Htelo target coated SA beads will provide background levels of SA recognition in the pool.

If the round 3 amplified stock has been evolved to target SA and not B-Htelo, then the pfu / 10µL count for incubations of the round 3 stock with the non-coated beads will be analogous to that of the SA phage + noncoated beads. If round 3 does not contain SA binding phage, then the pfu / 10 µL count should be on the order of the background levels of SA binding phage in the pool (approx. 100X less). If there is SA contamination, but not complete convergence to SA binding phage motif, then the pfu / 10 µL will reside somewhere in between.

By comparing the relative levels of recognition of the round 3 amplified stock for SA coated beads as compared to target coated beads, it is possible to evaluate the selection pool for wildtype phage contamination. If the evolved pool has greater recognition for the non coated beads than the target coated beads, this supports that the stock is evolving to recognize SA.

If the stock has significantly greater recognition for the target coated beads than the SA coated beads along with relatively low levels of recognition of the SA beads (see above), then it is evidence that the pool has been evolved for target recognition. If the evolved pool shows no preference for either the noncoated beads or the target coated beads with reduced recognition to both as compared to the SA pool : SA bead scenario, this indicates that the evolved pool contains significant wild-type contamination. This analysis of the Progress Report Assay is summarized in **Figure 5.10**.

The results for the SA-binding phage stock are analogous to what we have seen previously with the Bead Binding Assay. The SA binding phage exhibit a 100 fold increase in the recognition of the SA coated beads (no target) compared to the target coated beads. When

<table>
<tr><th></th><th>SA-Binding Phage Stock</th><th>Round 3 Amplified Stock</th><th colspan="2">Results & Analysis</th></tr>
<tr><td rowspan="2">SA-coated Beads (No Target)</td><td rowspan="2">↑
Control:
100% SA Binding Phage</td><td>↑</td><td colspan="2">Round 3 amplified contains SA binding phage</td></tr>
<tr><td>↓</td><td>Round 3 amplified contains limited to no SA binding phage</td><td rowspan="2">Round 3 amplified has probable wild type contamination</td></tr>
<tr><td rowspan="2">Beads loaded with B-Htelo (Target)</td><td rowspan="2">↓
Control:
Background Levels of SA Binding Phage</td><td>↓</td><td>Round 3 amplified does not recognize B-Htelo (Target)</td></tr>
<tr><td>↑</td><td colspan="2">Round 3 amplified has evolved to recognize B-Htelo (Target)</td></tr>
</table>

↑Represents relatively high pfu / 10 uL counts, ↓represents relatively low pfu / 10 uL counts

Figure 5.10. Progress Report Assay Analysis

evaluating the round 3 amplified stock, there are two things to note. The first note is that the round 3 amplified stock did not exhibit as high of phage titer count when incubated with the SA-coated beads as the SA-binding phage stock. This indicates that the pool has not converged to yield SA-binding phage. The second item to note is that the round 3 amplified stock phage show little to no preference for either the SA-coated beads (no target) or the B-Htelo loaded leads. This data (**Figure 5.11**) combined with the observation of a higher rate of amplification during the last round of selection indicate that the stock is probably contaminated with wild-type phage.

	SA-Binding Phage Stock	Round 3 Amplified Stock
SA-coated Beads (No Target)	3.0×10^5	7.5×10^4
Beads loaded with B-Htelo (Target)	3.0×10^3	5.1×10^4

Figure 5.11. Results from Progress Report Assay for Rd. 3 amplified B-Htelo selection experiment 2.

During our first attempt at selection with B-Htelo, we loaded 10 nM target and the sequencing results showed that we evolved a pool of SA binders, not Htelo binders. After evaluating the loading density from the bead binding assay, it was clear that the non-coordinated SA sites were still very accessible to the phage at that loading density and that we could decrease the probability of the selection to yield SA binding phage by increasing the loading of the beads. We also started the first round with a negative selection of the starting library against the SA coated beads to try and remove those binders from the pool while their relative copy number was very low (approx. 10). The bead binding assay showed that by increasing the loading of the beads to 100 nM, we could block 99% of the SA binding phage from recognizing the free SA sites even though we are still only loading 20% of the available coordination sites according to the product literature.

The Progress Report assay completed after Round 3 of the second attempt at selection along with the Round 3 amplified phage titer indicated that the evolved phage pool had significant wildtype contamination. Wildtype M13 phage have increased rates of infectivity compared to that of engineered M13 phage. During selection, if there is little selective pressure because of lack of any strong binding interaction, the wild type phage population will take over during iterative rounds of amplification. In this attempt at selection, there are two possible causes for the wild type contamination. The first explanation would be that the Htelo target was loaded too densely and that the phage were not able to efficiently access the 3-dimensional G-quadruplex structure, therefore not allowing for a significant binding interaction. The second explanation is just simply that the cyclic peptide library does not contain the necessary architecture to effectively target the large complex structure.

To eliminate the possibility that the perceived inability to evolve an Htelo binder during the first two rounds was not due to loading issues (under loading or over loading), a third attempt at the selection process was made doing side by side selections of 2 intermediate loading concentrations. Previous results have shown that 10 nM binding concentrations yield SA binders indicating that the target loading is too low and that 100 nM binding concentrations yield wild type phage contamination indicating that it is possible that the loading is too high. For the final attempt at selection I investigated loading concentrations of 20 nM and 50 nM.

By using the bead binding assay, I was able to assess how these loading concentrations would effect the 3-dimensional landscape of the bead surface (**Figure 5.12**).

B-Htelo loading experiment #2 - 2/26

Coating	Phage	pfu/10uL	Ratio	% open	% loaded
TBS	SA	2.30E+05			
10nM B-htelo	SA	2.10E+05	9.13E-01	91.304	8.696
20nM B-htelo	SA	9.80E+04	4.26E-01	42.609	57.391
50nM B-htelo	SA	1.13E+04	4.91E-02	4.913	95.087
100nM B-htelo	SA	4.70E+02	2.04E-03	0.204	99.796

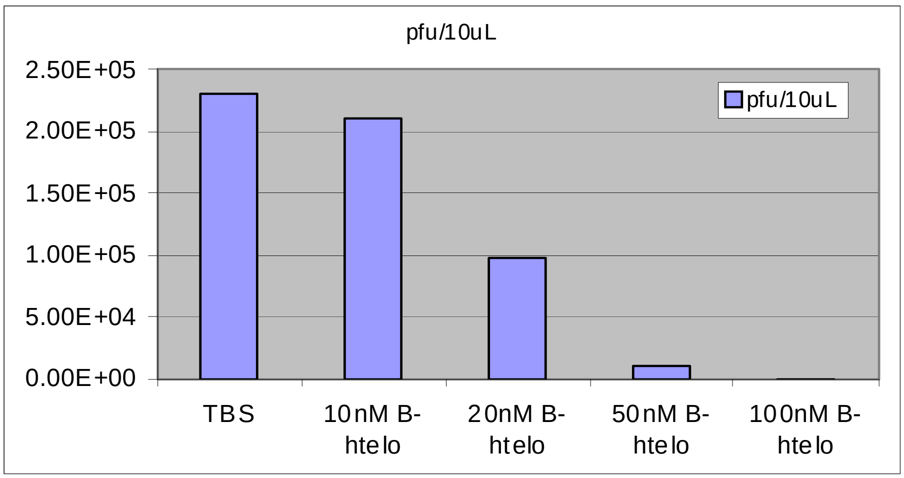

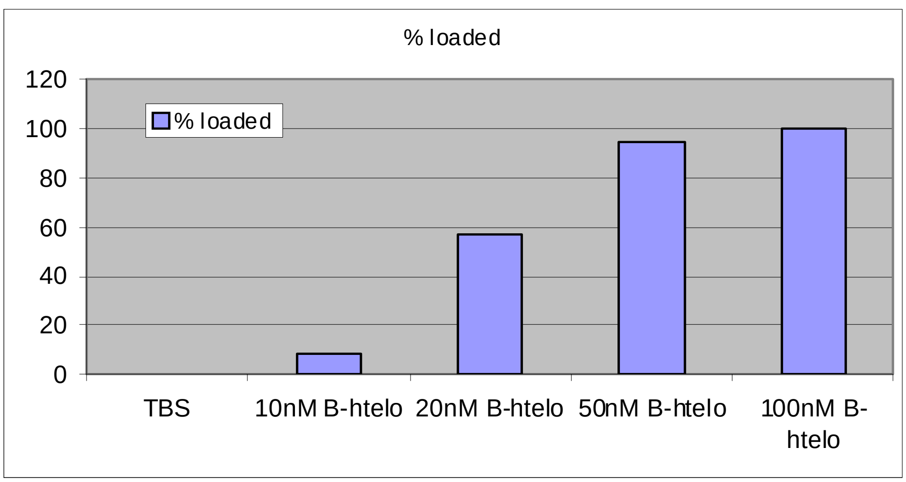

Figure 5.12. Results of bead binding assay testing 0, 10, 20,50,and 100 nM B-Htelo concentrations.

According to the product literature 50 μL of the supplied magnetic beads solution should have a binding capacity of greater than 200 nmol of free biotin or 100 nmol of single stranded biotinylated oligonucleotide. Due to the relatively large size of the G-quadruplex structure, the data indicates that it effectively blocks phage recognition of free SA sites on the bead surface more effectively than reported for the single stranded biotinylated oligonucleotide. For example, at 10 nM loading, this means 2 pmol of B-Htelo are incubated with the bead in 200 uL of solution. This would lead to a theoretical loading of 2% (based on binding capacity of beads for single-stranded oligonucleotides), although the Binding Assay indicated that this degree of loading resulted in the blocking of around 8.7% of the SA sites. As the loading was increased, the discrepancy between the theoretical loading and the resulting blockage of SA sites increased even greater. Overall, the data indicate that the binding capacity for the beads for our target, B-Htelo, is about 4-5X less than that of single stranded oligonucleotides. It is interesting to note that the G-quadruplex structure is comprised of a tetrad, with a diameter roughly 4X that of linear single-stranded DNA.

Three rounds of selection were completed in the third and final selection experiment to evolve cyclic peptide scaffolds for targeting G-quadruplex Htelo DNA. There was an indication in round 2 that there was a potential wildtype contamination as evidenced by the fact that the titer was 1000X higher than normal. A Progress Report Assay was completed to evaluate how the selection was proceeding. Results did not indicate that the evolved pool had any signs of preferential binding to the target coated beads over the non-coated beads. Given the inability to evolve cyclic peptide scaffolds over a range of target loading concentrations, it was concluded that under the selection conditions, there was not enough selective pressure provided by binding interactions between the cysteine constrained heptapeptide phage library and Htelo G-quadruplex for the evolution of binding scaffolds. No further studies have been completed for targeting B-Htelo.

III. Summary and Conclusions

Broadly speaking, the Bead Binding Assay that has been developed here is a technique that can be used with any streptavidin / biotin based system for the evaluation of biotinylated target loading and packing density. For the phage display application developed here, it can provide critical insight into the three dimensional landscape of the bead after the targets are loaded. This information can then be used to ensure the proper amount of packing density to minimize evolution of SA binders while still ensuring accessibility of the target to the phage library during the selection. The Progress Report Assay allows for relatively easy monitoring of the selection process at any point in the experiment and provides a method for quick screening of an evolved pool for the presence of SA binding phage and or wildtype phage before the investment in sequencing.

The summation of all the experimental data seemed to imply that the cysteine constrained heptapeptide scaffold did not contain the necessary architecture to efficiently bind the relatively large and complex G-quadruplex structure. Given the limited opportunities for hydrogen bonding interactions due to the cyclic Hoogsteen hydrogen bonding arrangement, groove based interactions would be limited for stabilizing the cyclic peptide interactions.

Htelo G-quadruplex DNA provides an extreme example of nucleic acid secondary structure and perhaps brings to attention the limitations of this approach.

CHAPTER 6: EXPERIMENTALS

I. Chapter 2 Experimental

Materials

The biotinylated bTAR RNA, non-biotinylated bTAR RNA, and biotinylated negative randomer used for the selections and biophysical characterizations were purchased from Dharmacon. The Ph.D.-C7C™ Phage Display Peptide Library Kit was obtained from New England Biolabs (NEB). Streptavidin coated magnetic beads were also purchased from NEB. The Tat peptide used during selections for Tat specific elution was obtained from Sigma Genosys. RNase Zap® Wipes were purchased from Ambion. All other reagents were purchased from Fisher Scientific.

Instrumentation

UV-Vis quantitation of peptides and RNA was performed using a Genesys 10uV Scanning UV-VIS from Thermo Electron Corporation. Polyacrylamide gels were run using the Mini-Protean III Cell and Mini-Transblot Electrophoretic System from BioRad. Agarose gels were run using the Sub-Cell GT Agarose Gel Electrophoresis System.

Mitigation of RNAse Contamination

All buffers or tubes that were used during the selection portion of the assay were either purchased as nuclease free and / or baked at 450 ºF overnight to ensure they were RNAse free. Also all benchtop surfaces were cleaned every day with RNase Zap® wipes prior to starting experiments. All reagants were purchased at highest purity and, where possible, nuclease free. Proper care and techniques were used when using these reagants to ensure they remained RNAse free.

Buffers and Solutions

All buffers used during the selection were made according to the Ph.D.-C7C™ Phage Display Peptide Library Kit protocol with the exception of a Tris-HCl buffer system containing 50 mM Tris-HCl, pH 7.5 with 20 mM KCl (TK buffer) in lieu of TBS during the binding and wash phases. The TK buffer was made fresh for each round of selection to limit the chance for RNase contamination.

Culturing ER2738 Cells for Amplification / Titers

ER2738 cells were provided with the Ph.D.-C7C™ Phage Display Peptide Library Kit. Cell stocks were stored according to specifications at -80 ºC. Cells were cultured according to kit protocols: grown on LB/ Agar + tetracyclin plates overnight at 37 ºC and stored at 4 ºC wrapped in parafilm for up to 1 month. Plates were restreaked at least once a month for the duration of the project.

Characterization of bTAR RNA Stock by Gel Electrophoresis

Samples were run on a 10% denaturing TBE PAGE gel with 7 M urea (100 mL: 25 mL of 40% Acrylamide, 10 mL of 10X TBE, 42 g urea, filter sterilize and stored at room temp).

The gel was cast and pre-heated for 20 minutes before loading the samples. Samples were prepared in TBE buffer at 1 nmol of RNA / lane. All samples were heated for 5 minutes at 95 ºC prior to loading the gel.

Characterization of bTAR RNA Stock by Circular Dichroism Spectroscopy

The first attempt to determine bTAR RNA hairpin structure using cirucular dichroism spectroscopy was completed in TK-T buffer (0.1% Tween) with RNAsecure. This attempt was unsuccessful due to the presence of the detergent Tween 20 and, to a larger extent, the RNAsecure. The second attempt was performed with 20 μM bTAR RNA in TK buffer without tween or RNAsecure. Samples were tested at 4, 23, and 90 ºC. Background spectra of the TK buffer were also taken at all three temperatures.

Data was collected using the Applied Photophysics Pistar 180 Spectrapolarimeter and analyzed with the associated Pistar software package. The parameters were set to report the data in millidegrees for the spectrum of 200 - 300 nm collecting data at 1 nm intervals with a sampling time of 0.8 sec. / point. Each sample was allowed to equilibrate to the set temperature for 5 minutes and then scanned 10 times. The scans were averaged and smoothed over 5 points to give the final spectra. Spectra were completed for all four experimental samples and for their relative buffers (**Appendix A.1**).

Positive Selection Scheme

This optimized protocol was based on the protocol provided with the Ph.D.-C7C™ Phage Display Peptide Library Kit from New England Biolabs (NEB) with a few modifications. A solution-binding scenario was also implemented for all rounds of selection. Two picomoles of the biotinylated bTAR RNA were placed in 200 µL of TK buffer (total RNA concentration of 10 nM), heated to 95 ºC for 1 minute and then cooled to room temperature (to ensure proper RNA folding), and subsequently incubated with 10 µL of phage solution containing 2.0×10^{11} plaque forming units (pfu's) for 20 minutes at room temperature. 50 µL of a streptavidin magnetic bead solution (binding capacity: approx. 2000 picomoles / mL, purchased from NEB) was pre-blocked with bovine serum albumin (BSA) to prevent non-specific binding then added to the RNA/phage solution. The bead/RNA/phage complexes were magnetically pooled to the bottom of the tube and the supernatant was discarded. The beads were washed 10 times with TK buffer, and the binding phage were non-specifically eluted with a 0.2 M glycine-HCl solution (pH = 2.2), containing 1 mg/mL BSA. The phage eluent was neutralized and subsequently amplified in bacterial cell culture

Negative Selection Scheme

The enriched library, resulting from the amplified pool from the previous selection round, was incubated with two picomoles of the 5'-biotinylated negative control RNA (5'–(Biotin) GCAAUGUUGACGACAGUUAGAUUACAGA–3') under the exact same conditions used during positive rounds. Streptavidin coated magnetic beads were used to capture negative control RNA along with any bound phage. Non-binding phage were then isolated in the supernatant and utilized directly for the subsequent round of positive selection (without amplification).

Final Elution

In the fourth and final round of selection, the round 3 amplified phage pool was carried forward in two parallel positive selection experiments that were performed varying only the elution conditions. In the first experiment, non-specific conditions (0.2 M glycine-HCl solution, pH = 2.2) were employed. In our second experiment, binding phage were eluted with 1 mL of 100 μM bTat peptide (H-GPRPRGTRGKGRRIRR-OH). Phage were then isolated and sequenced with the help of the Genome Research Laboratories of North Carolina State University.

Sequencing

Sequencing was performed by PCR, amplifying the library insert region of the host DNA using a single, complementary downstream primer provided by NEB (96 gIII sequencing primer) in coordination with the Big Dye ™ sequencing kit from Promega. The resulting fluorescently labeled complementary transcript was then read, using automated machinery, with the help of the Genome Research Laboratories (GRL) at North Carolina State University. Sequences were analyzed using BioEdit™ software to obtain the library insert sequence and then translated to obtain the cyclic peptide motif responsible for the binding interaction.

II. Chapter 3 Experimental

Materials

Cysteine constrained peptides used for all biophysical characterization were purchased from Biopeptide and non-biotinylated bTAR RNA was purchased from Dharmacon. The 17-mer Tat peptide used for EMSA was obtained from Sigma Genosys. Full length Tat protein was expressed from a plasmid obtained from a collaborator, Hal Bogerd, at Duke University. All other materials were obtained from Fisher Scientific.

Instrumentation

UV-Visible spectroscopy quantitation of all peptides and RNA was performed on a Nanodrop ND-1000. Polyacrylamide gels were run using the Mini-Protean III Cell and Mini-Transblot Electrophoretic System from BioRad. Agarose gels were run using the Sub-Cell GT Agarose Gel Electrophoresis System. Fluorescence quenching experiments were completed using a C-61 Spectrofluorometer from Photon Technology International (PTI) combined with the Felix Software package. Kaleidagraph was used to fit fluorescence quenching data to Equation 1 to obtain K_d values.[1]

Expression of GST::bTat Protein

The plasmid was obtained from Hal Bogerd (Duke University) and the GST::bTat protein was expressed according to published protocol.[N1] The plasmid was transformed into BL21

Gold (DE3) protease minus cells purchased from Stratagene according to the Stratagene protocol. 5 colonies were picked and restreaked on separate plates to assess for levels of protein production. Cell stocks of each of the 5 clones were prepared in LB-Amp and expression was induced using 1 mM IPTG. Each clone was assessed for its relative level of GST::bTAT expression by Western blot analysis using an anti-GST-HRP conjugated antibody. The clone displaying the highest level of GST expression was then taken forward for large scale production and subsequent purification of the GST::bTAT antibody using a B-PER GST spin purification kit. Bradford assay was used to quantitate the protein stock and ELISA was performed to assess purity.

EMSA with GST::Tat Protein

0.2 pmol of labeled bTAR RNA was incubated with varying concentrations of protein in 15 μL binding reactions (TK buffer) at 4 ºC for 30 minutes. Samples were then loaded on a 10% native PAGE gel. GST::bTAT protein was tested at 0, 0.02, 0.1, 0.2, 0.4, 1, 2, 4, and 10 pmol.

EMSA with Tat Peptide

0.1 nM labeled bTAR was incubated with bTat peptide with increasing concentrations at 4 ºC for 30 minutes. Binding interactions were visualized by 13.3% native PAGE, 0.5X TBE. bTAT peptide concentrations were tested at 0, 0.0025, 0.025, 0.25, 2.5, 25, and 250 nM.

TM

Completed by Darnell Graham, NCSU Biochemistry Department

Experiments were performed with low micromolar concentrations of bTAR RNA and a 1:15 ratio of bTAR RNA to cyclic peptide in TK buffer. UV absorbance at 260 nm was measured as a function of temperature as samples were heated from 4 – 95 ºC. A total of 6 cycles were completed and averaged for each test sample and the data is shown in **Appendix A.2**.

ITC

Completed by Darnell Graham, NCSU Biochemistry Department

Experiments were performed by monitoring the temperature of 1.4 mL of 40 μM bTAR RNA as the cyclic peptide was titrated in over a series of 5 μL injections of 400 μM cyclic peptide stock. A total of 40 injections were performed which allowed for a peptide concentration range from 0 – 1.25X bTAR concentration.

Fluorescence Quenching - bTAR

The intrinsic fluorescence emission of the tryptophan residue was used to determine the K_d's of cyclic peptides **P1** and **P2** for non-biotinylated bTAR RNA. Experiments were performed using a Hellma quartz cuvette (1.0cm x 0.4cm, oriented with the 0.4 cm along the emission pathlength) with an initial volume of 700 μL of TK buffer. All readings were taken in triplicate as samples were scanned from 330 – 360 nm. Peptide was then added and measurements of max emission was taken and subsequently monitored during titration of bTAR RNA into the cuvette. Dilution curves and photobleaching curves were used to correct

The data set for the dilution of peptide during titrations of bTAR RNA and repeated exposure of sample to light. **Appendices A.4 – A.5** give specific information including peptide and RNA concentration, injection volume, and the resulting quenching curves for **P1** and **P2.**

$$F_{\mathrm{ratio}} = 1 - \Phi \left[\frac{(K_{\mathrm{d}} + nP_0 + L_{\mathrm{T}}) - \sqrt{(K_{\mathrm{d}} + nP_0 + L_{\mathrm{T}})^2 - (4nP_0 \cdot L_{\mathrm{T}})}}{2nP_0} \right] \qquad \textbf{(1)}$$

The change in emission intensity at 350 nm was monitored. The corrected values for the observed fluorescence emission ratio (F_{obs}/F_0, $F_0 = Em_{max}$) was then plotted as a function of RNA concentration and fit to Equation **1**[1] where F_{ratio} is the observed fluorescent ratio, Φ is the fluorescent ratio change amplitude (= $1 - F^{\infty}_{\mathrm{ratio}}$), P_0 is the protein concentration, K_d is the dissociation constant, n is the stoichiometry, and L_T is the total ligand concentration (**Appendix A.3)**. The fluorescence quenching data of **P1** and **P2** fit to Equation **1** are depicted in Figures 3and 4, respectively.

Fluorescence Quenching: Negative Control RNA

Fluorescence quenching experiments with N1-RNA and N2-RNA were performed under the same experimental conditons as the bTAR experiment (see above).

III. Chapter 4 Experimental

Materials

All peptides were synthesized and characterized by Anne Basso. RNA oligonucleotides N1 and bTAR were purchased from Dharmacon. All other reagants were purchased from Fisher Scientific**.**

Instrumentation

UV-Vis quantitation of all peptides and RNA was performed on a Nanodrop ND-1000. Fluorescence quenching experiments were completed using a C-61 Spectrofluorometer from Photon Technology International (PTI) combined with the Felix Software package. Kaleidagraph was used to fit fluorescence quenching data to Equation 1 to obtain K_d values.[1] Circular dichroism experiments were performed on the Applied Photophysics Pistar 180 Spectrapolarimeter equipped with a Series 800 temperature controller from Alpha Omega Intstruments. Data was analyzed via the Pistar software package.

Preparation of Peptide Stocks

Lyophilized peptide constructs were re-suspended in a small volume of nuclease free H_2O and the concentration was quantitated for each using UV-Visible absorbance at 280 nm based on a calculated extinction coefficient of 5690 M^{-1} cm^{-1} (from tryptophan residue). Stocks were subsequently diluted with nuclease free H_2O to yield 1 mM stocks for storage and actual storage stock concentrations were determined. Quantitation was performed using a

Nanodrop ND-1000 and measurements were based on the average of three separate 2 μL aliquots of the storage stock.

Table 6.1. Quantitation of Analogues

	P2 C-C Flag	P2 C=C Flag	P1 C=C Flag
Abs: 280nM	3.78 3.79 3.772	4.984 5.101 5.057	5.222 5.188 5.158
Average Absorbance	3.781	5.047	5.189
Pathlength	1	1	1
Extinction Coefficient	5690	5690	5690
Concentration (μM)	664	887	912

Fluorescence quenching experiments were completed with peptide concentrations at approximately 1 nM in 700 – 800 uL of TK buffer (50 mM Tris-HCl pH 7.5; 20 mM KCl). Since the storage stock concentration was on the order of 10^6 times more concentrated than the final experimental [peptide], working stocks were made by direct serial dilutions of the storage stock with 1X TK buffer.

1X TK buffer was prepared in 50 mL conical tubes by combining 2.5 mL of 1M nuclease free Tris-HCl pH 7.4, 500 μL of 2 M nuclease free KCl, and 47 mL of nuclease free H_2O. Solutions were mixed thoroughly by vortexing.

Storage stocks were diluted with 1X TK buffer to make working stocks to use for fluorescence quenching experiments. Attention was given to making sure that all stocks were to be prepared using 1 single 20 μL pipette. Storage stocks were diluted based on their relative concentrations (determined from prior UV-Visible absorption data) in order to yield 500 μL of 20 μM working stocks.

Table 6.2. Preparation of Analogue stocks

	Vol. of Stock (μL)	Vol.TK buffer (μL)	Final Vol. (μL)	[Final] (μM)
P2 C-C Flag	15.06	484.94	500	20
P2 C=C Flag	11.27	488.73	500	20
P1 C=C Flag	10.96	489.04	500	20

Preparation of RNA Stocks

Both the N1 RNA and bTAR RNA stocks were ordered from Dharmacon. Samples were delivered lyophilized with the total amount of product split evenly between two tubes. 324.4 nmol of N1 RNA was delivered with approx. 162.2 nmol / tube and a calculated molecular weight of 9050.5 g/mol. There was a total of 307.2 nmol of bTAR RNA with approx. 153.6 nmol / tube and a calculated molecular weight of 8867.3 g/mol.

All working stocks were made from the lyophilized samples via a serial dilution scheme that yielded the desired volume and working concentrations for the fluorescence quenching experiments. Lyophilized samples were re-suspended in 1X TK buffer to give final RNA concentrations of 800 μM. Subsequent dilutions were performed using 1X TK buffer to yield working stocks of concentrations 800, 400, 200, 100, 50, and 25 μM. Final working stock concentrations were quantitated using the UV-Visible absorbance at 260 nm.

Fluorescence Quenching Experimental Scheme

Fluorescence quenching experiments with **$P1_1$**, **$P2_1$** and **$P2_2$** were performed comparable to the quenching studies with cysteine constrained **P1** and **P2**. The same experimental parameters (equipment and analytical) were used to test binding of **$P2_1$** and **$P2_2$** with both bTAR and N1-RNA aptamers.

Competitive Fluorescence Quenching

All test cyclic peptide analogue stocks were prepared at 20 μM in TK buffer. bTat peptide stock concentration was prepared at 120 μM in TK buffer, and bTAR stock concentrations were calculated to be 16.4 μM in TK buffer. Fluorescence spectra were collected with the same parameters previously used for fluorescence quenching experiments. 670 μL of TK buffer was added to the cuvette and the background spectra were taken. 30 μL of 20 μM stock was then added to the TK buffer and a second spectrum was taken. Quenching was measured by then adding 20 μL of the bTAR RNA stock. In the final step, 5 μL of the 120 μM bTat peptide was added to the cuvette and spectra were collected. The resulting data is shown in **Appendices A.6 – A.8**

Circular Dichroism

All CD spectra were collected at 20 and 80 μM bTAR (where applicable) in TK buffer. 2X stocks were prepared for each test peptide and bTAR RNA. Samples were prepared prior to scanning by mixing equal volumes of bTAR stock and peptide stock resulting in 1X concentration for each. For unbound bTAR scans: background spectra were collected using

TK buffer, and free bTAR spectra were collected by diluting bTAR 2X stock 1:1 with TK buffer. For bTAR + peptide scans, background spectra of peptide only in TK buffer were prepare by diluting peptide 2X stock 1:1 with TK buffer.

Data were collected using the Applied Photophysics Pistar 180 Spectrapolarimeter and analyzed with the associated Pistar software package. The parameters were set to report the data in millidegrees for the spectrum of 200 - 300 nm collecting data at 1 nm intervals with a sampling time of 0.8 sec. / point. Each sample was allowed to equilibrate to the set temperature for 10 minutes and then scanned 10 times. The scans were averaged and smoothed over 5 points to give the final spectra (**Appendix 1.9)**.

IV. Chapter 5 Experimental

Materials

Biotinlylated and non-biotinylated Htelo DNA were purchased from Sigma Genosys.

The Ph.D.-C7C™ Phage Display Peptide Library Kit was obtained from New England Biolabs (NEB). Streptavidin coated magnetic beads were also purchased from NEB. All other reagants were obtained from Fisher Scientific.

Instrumentation

Polyacrylamide gels were run using the Mini-Protean III Cell and Mini-Transblot Electrophoritic System from BioRad. Agarose gels were run using the Sub-Cell GT Agarose Gel Electrophoresis System. UV-Visible spectroscopy quantitation of DNA was performed with a Nanodrop ND-1000. Circular dichroism experiments were performed on the Applied Photophysics Pistar 180 Spectrapolarimeter equipped with a Series 800 temperature controller from Alpha Omega Intstruments. Data was analyzed via the Pistar software package.

Preparation of Biotinylated Htelo DNA

Biotinylated Htelo DNA (5' – 7GGTTAGGGTTAGGGTTAGGGTTAGGGTTAG – 3') was shipped lyophilized and the tube was quantitated by Sigma Genosys to contain 13.1 nmol / tube with a molecular weight of 9889 g/mol. The sample tube was briefly spun for 2 minutes At 15,000 rpm in a tabletop centrifuge and then 262 μL of nuclease free H_2O was added to the tube and the sample was resuspended through an iterative process of vortexing and centrifugation to yield a final target concentration of 50 μM. A 100X working stock of 1 μM Htelo in nuclease free water was made via serial dilutions and then aliquoted for storage at -20 ºC.

Preparation of non-biotinylated Htelo DNA

157 nmol of lyophilized Htelo DNA was received from the supplier. The tube was briefly spun for 2 minutes at 15,000 rpm in a tabletop centrifuge and then 157.0 μL of H_2O was

added and the sample was resuspended through an iterative process of vortexing and centrifugation to yield a final target concentration of 1 mM Htelo in nuclease free H_2O. All working stocks were obtained through serial dilutions of the 1 mM Htelo stock using nuclease free H_2O.

Testing ppurity of Bbiotinylated and Non-Biotinylated Htelo by Gel Electrophoresis

Biotinylated and non-biotinylated Htelo 50 μM stocks were analyzed by native polyacrylamide gel electrophoresis to evaluate the purity of the sample, the presence of the biotin group and linker, and to determine detection limits.

Table 6.3. Samples Preparation for B-Htelo and Htelo Test Gel.

Lane	DNA	[DNA] Stock (μM)	Vol. DNA (μL)	Vol. water (μL)	Vol. loading dye (μL)	Total Vol. (μL)	DNA pmol
1	BLANK						
2	biotinylated Htelo	50	5	10	3	18	250
3	biotinylated Htelo	50	10	5	3	18	500
4	biotinylated Htelo	50	15	0	3	18	750
5	BLANK						
6	non-biotinylated Htelo	50	5	10	3	18	250
7	non-biotinylated Htelo	50	10	5	3	18	500
8	non-biotinylated Htelo	50	15	0	3	18	750
9	BLANK						
10	BLANK						

To test the purity of the DNA stocks, samples were prepared according to **Table 6.3** with the addition of 6X loading dye (30% glycerol, 0.3% bromophenol blue, 0.3% xylene cyanol in nuclease free H_2O) and then loaded onto a 15% native polyacrylamide mini gel. The gel was cast and run on the BioRad apparatus (Mini-Protean III cell) according to manufacturer's protocols. DNA was visualized using methylene blue staining (0.002% w/v in ddH_20).

Testing for Formation of G-Quadruplex Structure via Circular Dichroism

All Htelo solutions used for CD analysis of Htelo folding were prepared from a 1 mM non-biotinylated Htelo storage stock which was diluted 1:100 in the buffer of choice to yield 10 μM working solutions. Two different buffers were analyzed using CD, the first is the TBS buffer that was used during selections, the second was a "no salt" buffer containing 50 mM Tris-HCl (pH 7.5) in H_2O. All samples were heated and cooled according to standard folding protocols to allow formation of G-quadruplex structure if possible. Both buffer conditions were tested for G-quadruplex formation at 22 - 90 ºC. A background spectrum was also taken for both the TBS and no salt buffer at both experimental temperatures.

Data were collected using the Applied Photophysics Pistar 180 Spectrapolarimeter and analyzed with the associated Pistar software package. The parameters were set to report the data in millidgrees for the spectrum of 200 - 320 nm collecting data at 1 nm intervals with a sampling time of 1.00 sec. per point. Each sample was allowed to equilibrate to the set temperature for 10 minutes and then scanned 5 times. The scans were averaged and smoothed over 5 points to give the final spectra. Spectra were completed for all four experimental samples and for their relative buffers (**Appendices A.1 – A.13)**.

Testing Recognition of Free Streptavidin by Biotinylated Htelo Oligonucleotide

To test the ability of the biotinylated Htelo to recognize and bind streptavidin *in vitro* under the selection conditions, a second gel experiment was designed with the idea that complexed biotinylated Htelo + free streptavidin would elicit a visible shift as compared to noncomplexed biotinylated Htelo. Experimental conditions were set to mimic the selection protocol using the same TBS-T buffer (50 mM Tris-HCl pH 7.5, 100 mM KCl, 0.1 % Tween and analogous binding time and temperature (20 min. at room temp). The free streptavidin used was obtained from the Ph.D.-C7C™ Phage Display Peptide Library Kit, and the lyophilized stock was resuspended in TBS-T buffer to make a 100 μM stock. Four DNA samples were prepared for the experiment as summarized in (**TABLE 6.4**), two samples of non-biotinylated Htelo for negative control purposes and two samples of biotinylated Htelo. All samples were folded to ensure G-quadruplex formation by heating to 95 ºC for 2 minutes and the cooling to 4 ºC at an average rate of 2 ºC / minute. One of the samples from the biotinylated and non-biotinylated Htelo DNA was then incubated with 2.5 μL of the 100 μM streptavidin while the other two samples were incubated with TBS-T. Following the incubations 3 μL of 6X loading dye was added to each of the 4 tubes and samples were loaded and run on a 15% native PAGE minigel using the Mini-Protean III Cell from BioRad and according to equipment protocols.

Table 6.4. Sample preparation for free SA binding gel.

Lane	DNA	[DNA] (μM)	Vol. DNA (μL)	Vol.TBS-T (μL)	Vol. of 100 uM Streptavidin	Vol. loading dye (μL)	Total Vol. (μL)	pmol of DNA
1	biotinylated Htelo	50	2.5	12.5	0	3	18	125
2	biotinylated Htelo	50	2.5	10	2.5	3	18	125
3	BLANK							
4	non-biotinylated Htelo	50	2.5	12.5	0	3	18	125
5	non-biotinylated Htelo	50	2.5	10	2.5	3	18	125

Bead Binding Assay

SA binding phage were obtained from samples we collected and sequenced from our first selection attempt. By comparing the sequencing data directly to the samples that were saved from each clone submitted for sequencing for ELISA, it was possible to combine all clones with the known SA binding consensus sequence of CGSWSHPQC.

A viability test of the SA binding phage stock was completed by performing phage titers on IPTG / X-Gal Plates of 10^0, 10^2, 10^4, 10^6, 10^8, 10^{10} dilutions of the pooled stock. Plates were inverted and incubated overnight at 37 ºC. The next day, plaque forming units were counted and stock the concentration was estimated by accounting for dilution. Amplification of the pooled stock was completed by standard assay protocols.

The bead binding assay conditions for loading targets were designed to mimic those conditions used for target loading during the selection. 50 uL of beads were aliquoted from the stock solution and added to 1 mL of TBS-T (0.1%). Beads were then washed with an additional 1 mL of TBS-T (0.1%) and subsequently blocked for at least 1 hour at 4 ºC in 1 mL of blocking buffer. Following the blocking step, the beads were washed 2X in 1 mL TBS-T (0.1%) to remove any residual blocking buffer before incubation with the samples.

All samples were prepared and folded, regardless of their content, according to the selection folding protocols for rigidity in the handling of the samples. In this experiment, 9 different samples were tested: no target, 10 nM B-Htelo, 100 nM B-Htelo, 500 nM B-Htelo, 100 nM

Htelo, 500 nM Htelo, 10 nM free biotin, 100 nM free biotin, and 500 nM free biotin. Each sample was prepared to a final volume of 200 μL TBS-T (0.1%).

Samples were added to the blocked and washed beads and incubated for 20 minutes at room temperature. Following the incubation, the non-binding target was removed by gently washing the beads 2X in 1 mL of TBS-T (0.1%). Target coated beads were then incubated with 10 μL of the SA binding phage stock + 190 μL of TBS-T (0.1%) for 30 minutes at room temperature. Non-binding phage were removed by gently washing the beads 5X in TBS-T (0.1%). Phage were eluted using a non-specific glycine elution buffer and then the resulting solution was neutralized under the same assay conditions as the selection. By trial and error, the correct dilution ranges were determined in order to obtain approximately 100 pfu / plate.

Progress Report Assay

This assay evaluates the ability of a pool of phage to bind its target molecule as compared to its binding with streptavidin. All samples and beads were prepared according to standard selection protocols. The evolved pool to be tested was incubated with both non-coated beads (free SA) and beads loaded with 100 nM target. Non-binding phage are removed using TBS-T (0.1%). Binding phage are eluted with a non-specific glycine elution buffer and neutralized according to standard protocols. Phage titers are performed to determine the relative binding capabilities of the pool for both the SA beads and target loaded beads. **Figure 6.1** gives an overview of the assay in flowchart form. The same assay was completed using the SA binding phage stock as the test phage for control purposes.

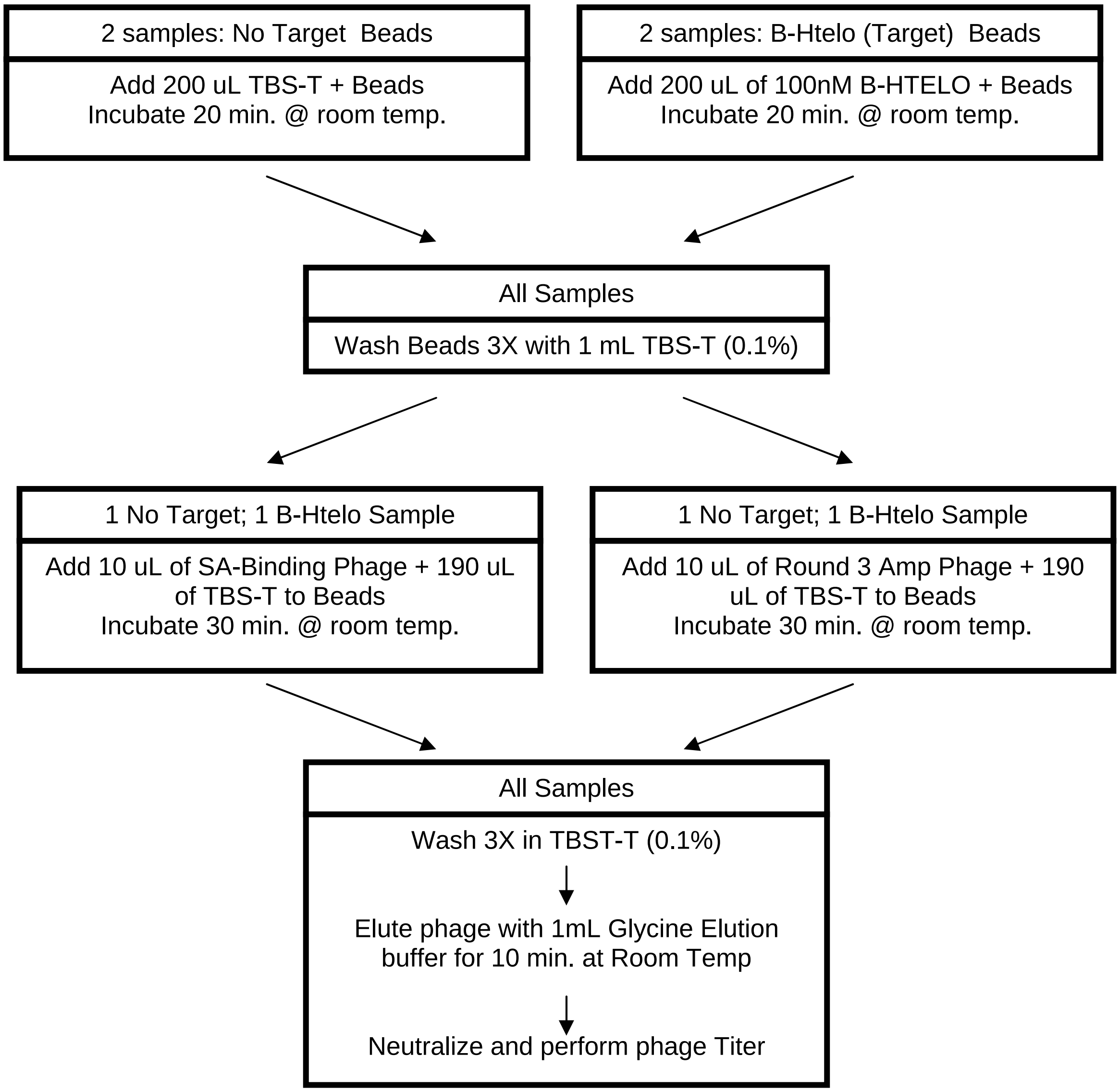

Figure 6.1. Protocol for Progress Report Assay.

Selection Assay: First attempt

The first attempt at phage selection for the B-Htelo target was completed using the same general assay that had been developed to target bTAR RNA with the exception of using TBS-T buffer for binding and wash steps (50 mM Tris-HCl pH 7.5, 100 mM KCl, 0.1% Tween). The first two rounds were completed with side-by-side binding protocols (bead binding and solution binding) to evaluate whether one approach was better than the other. Beads were prepared by blocking and washing according to standard protocol. 1 μM B-Htelo solution was prepared and folded by heating to 95 ºC for 2 minutes and then cooling to 4 ºC at an average rate of 2 ºC / min. Folded stocks were then diluted to 10 nM with TBS-T.

In the solution binding scenario, the phage were first incubated with the target in solution and subsequently captured by the SA coated magnetic beads. 2 μL of the 1 μM folded B-Htelo stock + 10 μL of the phage library were added to 188 μL of TBS-T buffer and incubated at room temp for 20 minutes. Following the B-Htelo / phage binding, this solution was added to the blocked and washed SA coated magnetic beads and incubated for another 20 minutes at room temperature. In contrast, the bead binding scenario allowed for the capture of the biotinylated target by the SA coated bead first; then allowed for incubation with the phage. Two μL of 1 μM folded B-Htelo + 198 uL of TBS-T were added to the blocked and washed beads and incubated for 20 minutes at room temperature. Non-binding B-Htelo were removed by washing the beads 2-3X with 1 mL of TBS-T. The phage solution consisting of 10 μL of phage stock + 190 μL of TBS-T was then added to the target coated beads and incubated for 30 minutes. at room temperature. In both scenarios, non-binding phage were removed by washing the beads 10X in 1 mL TBS-T. Binding phage were eluted from the beads with a nonspecific glycine buffer and amplified for subsequent rounds of selection.

Selection Assay: Second Attempt

The results from the first attempt at phage selection to target Htelo, along with the insight that was gained with the bead binding assay, prompted some modifications in the approach used during the second attempt. The first modification was that the B-Htelo binding solution would be 200 µL of 100 nM B-Htelo (20 pmol) rather than 200 µL of 10 nM B-Htelo (2 pmol). The second change was that there would be no Tween added to the TBS used for the folding step of the DNA. The 100 nM B-Htelo binding solution was made by adding 4 µL of 50 µM B-Htelo stock + 16 µL of TBS (no Tween) to give 20 µL of 10 µM B-Htelo solution. This solution was then heated to 95 ºC for 2 minutes. and cooled to 4 degrees Celsius at 2 ºC / min. to ensure the formation of the G-quadruplex structure.

Following folding, 1.98 mL of TBS-T (0.1%) was added to the 20 µL of 10 µM B-Htelo to yield a total of 2 mL of 100 nM B-Htelo stock for selections.

There were also two changes to the selection assay: 1. Every round of selection included a negative selection that preceeded the positive selection including the first round, 2. more aggressive elution practices. To maximize the phage recovery during the elution step of the assay, samples were agitated during the 10 minute elution with glycine buffer at room temperature. The resulting assay for the second attempt at selection is summarized in **Figure 6.2.**

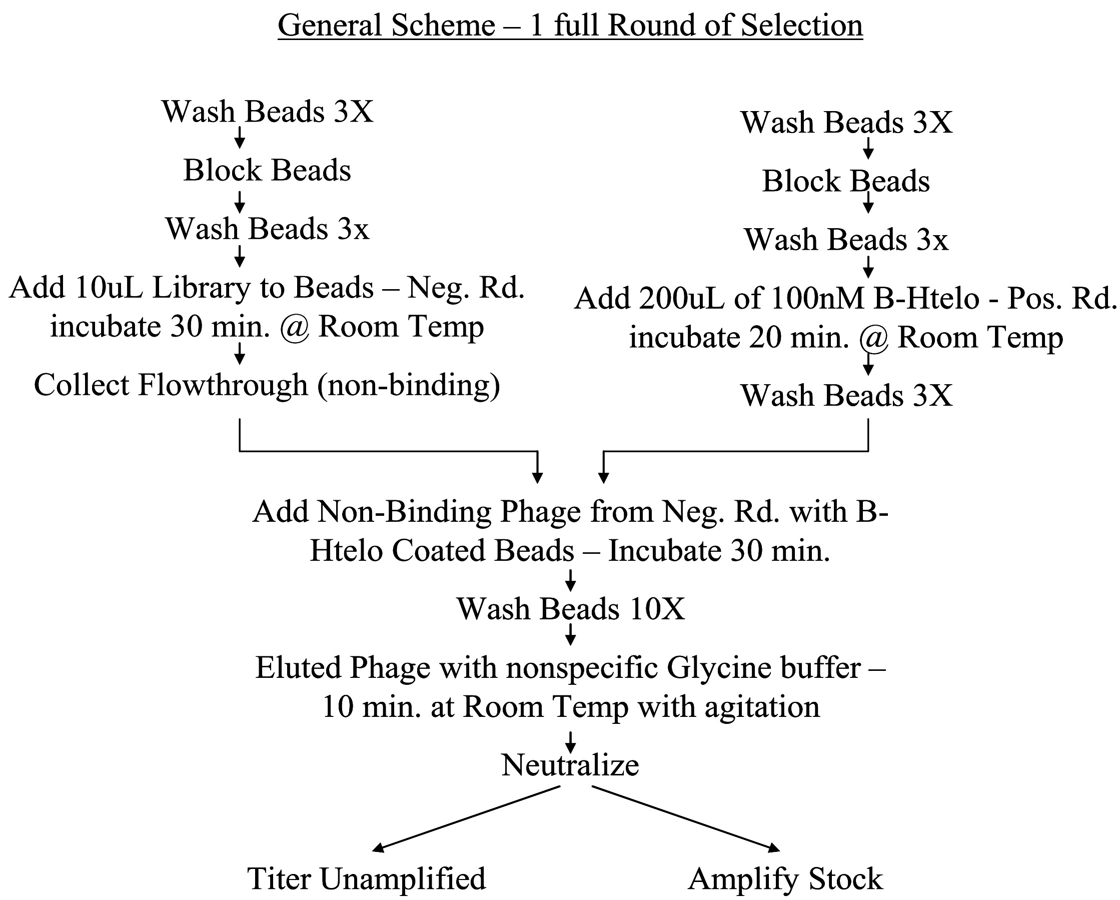

Figure 6.2. General Scheme of Selection Experiments with Htelo

Selection Assay: Third and Final Attempt

In the final attempt at phage selection to target Htelo G-quadruplexes, two different B-Htelo loading concentrations were tested: 20 nM (4 pmol) and 50 nM (10 pmol). Samples were prepared by 1:5 and 1:2 dilutions of the 100 nM B-Htelo stock that was made for the second round of selections. The 500 µL 100 nM B-Htelo stock + 500 µL of TBS-T yielded 1 mL of 50 nM stock. The 200 µL of 100 nM B-Htelo stock + 800 µL of TBS-T yielded 1 mL of 20 nM stock. All other assay conditions were the same as those developed for the second attempt.

REFERENCES

1. Crick, F., Central Dogma of Molecular Biology. *Nature* **1970,** *227* (5258), 561-&.

2. Basu, H. S.; Feuerstein, B. G.; Zarling, D. A.; Shafer, R. H.; Marton, L. J., Recognition of Z-RNA and Z-DNA determinants by polyamines in solution: experimental and theoretical studies. *J Biomol Struct Dyn* **1988,** *6* (2), 299-309.

3. Burge, S.; Parkinson, G. N.; Hazel, P.; Todd, A. K.; Neidle, S., Quadruplex DNA: sequence, topology and structure. *Nucleic Acids Res* **2006,** *34* (19), 5402-15.

4. Ghosh, A.; Bansal, M., A glossary of DNA structures from A to Z. *Acta Crystallogr D Biol Crystallogr* **2003,** *59* (Pt 4), 620-6.

5. Griffith, J. D.; Comeau, L.; Rosenfield, S.; Stansel, R. M.; Bianchi, A.; Moss, H.; de Lange, T., Mammalian telomeres end in a large duplex loop. *Cell* **1999,** *97* (4), 503-14.

6. Leslie, A. G.; Arnott, S.; Chandrasekaran, R.; Ratliff, R. L., Polymorphism of DNA double helices. *J Mol Biol* **1980,** *143* (1), 49-72.

7. Lu, X. J.; Shakked, Z.; Olson, W. K., A-form conformational motifs in ligand-bound DNA structures. *J Mol Biol* **2000,** *300* (4), 819-40.

8. Parkinson, G. N.; Lee, M. P.; Neidle, S., Crystal structure of parallel quadruplexes from human telomeric DNA. *Nature* **2002,** *417* (6891), 876-80.

9. Wahl, M. C.; Sundaralingam, M., Crystal structures of A-DNA duplexes. *Biopolymers* **1997,** *44* (1), 45-63.

10. Wright, W. E.; Tesmer, V. M.; Huffman, K. E.; Levene, S. D.; Shay, J. W., Normal human chromosomes have long G-rich telomeric overhangs at one end. *Genes Dev* **1997,** *11* (21), 2801-9.

11. Oh, D. B.; Kim, Y. G.; Rich, A., Z-DNA-binding proteins can act as potent effectors of gene expression in vivo. *Proc Natl Acad Sci U S A* **2002,** *99* (26), 16666-71.

12. Greider, C. W.; Blackburn, E. H., Identification of a specific telomere terminal transferase activity in Tetrahymena extracts. *Cell* **1985,** *43* (2 Pt 1), 405-13.

13. Harrison, P. M.; Gerstein, M., Studying genomes through the aeons: protein families, pseudogenes and proteome evolution. *J Mol Biol* **2002,** *318* (5), 1155-74.

14. Harrison, P. M.; Hegyi, H.; Balasubramanian, S.; Luscombe, N. M.; Bertone, P.; Echols, N.; Johnson, T.; Gerstein, M., Molecular fossils in the human genome: identification and analysis of the pseudogenes in chromosomes 21 and 22. *Genome Res* **2002,** *12* (2), 272-80.

15. Nugent, C. I.; Lundblad, V., The telomerase reverse transcriptase: components and regulation. *Genes Dev* **1998,** *12* (8), 1073-85.

16. Pidoux, A. L.; Allshire, R. C., The role of heterochromatin in centromere function. *Philos Trans R Soc Lond B Biol Sci* **2005,** *360* (1455), 569-79.

17. Baker, B. F., The role of antisense oligonucleotides in the wave of genomic information. *Nucleosides Nucleotides Nucleic Acids* **2001,** *20* (4-7), 397-9.

18. van Ommen, G. J.; Bakker, E.; den Dunnen, J. T., The human genome project and the future of diagnostics, treatment, and prevention. *Lancet* **1999,** *354 Suppl 1*, SI5-10.

19. Nahvi, A.; Sudarsan, N.; Ebert, M. S.; Zou, X.; Brown, K. L.; Breaker, R. R., Genetic control by a metabolite binding mRNA. *Chemistry & Biology* **2002,** *9* (9), 1043-1049.

20. Winkler, W.; Nahvi, A.; Breaker, R. R., Thiamine derivatives bind messenger RNAs directly to regulate bacterial gene expression. *Nature* **2002,** *419* (6910), 952-956.

21. Winkler, W. C.; Cohen-Chalamish, S.; Breaker, R. R., An mRNA structure that controls gene expression by binding FMN. *Proceedings of the National Academy of Sciences of the United States of America* **2002,** *99* (25), 15908-15913.

22. Mironov, A. S.; Gusarov, I.; Rafikov, R.; Lopez, L. E.; Shatalin, K.; Kreneva, R. A.; Perumov, D. A.; Nudler, E., Sensing small molecules by nascent RNA: A mechanism to control transcription in bacteria. *Cell* **2002,** *111* (5), 747-756.

23. Winkler, W. C.; Nahvi, A.; Sudarsan, N.; Barrick, J. E.; Breaker, R. R., An mRNA structure that controls gene expression by binding S-adenosylmethionine. *Nature Structural Biology* **2003,** *10* (9), 701-707.

24. Mandal, M.; Boese, B.; Barrick, J. E.; Winkler, W. C.; Breaker, R. R., Riboswitches control fundamental biochemical pathways in Bacillus subtilis and other bacteria. *Cell* **2003,** *113* (5), 577-586.

25. Barrick, J. E.; Corbino, K. A.; Winkler, W. C.; Nahvi, A.; Mandal, M.; Collins, J.; Lee, M.; Roth, A.; Sudarsan, N.; Jona, I.; Wickiser, J. K.; Breaker, R. R., New RNA motifs suggest an expanded scope for riboswitches in bacterial genetic control. *Proceedings of*

the National Academy of Sciences of the United States of America **2004,** *101* (17), 6421-6426.

26. Nudler, E.; Mironov, A. S., The riboswitch control of bacterial metabolism. *Trends in Biochemical Sciences* **2004,** *29* (1), 11-17.

27. Winkler, W. C.; Nahvi, A.; Roth, A.; Collins, J. A.; Breaker, R. R., Control of gene expression by a natural metabolite-responsive ribozyme. *Nature* **2004,** *428* (6980), 281-286.

28. Ebralidze, A.; Wang, Y.; Petkova, V.; Ebralidse, K.; Junghans, R. P., RNA leaching of transcription factors disrupts transcription in myotonic dystrophy. *Science* **2004,** *303* (5656), 383-387.

29. McDaniel, B. A.; Grundy, F. J.; Henkin, T. M., A tertiary structural element in S box leader RNAs is required for S-adenosylmethionine-directed transcription termination. *Molecular Microbiology* **2005,** *57* (4), 1008-1021.

30. Robertson, M. P.; Igel, H.; Baertsch, R.; Haussler, D.; Ares, M.; Scott, W. G., The structure of a rigorously conserved RNA element within the SARS virus genome. *Plos Biology* **2005,** *3* (1), 86-94.

31. Ecker, D. J.; Griffey, R. H., RNA as a small-molecule drug target: doubling the value of genomics. *Drug Discovery Today* **1999,** *4* (9), 420-429.

32. Mingeot-Leclercq, M. P.; Glupczynski, Y.; Tulkens, P. M., Aminoglycosides: Activity and resistance. *Antimicrobial Agents and Chemotherapy* **1999,** *43* (4), 727-737.

33. Tor, Y., Targeting RNA with small molecules. *Chembiochem* **2003,** *4* (10), 998-1007.

34. Hamy, F.; Felder, E. R.; Heizmann, G.; Lazdins, J.; Aboul-ela, F.; Varani, G.; Karn, J.; Klimkait, T., An inhibitor of the Tat/TAR RNA interaction that effectively suppresses HIV-1 replication. *Proc Natl Acad Sci U S A* **1997,** *94* (8), 3548-53.

35. Zapp, M. L.; Stern, S.; Green, M. R., Small Molecules That Selectively Block Rna-Binding of Hiv-1 Rev Protein Inhibit Rev Function and Viral Production. *Cell* **1993,** *74* (6), 969-978.

36. Hermann, T., Chemical and functional diversity of small molecule ligands for RNA. *Biopolymers* **2003,** *70* (1), 4-18.

37. Cheng, A. C.; Calabro, V.; Frankel, A. D., Design of RNA-binding proteins and ligands. *Current Opinion in Structural Biology* **2001,** *11* (4), 478-484.

38. van Dijk, A. D. J.; de Vries, S. J.; Dominguez, C.; Chen, H.; Zhou, H. X.; Bonvin, A. M. J. J., Data-driven docking: HADDOCK's adventures in CAPRI. *Proteins-Structure Function and Bioinformatics* **2005,** *60* (2), 232-238.

39. Dominguez, C.; Boelens, R.; Bonvin, A. M. J. J., HADDOCK: A protein-protein docking approach based on biochemical or biophysical information. *Journal of the American Chemical Society* **2003,** *125* (7), 1731-1737.

40. Mclafferty, M. A.; Kent, R. B.; Ladner, R. C.; Markland, W., Bacteriophage-M-13 Displaying Disulfide-Constrained Microproteins. *Gene* **1993,** *128* (1), 29-36.

41. Parmley, S. F.; Smith, G. P., Antibody-Selectable Filamentous Fd Phage Vectors - Affinity Purification of Target Genes. *Gene* **1988,** *73* (2), 305-318.

42. Dervan, P. B., Design of Sequence Specific DNA-Binding Molecules. *Abstracts of Papers of the American Chemical Society* **1986,** *192*, 122-ORGN.

43. Dervan, P. B.; Edelson, B. S., Recognition of the DNA minor groove by pyrrole-imidazole polyamides. *Current Opinion in Structural Biology* **2003,** *13* (3), 284-299.

44. Alper, P. B.; Hendrix, M.; Sears, P.; Wong, C. H., Probing the specificity of aminoglycoside ribosomal RNA interactions with designed synthetic analogs. *Journal of the American Chemical Society* **1998,** *120* (9), 1965-1978.

45. Gonda, M. A.; Luther, D. G.; Fong, S. E.; Tobin, G. J., Bovine Immunodeficiency Virus - Molecular-Biology and Virus-Host Interactions. *Virus Research* **1994,** *32* (2), 155-181.

46. Johnson, E. C.; Feher, V. A.; Peng, J. W.; Moore, J. M.; Williamson, J. R., Application of NMR SHAPES screening to an RNA target. *Journal of the American Chemical Society* **2003,** *125* (51), 15724-15725.

47. Michael, K.; Tor, Y., Designing novel RNA binders. *Chemistry-a European Journal* **1998,** *4* (11), 2091-2098.

48. Pilch, D. S.; Kaul, M.; Barbieri, C. M., Ribosomal RNA recognition by aminoglycoside antibiotics. *DNA Binders and Related Subjects* **2005,** *253*, 179-204.

49. Smith, G. P., Filamentous Fusion Phage - Novel Expression Vectors That Display Cloned Antigens on the Virion Surface. *Science* **1985,** *228* (4705), 1315-1317.

50. Carlson, C. B.; Stephens, O. M.; Beal, P. A., Recognition of double-stranded RNA by proteins and small molecules. *Biopolymers* **2003,** *70* (1), 86-102.

51. Gooch, B. D.; Beal, P. A., Recognition of duplex RNA by helix-threading peptides. *Journal of the American Chemical Society* **2004,** *126* (34), 10603-10610.

52. Gooch, B. D.; Krishnamurthy, M.; Shadid, M.; Beal, P. A., Binding of helix-threading peptides to E-coli 16S ribosomal RNA and inhibition of the S15-16S complex. *Chembiochem* **2005,** *6* (12), 2247-2254.

53. Hwang, S.; Tamilarasu, N.; Ryan, K.; Huq, I.; Richter, S.; Still, W. C.; Rana, T. M., Inhibition of gene expression in human cells through small molecule-RNA interactions. *Proceedings of the National Academy of Sciences of the United States of America* **1999,** *96* (23), 12997-13002.

54. Krishnamurthy, M.; Gooch, B. D.; Beal, P. A., RNA binding and thiolytic stability of a quinoline-containing helix-threading peptide. *Organic & Biomolecular Chemistry* **2006,** *4* (4), 639-645.

55. Lajiness, M. S.; Vieth, M.; Erickson, J., Molecular properties that influence oral drug-like behavior. *Current Opinion in Drug Discovery & Development* **2004,** *7* (4), 470-477.

56. Tamilarasu, N.; Huq, I.; Rana, T. M., Design, synthesis, and biological activity of a cyclic peptide: An inhibitor of HIV-1 Tat-TAR interactions in human cells. *Bioorganic & Medicinal Chemistry Letters* **2000,** *10* (9), 971-974.

57. Austin, R. J.; Xia, T. B.; Ren, J. S.; Takahashi, T. T.; Roberts, R. W., Designed arginine-rich RNA-binding peptides with picomolar affinity. *Journal of the American Chemical Society* **2002,** *124* (37), 10966-10967.

58. Barrick, J. E.; Takahashi, T. T.; Balakin, A.; Roberts, R. W., Selection of RNA-binding peptides using mRNA-peptide fusions. *Methods* **2001,** *23* (3), 287-293.

59. Barrick, J. E.; Takahashi, T. T.; Ren, J. S.; Xia, T. B.; Roberts, R. W., Large libraries reveal diverse solutions to an RNA recognition problem. *Proceedings of the National Academy of Sciences of the United States of America* **2001,** *98* (22), 12374-12378.

60. Huq, I.; Ping, Y. H.; Tamilarasu, N.; Rana, T. M., Controlling human immunodeficiency virus type 1 gene expression by unnatural peptides. *Biochemistry* **1999,** *38* (16), 5172-5177.

61. Mucha, P.; Szyk, A.; Rekowski, P.; Weiss, P. A.; Agris, P. F., Anticodon domain methylated nucleosides of yeast tRNA(Phe) are significant recognition determinants in the binding of a phage display selected peptide. *Biochemistry* **2001,** *40* (47), 14191-14199.

62. Pustowka, A.; Dietz, J.; Ferner, J.; Baumann, M.; Landersz, M.; Konigs, C.; Schwalbe, H.; Dietrich, U., Identification of peptide ligands for target RNA structures derived from the HIV-1 packaging signal psi by screening phage-displayed peptide libraries. *Chembiochem* **2003,** *4* (10), 1093-1097.

63. Agris, P. F.; Marchbank, M. T.; Newman, W.; Guenther, R.; Ingram, P.; Swallow, J.; Mucha, P.; Szyk, A.; Rekowski, P.; Peletskaya, E.; Deutscher, S. L., Experimental models of protein-RNA interaction: Isolation and analyses of tRNA(Phe) and U1 snRNA-binding peptides from bacteriophage display libraries. *Journal of Protein Chemistry* **1999,** *18* (4), 425-435.

64. Athanassiou, Z.; Dias, R. L. A.; Moehle, K.; Dobson, N.; Varani, G.; Robinson, J. A., Structural mimicry of retroviral Tat proteins by constrained, beta-hairpin peptidomimetics: Ligands with high affinity and selectivity for viral TAR RNA regulatory elements. *Journal of the American Chemical Society* **2004,** *126* (22), 6906-6913.

65. Frugier, M.; Schimmel, P., Subtle atomic group discrimination in the RNA minor groove. *Proceedings of the National Academy of Sciences of the United States of America* **1997,** *94* (21), 11291-11294.

66. Gelman, M. A.; Richter, S.; Cao, H.; Umezawa, N.; Gellman, S. H.; Rana, T. M., Selective binding of TAR RNA by a tat-derived beta-peptide. *Organic Letters* **2003,** *5* (20), 3563-3565.

67. Huq, I.; Wang, X. L.; Rana, T. M., Specific recognition of HIV-1 TAR RNA by a D-Tat peptide. *Nature Structural Biology* **1997,** *4* (11), 881-882.

68. Runyon, S. T.; Puglisi, J. D., Design of a cyclic peptide that targets a viral RNA. *Journal of the American Chemical Society* **2003,** *125* (51), 15704-15705.

69. Chen, L.; Frankel, A. D., An Rna-Binding Peptide from Bovine Immunodeficiency Virus Tat Protein Recognizes an Unusual Rna Structure. *Biochemistry* **1994,** *33* (9), 2708-2715.

70. Battiste, J. L.; Tan, R. Y.; Frankel, A. D.; Williamson, J. R., Binding of an Hiv Rev Peptide to Rev Responsive Element Rna Induces Formation of Purine-Purine Base-Pairs. *Biochemistry* **1994,** *33* (10), 2741-2747.

71. Das, C.; Frankel, A. D., Sequence and structure space of RNA-binding peptides. *Biopolymers* **2003,** *70* (1), 80-85.

72. Clackson, T.; Wells, J. A., In-Vitro Selection from Protein and Peptide Libraries. *Trends in Biotechnology* **1994,** *12* (5), 173-184.

73. Lowman, H. B., Bacteriophage display and discovery of peptide leads for drug development. *Annual Review of Biophysics and Biomolecular Structure* **1997,** *26*, 401-424.

74. Sidhu, S. S.; Weiss, G. A.; Wells, J. A., High copy display of large proteins on phage for functional selections. *Journal of Molecular Biology* **2000,** *296* (2), 487-495.

75. Smith, G. P.; Petrenko, V. A., Phage display. *Chemical Reviews* **1997,** *97* (2), 391-410.

76. Adessi, C.; Frossard, M. J.; Boissard, C.; Fraga, S.; Bieler, S.; Ruckle, T.; Vilbois, F.; Robinson, S. M.; Mutter, M.; Banks, W. A.; Soto, C., Pharmacological profiles of peptide drug candidates for the treatment of Alzheimer's disease. *Journal of Biological Chemistry* **2003,** *278* (16), 13905-13911.

77. Veber, D. F.; Johnson, S. R.; Cheng, H. Y.; Smith, B. R.; Ward, K. W.; Kopple, K. D., Molecular properties that influence the oral bioavailability of drug candidates. *Journal of Medicinal Chemistry* **2002,** *45* (12), 2615-2623.

78. Williamson, J. R., Molecular biology - Small subunit, big science. *Nature* **2000,** *407* (6802), 306-307.

79. Knipp, G. T.; Audus, K. L.; Soares, M. J., Nutrient transport across the placenta. *Advanced Drug Delivery Reviews* **1999,** *38* (1), 41-58.

80. Adessi, C.; Soto, C., Converting a peptide into a drug: Strategies to improve stability and bioavailability. *Current Medicinal Chemistry* **2002,** *9* (9), 963-978.

81. Davies, J. S., The cyclization of peptides and depsipeptides. *Journal of Peptide Science* **2003,** *9* (8), 471-501.

82. Friedler, A.; Friedler, D.; Luedtke, N. W.; Tor, Y.; Loyter, A.; Gilon, C., Development of a functional backbone cyclic mimetic of the HTV-1 Tat arginine-rich motif. *Journal of Biological Chemistry* **2000,** *275* (31), 23783-23789.

83. Okumu, F. W.; Pauletti, G. M.; VanderVelde, D. G.; Siahaan, T. J.; Borchardt, R. T., Effect of restricted conformational flexibility on the permeation of model hexapeptides across Caco-2 cell monolayers. *Pharmaceutical Research* **1997,** *14* (2), 169-175.

84. Fairlie, D. P.; Abbenante, G.; March, D. R., Macrocyclic Peptidomimetics - Forcing Peptides into Bioactive Conformations. *Current Medicinal Chemistry* **1995,** *2* (2), 654-686.

85. Raja, C.; Ferner, J.; Dietrich, U.; Avilov, S.; Ficheux, D.; Darlix, J. L.; de Rocquigny, H.; Schwalbe, H.; Mely, Y., A tryptophan-rich hexapeptide inhibits nucleic acid destabilization chaperoned by the HIV-1 nucleocapsid protein. *Biochemistry* **2006,** *45* (30), 9254-9265.

86. McPhillips, M. G.; Veerapraditsin, T.; Cumming, S. A.; Karali, D.; Milligan, S. G.; Boner, W.; Morgan, I. M.; Graham, S. V., SF2/ASF binds the human papillomavirus type 16 late RNA control element and is regulated during differentiation of virus-infected epithelial cells. *Journal of Virology* **2004,** *78* (19), 10598-10605.

87. Roy, S., Fluorescence quenching methods to study protein-nucleic acid interactions. *Energetics of Biological Macromolecules, Pt D* **2004,** *379*, 175-187.

88. Tang, S.; Tao, M. F.; McCoy, J. P.; Zheng, Z. M., The E7 oncoprotein is translated from spliced E6*I transcripts in high-risk human papillomavirus type 16-or type 18-positive cervical cancer cell lines via translation reinitiation. *Journal of Virology* **2006,** *80* (9), 4249-4263.

89. Ausubel, F. M., Current Protocols in Molecular Biology. Chichester, Ed. John Wiley & Sons: 1994.

90. Barboric, M.; Taube, R.; Nekrep, N.; Fujinaga, K.; Peterlin, B. M., Binding of Tat to TAR and recruitment of positive transcription elongation factor b occur independently in bovine immunodeficiency virus. *J Virol* **2000,** *74* (13), 6039-44.

91. Bogerd, H. P.; Wiegand, H. L.; Bieniasz, P. D.; Cullen, B. R., Functional differences between human and bovine immunodeficiency virus tar transcription factors. *Journal of Virology* **2000,** *74* (10), 4666-4671.

92. Mergny, J. L.; Lacroix, L., Analysis of thermal melting curves. *Oligonucleotides* **2003,** *13* (6), 515-37.

93. Garbesi, A.; Hamy, F.; Maffini, M.; Albrecht, G.; Klimkait, T., TAR-RNA binding by HIV-1 Tat protein is selectively inhibited by its L-enantiomer. *Nucleic Acids Res* **1998,** *26* (12), 2886-90.

94. Metzger, A. U.; Schindler, T.; Willbold, D.; Kraft, M.; Steegborn, C.; Volkmann, A.; Frank, R. W.; Rosch, P., Structural rearrangements on HIV-1 Tat (32-72) TAR complex formation. *FEBS Lett* **1996,** *384* (3), 255-9.

95. Tok, J. B.; Bi, L., A comparative binding study of BIV Tat peptide against its TAR RNA duplex, RNA-DNA heteroduplex and DNA duplex. *Bioorg Med Chem Lett* **2005,** *15* (1), 129-33.

96. Feig, A. L., Applications of isothermal titration calorimetry in RNA biochemistry and biophysics. *Biopolymers* **2007,** *87* (5-6), 293-301.

97. Ennifar, E.; Paillart, J. C.; Marquet, R.; Ehresmann, B.; Ehresmann, C.; Dumas, P.; Walter, P., HIV-1 RNA dimerization initiation site is structurally similar to the ribosomal A site and binds aminoglycoside antibiotics. *J Biol Chem* **2003,** *278* (4), 2723-30.

98. Gilbert, S. D.; Stoddard, C. D.; Wise, S. J.; Batey, R. T., Thermodynamic and kinetic characterization of ligand binding to the purine riboswitch aptamer domain. *J Mol Biol* **2006,** *359* (3), 754-68.

99. Hermann, T.; Westhof, E., Aminoglycoside binding to the hammerhead ribozyme: a general model for the interaction of cationic antibiotics with RNA. *J Mol Biol* **1998,** *276* (5), 903-12.

100. Talkington, M. W.; Siuzdak, G.; Williamson, J. R., An assembly landscape for the 30S ribosomal subunit. *Nature* **2005,** *438* (7068), 628-32.

101. Windbichler, N.; Werner, M.; Schroeder, R., Kissing complex-mediated dimerisation of HIV-1 RNA: coupling extended duplex formation to ribozyme cleavage. *Nucleic Acids Res* **2003,** *31* (22), 6419-27.

102. Bauer, G.; Suess, B., Engineered riboswitches as novel tools in molecular biology. *Journal of Biotechnology* **2006,** *124* (1), 4-11.

103. Cho, C. W.; Poo, H.; Cho, Y. S.; Cho, M. C.; Lee, K. A.; Lee, S. J.; Park, S. N.; Kim, I. K.; Jung, Y. K.; Choe, Y. K.; Yeom, Y. I.; Choe, I. S.; Yoon, D. Y., HPV E6 antisense induces apoptosis in CaSki cells via suppression of E6 splicing. *Experimental and Molecular Medicine* **2002,** *34* (2), 159-166.

104. Epshtein, V.; Mironov, A. S.; Nudler, E., The riboswitch-mediated control of sulfur metabolism in bacteria. *Proceedings of the National Academy of Sciences of the United States of America* **2003,** *100* (9), 5052-5056.

105. McDaniel, B. A. M.; Grundy, F. J.; Artsimovitch, I.; Henkin, T. M., Transcription termination control of the S box system: Direct measurement of S-adenosylmethionine by the leader RNA. *Proceedings of the National Academy of Sciences of the United States of America* **2003,** *100* (6), 3083-3088.

106. Agris, P. F.; Marchbank, M. T.; Newman, W.; Guenther, R.; Ingram, P.; Swallow, J.; Mucha, P.; Szyk, A.; Rekowski, P.; Peletskaya, E.; Deutscher, S. L., Experimental models of protein-RNA interaction: isolation and analyses of tRNA(Phe) and U1 snRNA-binding peptides from bacteriophage display libraries. *J Protein Chem* **1999,** *18* (4), 425-35.

107. Puglisi, J. D.; Chen, L.; Blanchard, S.; Frankel, A. D., Solution Structure of a Bovine Immunodeficiency Virus Tat-Tar Peptide-Rna Complex. *Science* **1995,** *270* (5239), 1200-1203.

108. Long, K. S.; Crothers, D. M., Interaction of human immunodeficiency virus type 1 Tat-derived peptides with TAR RNA. *Biochemistry* **1995,** *34* (27), 8885-95.

109. Tan, R.; Frankel, A. D., Circular dichroism studies suggest that TAR RNA changes conformation upon specific binding of arginine or guanidine. *Biochemistry* **1992,** *31* (42), 10288-94.

110. Ambrus, A.; Chen, D.; Dai, J.; Jones, R. A.; Yang, D., Solution structure of the biologically relevant G-quadruplex element in the human c-MYC promoter. Implications for G-quadruplex stabilization. *Biochemistry* **2005,** *44* (6), 2048-58.

111. Duan, W.; Rangan, A.; Vankayalapati, H.; Kim, M. Y.; Zeng, Q.; Sun, D.; Han, H.; Fedoroff, O. Y.; Nishioka, D.; Rha, S. Y.; Izbicka, E.; Von Hoff, D. D.; Hurley, L. H., Design and synthesis of fluoroquinophenoxazines that interact with human telomeric G-quadruplexes and their biological effects. *Mol Cancer Ther* **2001,** *1* (2), 103-20.

112. Goncalves, D. P.; Ladame, S.; Balasubramanian, S.; Sanders, J. K., Synthesis and G-quadruplex binding studies of new 4-N-methylpyridinium porphyrins. *Org Biomol Chem* **2006,** *4* (17), 3337-42.

113. Granotier, C.; Pennarun, G.; Riou, L.; Hoffschir, F.; Gauthier, L. R.; De Cian, A.; Gomez, D.; Mandine, E.; Riou, J. F.; Mergny, J. L.; Mailliet, P.; Dutrillaux, B.; Boussin, F. D., Preferential binding of a G-quadruplex ligand to human chromosome ends. *Nucleic Acids Res* **2005,** *33* (13), 4182-90.

114. Green, J. J.; Ying, L.; Klenerman, D.; Balasubramanian, S., Kinetics of unfolding the human telomeric DNA quadruplex using a PNA trap. *J Am Chem Soc* **2003,** *125* (13), 3763-7.

115. Guittat, L.; Alberti, P.; Gomez, D.; De Cian, A.; Pennarun, G.; Lemarteleur, T.; Belmokhtar, C.; Paterski, R.; Morjani, H.; Trentesaux, C.; Mandine, E.; Boussin, F.; Mailliet, P.; Lacroix, L.; Riou, J. F.; Mergny, J. L., Targeting human telomerase for cancer therapeutics. *Cytotechnology* **2004,** *45* (1-2), 75-90.

116. Han, H.; Hurley, L. H.; Salazar, M., A DNA polymerase stop assay for G-quadruplex-interactive compounds. *Nucleic Acids Res* **1999,** *27* (2), 537-42.

117. Huppert, J. L.; Balasubramanian, S., Prevalence of quadruplexes in the human genome. *Nucleic Acids Res* **2005,** *33* (9), 2908-16.

118. Hurley, L. H.; Wheelhouse, R. T.; Sun, D.; Kerwin, S. M.; Salazar, M.; Fedoroff, O. Y.; Han, F. X.; Han, H. Y.; Izbicka, E.; Von Hoff, D. D., G-quadruplexes as targets for drug design. *Pharmacology & Therapeutics* **2000,** *85* (3), 141-158.

119. Jantos, K.; Rodriguez, R.; Ladame, S.; Shirude, P. S.; Balasubramanian, S., Oxazole-based peptide macrocycles: a new class of G-quadruplex binding ligands. *J Am Chem Soc* **2006,** *128* (42), 13662-3.

120. Kelland, L. R., Overcoming the immortality of tumour cells by telomere and telomerase based cancer therapeutics--current status and future prospects. *Eur J Cancer* **2005,** *41* (7), 971-9.

121. Keniry, M. A., Quadruplex structures in nucleic acids. *Biopolymers* **2000,** *56* (3), 123-146.

122. Kim, M. Y.; Vankayalapati, H.; Shin-Ya, K.; Wierzba, K.; Hurley, L. H., Telomestatin, a potent telomerase inhibitor that interacts quite specifically with the human telomeric intramolecular g-quadruplex. *J Am Chem Soc* **2002,** *124* (10), 2098-9.

123. Ladame, S.; Schouten, J. A.; Stuart, J.; Roldan, J.; Neidle, S.; Balasubramanian, S., Tetrapeptides induce selective recognition for G-quadruplexes when conjugated to a DNA-binding platform. *Org Biomol Chem* **2004,** *2* (20), 2925-31.

124. Mondello, C.; Scovassi, A. I., Telomeres, telomerase, and apoptosis. *Biochemistry and Cell Biology-Biochimie Et Biologie Cellulaire* **2004,** *82* (4), 498-507.

125. Olaussen, K. A.; Dubrana, K.; Dornont, J.; Spano, J. P.; Sabatier, L.; Soria, J. C., Telomeres and telomerase as targets for anticancer drug development. *Critical Reviews in Oncology Hematology* **2006,** *57* (3), 191-214.

126. Schouten, J. A.; Ladame, S.; Mason, S. J.; Cooper, M. A.; Balasubramanian, S., G-quadruplex-specific peptide-hemicyanine ligands by partial combinatorial selection. *J Am Chem Soc* **2003,** *125* (19), 5594-5.

127. Sharma, S.; Doherty, K. M.; Brosh, R. M., Jr., DNA helicases as targets for anti-cancer drugs. *Curr Med Chem Anticancer Agents* **2005,** *5* (3), 183-99.

128. Simonsson, T., G-quadruplex DNA structures--variations on a theme. *Biol Chem* **2001,** *382* (4), 621-8.

129. Tuntiwechapikul, W.; Salazar, M., Cleavage of telomeric G-quadruplex DNA with perylene-EDTA*Fe(II). *Biochemistry* **2001,** *40* (45), 13652-8.

130. Williamson, J. R., G-quartet structures in telomeric DNA. *Annu Rev Biophys Biomol Struct* **1994,** *23*, 703-30.

APPENDICES

A.1 CD Temperature Study of bTAR RNA Hairpin

wavelenth	TK 4	bTAR 4	bTAR - TK 4	TK 23	bTAR 23	bTAR - TK 23	TK 90	bTAR 90	bTAR - TK 90
300	1.380	1.151	-0.229	1.363	1.129	-0.234	1.210	1.124	-0.085
299	1.352	1.094	-0.258	1.387	1.191	-0.196	1.150	1.243	0.093
298	1.337	1.174	-0.163	1.360	1.273	-0.087	1.127	1.290	0.164
297	1.360	1.204	-0.157	1.330	1.320	-0.010	1.098	1.266	0.168
296	1.371	1.186	-0.184	1.316	1.313	-0.003	1.107	1.237	0.130
295	1.361	1.188	-0.173	1.289	1.320	0.032	1.116	1.208	0.092
294	1.357	1.230	-0.127	1.283	1.354	0.071	1.112	1.213	0.101
293	1.354	1.269	-0.086	1.274	1.385	0.111	1.112	1.258	0.145
292	1.335	1.349	0.013	1.272	1.447	0.175	1.113	1.319	0.206
291	1.311	1.431	0.120	1.276	1.538	0.262	1.100	1.388	0.288
290	1.295	1.539	0.245	1.248	1.637	0.390	1.087	1.429	0.342
289	1.263	1.623	0.360	1.245	1.725	0.480	1.074	1.477	0.402
288	1.229	1.698	0.468	1.233	1.799	0.566	1.062	1.499	0.437
287	1.199	1.776	0.578	1.206	1.873	0.667	1.048	1.526	0.478
286	1.166	1.882	0.715	1.160	1.962	0.802	1.028	1.560	0.531
285	1.128	2.000	0.872	1.138	2.059	0.921	0.990	1.609	0.619
284	1.103	2.138	1.035	1.118	2.179	1.061	0.956	1.687	0.731
283	1.090	2.264	1.174	1.069	2.286	1.217	0.927	1.755	0.828
282	1.067	2.388	1.321	1.039	2.413	1.373	0.893	1.804	0.911
281	1.040	2.504	1.464	1.012	2.540	1.528	0.871	1.830	0.958
280	1.030	2.624	1.594	0.965	2.666	1.702	0.856	1.841	0.985
279	0.999	2.746	1.747	0.957	2.798	1.841	0.853	1.861	1.007
278	0.966	2.879	1.914	0.922	2.932	2.010	0.835	1.872	1.036
277	0.942	3.024	2.082	0.887	3.072	2.185	0.822	1.916	1.094
276	0.920	3.185	2.266	0.861	3.228	2.367	0.823	1.944	1.121
275	0.888	3.331	2.442	0.832	3.357	2.525	0.797	1.962	1.165
274	0.853	3.464	2.611	0.822	3.465	2.643	0.798	1.968	1.170
273	0.822	3.555	2.733	0.797	3.548	2.750	0.763	1.943	1.179
272	0.804	3.610	2.806	0.792	3.614	2.822	0.751	1.934	1.183
271	0.773	3.645	2.872	0.798	3.677	2.879	0.733	1.923	1.191
270	0.760	3.671	2.912	0.788	3.732	2.943	0.734	1.897	1.163
269	0.741	3.676	2.935	0.785	3.749	2.964	0.727	1.869	1.142
268	0.735	3.632	2.897	0.764	3.728	2.963	0.699	1.808	1.109
267	0.721	3.567	2.846	0.747	3.669	2.922	0.680	1.732	1.052
266	0.714	3.484	2.770	0.718	3.591	2.873	0.687	1.648	0.961
265	0.693	3.375	2.681	0.683	3.436	2.753	0.663	1.575	0.911
264	0.673	3.230	2.557	0.658	3.295	2.636	0.661	1.499	0.838
263	0.690	3.058	2.368	0.632	3.119	2.487	0.638	1.388	0.750
262	0.701	2.855	2.154	0.604	2.944	2.340	0.640	1.269	0.629
261	0.692	2.643	1.951	0.614	2.754	2.139	0.625	1.152	0.526
260	0.678	2.461	1.783	0.619	2.548	1.930	0.621	1.054	0.433
259	0.672	2.260	1.588	0.625	2.348	1.723	0.587	0.940	0.354
258	0.646	2.015	1.369	0.627	2.132	1.504	0.555	0.829	0.274
257	0.606	1.836	1.230	0.616	1.949	1.334	0.519	0.722	0.204
256	0.592	1.623	1.031	0.587	1.755	1.168	0.481	0.649	0.167
255	0.557	1.407	0.849	0.563	1.541	0.978	0.445	0.580	0.136
254	0.529	1.214	0.684	0.530	1.378	0.848	0.395	0.520	0.125
253	0.549	1.040	0.491	0.497	1.214	0.717	0.370	0.413	0.042
252	0.524	0.879	0.355	0.467	1.047	0.580	0.338	0.318	-0.019
251	0.501	0.730	0.229	0.478	0.874	0.396	0.291	0.247	-0.044
250	0.471	0.637	0.166	0.458	0.740	0.282	0.252	0.164	-0.089
249	0.446	0.519	0.072	0.420	0.649	0.229	0.234	0.087	-0.147
248	0.401	0.406	0.005	0.382	0.552	0.170	0.235	0.037	-0.198
247	0.361	0.329	-0.032	0.341	0.498	0.157	0.218	-0.049	-0.267
246	0.334	0.211	-0.123	0.319	0.399	0.080	0.197	-0.113	-0.310
245	0.315	0.128	-0.187	0.301	0.297	-0.004	0.172	-0.181	-0.353
244	0.295	0.057	-0.238	0.290	0.204	-0.085	0.142	-0.239	-0.381
243	0.262	-0.013	-0.275	0.245	0.127	-0.118	0.085	-0.291	-0.376
242	0.223	-0.109	-0.332	0.216	0.035	-0.181	0.008	-0.321	-0.329
241	0.158	-0.225	-0.382	0.207	-0.072	-0.279	-0.064	-0.411	-0.346
240	0.142	-0.329	-0.471	0.137	-0.156	-0.292	-0.115	-0.504	-0.389
239	0.116	-0.433	-0.549	0.053	-0.239	-0.292	-0.183	-0.579	-0.396
238	0.044	-0.568	-0.612	-0.018	-0.357	-0.339	-0.217	-0.681	-0.464
237	-0.019	-0.665	-0.646	-0.100	-0.443	-0.343	-0.262	-0.786	-0.524
236	-0.101	-0.721	-0.620	-0.195	-0.524	-0.329	-0.337	-0.865	-0.527
235	-0.194	-0.814	-0.620	-0.300	-0.626	-0.327	-0.436	-0.956	-0.520
234	-0.341	-0.853	-0.512	-0.420	-0.748	-0.328	-0.558	-1.021	-0.464
233	-0.478	-0.928	-0.451	-0.533	-0.822	-0.289	-0.707	-1.055	-0.348
232	-0.616	-1.048	-0.431	-0.627	-0.883	-0.256	-0.841	-1.146	-0.304
231	-0.739	-1.158	-0.419	-0.711	-0.953	-0.242	-0.971	-1.264	-0.293
230	-0.817	-1.272	-0.455	-0.796	-1.043	-0.248	-1.073	-1.396	-0.323
229	-0.890	-1.376	-0.487	-0.867	-1.203	-0.336	-1.217	-1.515	-0.298
228	-0.979	-1.513	-0.534	-0.995	-1.330	-0.334	-1.315	-1.638	-0.323
227	-1.061	-1.569	-0.508	-1.105	-1.426	-0.321	-1.376	-1.729	-0.353
226	-1.207	-1.653	-0.446	-1.259	-1.553	-0.293	-1.468	-1.763	-0.295
225	-1.352	-1.757	-0.405	-1.401	-1.699	-0.298	-1.583	-1.864	-0.281
224	-1.510	-1.842	-0.332	-1.538	-1.857	-0.319	-1.693	-1.919	-0.226
223	-1.586	-1.956	-0.370	-1.597	-1.977	-0.380	-1.782	-1.953	-0.170
222	-1.614	-2.219	-0.606	-1.714	-2.134	-0.420	-1.885	-2.019	-0.134
221	-1.660	-2.503	-0.843	-1.777	-2.291	-0.514	-1.971	-2.095	-0.124
220	-1.728	-2.772	-1.044	-1.863	-2.500	-0.637	-2.060	-2.322	-0.262
219	-1.772	-3.130	-1.358	-1.969	-2.819	-0.851	-2.191	-2.468	-0.277
218	-1.813	-3.540	-1.727	-2.183	-3.069	-0.886	-2.253	-2.594	-0.341
217	-1.961	-3.880	-1.919	-2.250	-3.462	-1.213	-2.282	-2.660	-0.378
216	-2.140	-4.239	-2.099	-2.338	-3.774	-1.436	-2.378	-2.724	-0.346
215	-2.258	-4.444	-2.186	-2.408	-4.176	-1.768	-2.463	-2.867	-0.404
214	-2.415	-4.647	-2.232	-2.390	-4.518	-2.128	-2.500	-2.855	-0.355
213	-2.406	-4.837	-2.432	-2.282	-4.757	-2.475	-2.539	-2.962	-0.423
212	-2.372	-5.073	-2.701	-2.297	-4.829	-2.532	-2.633	-3.002	-0.369
211	-2.426	-5.106	-2.680	-2.286	-4.905	-2.620	-2.733	-3.065	-0.331
210	-2.442	-4.993	-2.551	-2.290	-4.855	-2.566	-2.804	-3.276	-0.472
209	-2.439	-4.925	-2.486	-2.190	-4.717	-2.527	-2.730	-3.404	-0.674
208	-2.360	-4.722	-2.362	-2.243	-4.348	-2.105	-2.614	-3.369	-0.755
207	-2.324	-4.195	-1.871	-2.199	-3.885	-1.686	-2.543	-3.100	-0.557
206	-2.280	-3.700	-1.420	-2.198	-3.189	-0.992	-2.503	-2.823	-0.320
205	-2.182	-2.694	-0.513	-2.312	-2.392	-0.079	-2.481	-2.450	0.031
204	-2.140	-1.773	0.367	-2.077	-1.419	0.658	-2.523	-1.877	0.646
203	-1.648	-0.591	1.057	-1.920	-0.338	1.582	-2.412	-1.001	1.410
202	-1.451	0.756	2.207	-1.741	0.723	2.464	-2.450	-0.486	1.964
201	-1.314	2.866	4.181	-1.459	1.564	3.024	-2.036	0.599	2.635
200	-0.918	2.482	3.399	-0.865	3.549	4.414	-1.438	2.397	3.836

A.2 UV Denaturation Analysis: Supplied by Darnell Graham, NCSU Biochemistry Depart.

Experiment	[RNA] (M)	[Peptide] (M)	ΔH (kcal/mol)	ΔS (cal/K*mol)	ΔG (kcal/mol, 37°)	Tm (°C)
bTAR	8.78E-07	1.32E-05	-22.16	-67.25	-1.3	56.39
bTAR	8.72E-07	1.31E-05	-21.46	-65.51	-1.14	54.46
bTAR	7.08E-07	1.06E-05	-21.01	-63.28	-1.39	58.93
bTAR	8.79E-07	1.32E-05	-19.08	-58.52	-0.93	52.84
bTAR	8.96E-07	1.34E-05	-26.04	-80.2	-1.17	51.57
		Averages:	-21.95	-66.95	-1.19	54.84
		Standard deviation:	2.56	8.10	0.18	2.91

Experiment	[RNA] (M)	[Peptide] (M)	ΔH (kcal/mol)	ΔS (cal/K*mol)	ΔG (kcal/mol, 37°)	Tm (°C)
bTAR / P1	1.38E-06	2.08E-05	-32.22	-98.37	-1.1	54.36
bTAR / P1	1.39E-06	2.08E-05	-59.56	-178.23	-4.28	61.02
bTAR / P1	1.38E-06	2.07E-05	-54.39	-165.62	-3.05	55.24
bTAR / P1	1.42E-06	2.12E-05	-18.78	-56.63	-1.22	58.49
bTAR / P1	1.42E-06	2.14E-05	-41.61	-126.9	-2.26	54.78
bTAR / P1	1.42E-06	2.13E-05	-21.33	-64.7	-1.27	56.57
		Averages:	-37.98	-115.08	-2.20	56.74
		Standard deviation:	16.89	50.82	1.27	2.58

Experiment	[RNA] (M)	[Peptide] (M)	ΔH (kcal/mol)	ΔS (cal/K*mol)	ΔG (kcal/mol, 37°)	Tm (°C)
bTAR / P2	1.37E-06	2.05E-05	-32.18	-97.68	-1.89	56.35
bTAR / P2	1.41E-06	2.12E-05	-43.17	-131.23	-2.47	55.79
bTAR / P2	1.40E-06	2.10E-05	-36.42	-109.92	-2.33	58.23
bTAR / P2	1.41E-06	2.11E-05	-31.91	-96.46	-1.99	57.67
bTAR / P2	1.40E-06	2.11E-05	-79.35	-241.87	-4.33	54.91
bTAR / P2	1.40E-06	2.10E-05	-48.16	-145.51	-3.03	57.79
		Averages:	-45.20	-137.11	-2.67	56.79
		Standard deviation:	17.90	54.82	0.91	1.31

Experiment	[RNA] (M)	[Peptide] (M)	ΔH (kcal/mol)	ΔS (cal/K*mol)	ΔG (kcal/mol, 37°)	Tm (°C)
bTAR / P3	1.04E-06	1.55E-05	-37.59	-114.79	-1.99	54.34
bTAR / P3	1.05E-06	1.58E-05	-34.16	-104.48	-1.76	53.85
bTAR / P3	1.05E-06	1.58E-05	-25.2	-46.65	-1.43	55.66
bTAR / P3	1.04E-06	1.57E-05	-68.36	-208.1	-3.82	55.35
bTAR / P3	1.05E-06	1.57E-05	-22.25	-66.89	-1.5	59.47
bTAR / P3	1.07E-06	1.60E-05	-26.52	-81.06	-1.38	54.04
bTAR / P3	1.06E-06	1.59E-05	-21.05	-63.25	-1.44	59.71
		Averages:	-33.59	-97.89	-1.90	56.06
		Standard deviation:	16.49	54.08	0.87	2.50

A.3 General Equation Used in the Fluorescence Quenching Analysis

$F_{ratio} = F_{obs}/F_o = 1\text{-}\Phi\ [((K_d + nP_0\ + L_T) – ((K_d + nP_o + L_T)^2 – (4nP_o{*}\ L_T))^{1/2}) / 2nP_o]$

Φ = Fluorescence Ratio Δ Amplitude (= $1\text{-}F^{\infty}{}_{ratio}$)
K_d = Dissociation Constant
n = Stoichiometry (assume = 1 at low concentration)
L_T = Ligand Concentration (RNA)
P_o = Peptide Concentration

Fitting Program : Kaleidagraph
Equation as entered:

```
1-(m1*((m2+(1*C2)+m0)-(sqrt(((m2+(1*C2)+m0)^2)-
(4*1*C2*m0))))/(2*1*C2));m1=1;m2=5e-6
```

m1 = Φ - starting value given as 1
m2 = Kd – starting value given as 5 μM
m3 = n – set to 1
m4 =[P] – referenced column of data points that took into account dilution factor.

A.4 Fluorescence Quenching Data: **P2** / bTAR RNA

"quant. uM"	Titration point	Vol Total uL	amt. Peptide pmol	Conc. Peptide uM	Vol. RNA uL	Conc. RNA added uM	amt. RNA sample pmol	Conc. RNA sample uM	Emission BG-corr	Emission max diluttion corr.	Avg. # readings per titration point	Emission max photobleach corr.	Emission Rati
	MAX	700	1115.000	1.593				0	40888.37667	40888.64	2	40816.77686	1.00175418
	T1	710	1115.000	1.570	10	25.36	253.6	0.357	38325.54333	40312.75	5	40133.08148	0.95496139
25	T2	720	1115.000	1.549	10	25.36	507.2	0.704	36012.17667	39752.85	8	39465.38322	0.91250037
	T3	730	1115.000	1.527	10	25.36	760.8	1.042	34548.87667	39208.29	11	38813.02467	0.89013616
	T4	740	1115.000	1.507	10	25.36	1014.4	1.371	33315.84333	38678.45	14	38175.38395	0.87270487
50	T5	750	1115.000	1.487	10	50.72	1521.6	2.029	30985.77667	38162.73	17	37551.87233	0.82514598
	T6	760	1115.000	1.467	10	50.72	2028.8	2.669	29436.11	37660.59	20	36941.93211	0.79682107
	T7	770	1115.000	1.448	10	91.3	2941.8	3.821	26052.27667	37171.49	23	36345.03451	0.71680429
90	T8	780	1115.000	1.429	10	91.3	3854.8	4.942	23237.71	36694.94	26	35760.6779	0.64981179
	T9	790	1115.000	1.411	9.7	91.3	4740.41	6.001	21024.77667	36230.44	29	35188.38604	0.59749193
200	T10	795	1115.000	1.403	5	217.86	5829.71	7.333	19028.01	36002.58	32	34852.72262	0.54595477
	T11	800	1115.000	1.394	5	217.86	6919.01	8.649	17371.81	35777.56	35	34519.9075	0.50324034

Photobleaching Correction

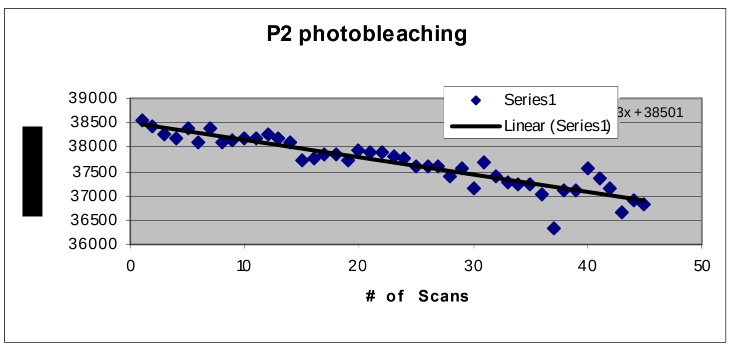

Quenching Profile and Fitted Data

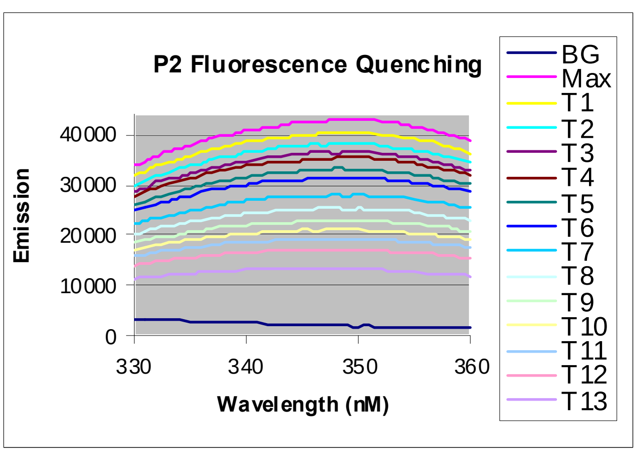

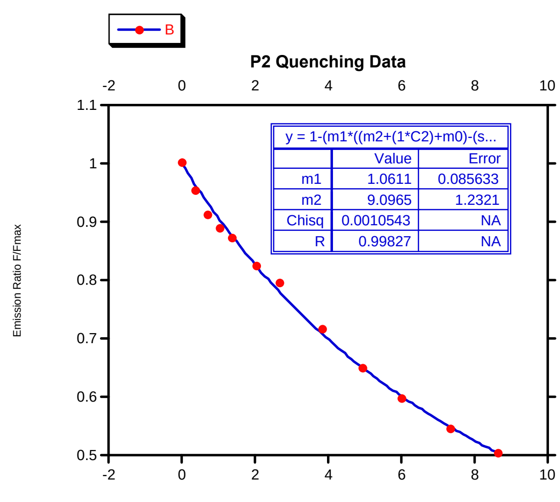

A.5 Fluorescence Quenching Data: **P1** / bTAR RNA

"quant. uM"	Titration point	Vol Total uL	amt. Peptide pmol	Conc. Peptide uM	Vol. RNA uL	Conc. RNA added uM	amt. RNA sample pmol	Conc. RNA sample uM	Emission BG-corr	Emission max dilution corr.	Avg. # readings per titration point
	MAX	700	522.000	0.746	10	0		0	32646.26	32633.94857	0
25	T1	710	522.000	0.735	10	25.36	253.600	0.357	30952.52	32174.31549	2
25	T2	720	522.000	0.725	10	25.36	507.200	0.704	28921.22	31727.45	5
25	T3	730	522.000	0.715	10	25.36	760.800	1.042	27693.79	31292.8274	8
25	T4	740	522.000	0.705	10	25.36	1014.400	1.371	25427.16	30869.95135	11
50	T5	750	522.000	0.696	10	50.72	1521.600	2.029	24175.26	30458.352	14
50	T6	760	522.000	0.687	10	50.72	2028.800	2.669	22570.66	30057.58421	17
100	T7	770	522.000	0.678	10	91.3	2941.800	3.821	19986.39	29667.22597	20
100	T8	780	522.000	0.669	10	91.3	3854.800	4.942	17806.02	29286.87692	23
100	T9	790	522.000	0.661	10	91.3	4767.800	6.035	16095.39	28916.15696	26
200	T10	795	522.000	0.657	5	217.86	5857.100	7.367	15062.09	28734.29434	29
200	T11	800	522.000	0.653	5	217.86	6946.400	8.683	13692.26	28554.705	32
400	T12	805	522.000	0.648	5	435.73	9125.050	11.335	11498.19	28377.34658	35
400	T13	810	522.000	0.644	5	435.73	11303.700	13.955	9822.39	28202.17778	38

Photobleaching Correction:

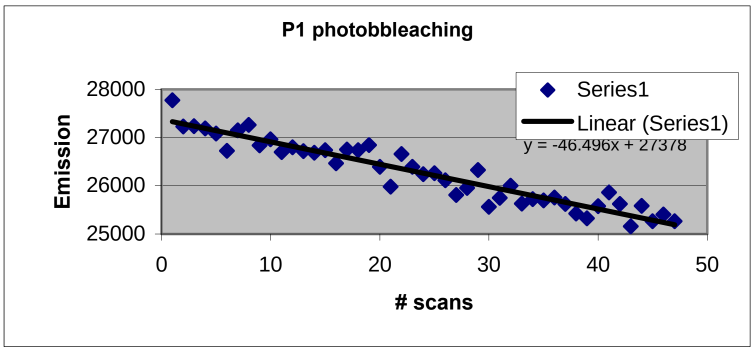

Quenching Profile and Fitted Data

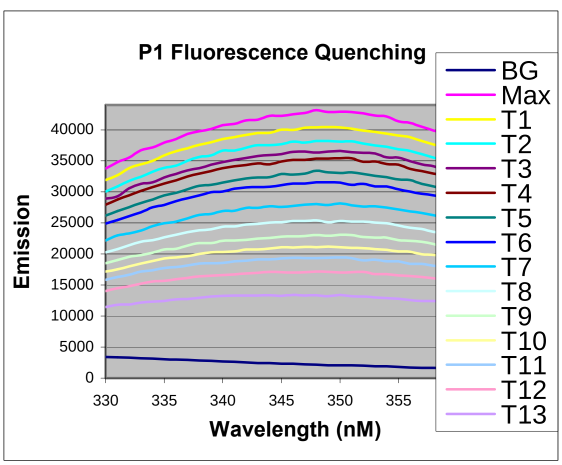

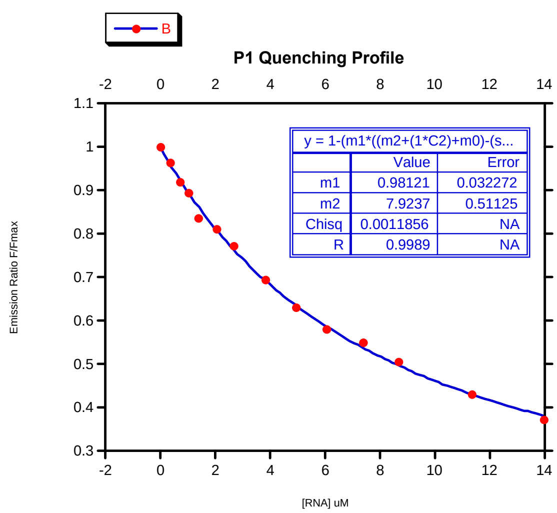

A.6 Competitive Quenching Data: **P1**$_1$

P1 C=C Competitive Quenching Data

Wavelength	smooth BG	smooth Max	smooth TK	Smooth Tat
333	4509.87667	52481.9667	51565.4667	50841.8333
334	4443.76333	53788.7667	52845.5	51991.7
335	4341.45	55073.5	54105.3	53143.9667
336	4257.33333	56278.5667	55282.2	54233.7667
337	4170.10667	57409.4	56244.2667	55240.6667
338	4094.58	58418.5667	57162.8333	56093.1667
339	4018.57333	59335.7	58057.9333	56869.0333
340	3961.83667	60086.3667	58949.4333	57657.8
341	3879.77667	60811.4667	59718	58436.6
342	3811.99	61511.5333	60464.2667	59191
343	3711.45667	62121.1333	60949.4333	59834.3
344	3628.83667	62616.6	61389.8667	60277.7333
345	3551.8	63093.3	61945.2	60627.2
346	3508.34	63512.4333	62341.5	60978.9333
347	3465.62	63916	62651.1667	61196
348	3445.41333	64183.2667	62880.4	61481.1667
349	3418.07667	64446.3	63001.2333	61747.2333
350	3384.57333	64501.4667	63020.2333	61855.3667
351	3341.25667	64420.1667	62982.9667	61857.4
352	3301.34333	64179.2333	62776.5	61711.1333
353	3248.20333	63824.8	62486.1667	61448.9
354	3193.25667	63450.9333	62094.7667	61045.0667
355	3119.13	63059.7333	61748.0333	60616.3333
356	3036.58667	62450.5	61305.8	59936.9333
357	2970.51	61702.9	60778.5	59299.2667

Wavelength	smooth BG	smooth Max	smooth TAR	Smooth Tat
333	4507.40667	52090.9333	22726.5	22644.7
334	4408.90667	53379.2667	23169.1	23094.5333
335	4324.77333	54574.7667	23622.7	23493.5667
336	4249.17333	55659.6333	24067.1667	23913.3333
337	4165.41667	56717.4	24421.7	24203.4
338	4088.88667	57567.6	24757.8667	24518.0333
339	4032.51	58341.6	25033.1667	24875.3333
340	3918.51	59122.6667	25241.2333	25203.0333
341	3828.19667	59768.8333	25477.1667	25439.4333
342	3754.98333	60509.7	25701.6667	25683.8
343	3686.45333	61133.1	25868.8333	25823.6
344	3608.85667	61699.1667	26071.9333	25973.1333
345	3550.61	62218.4	26225.5	26087.8333
346	3492.08667	62664.1667	26361.7	26199.5333
347	3451.79	63024.1667	26399.6333	26229.1667
348	3425.56667	63384.7	26427.6	26315.6333
349	3395.4	63413.0333	26421.1	26309.5
350	3350.24	63458.6	26454.4667	26307.5667
351	3302.26667	63347.6333	26407.2	26259.0333
352	3264.02667	63201.7333	26322.5667	26232.1667
353	3205.83333	63071.1	26205.0667	26011.5333
354	3149.16667	62776.1667	25976.3	25823.1
355	3074.74	62202.5	25750.0667	25572.7
356	3005.10667	61622.4333	25528.6333	25318.4667
357	2930.18333	60806.3	25224.4667	25049.2667

BG correction

Wavelength	smooth Max	smooth TK	Smooth Tat
333	48026.2067	47109.7067	46386.0733
334	49333.0067	48389.74	47535.94
335	50617.74	49649.54	48688.2067
336	51822.8067	50826.44	49778.0067
337	52953.64	51788.5067	50784.9067
338	53962.8067	52707.0733	51637.4067
339	54879.94	53602.1733	52413.2733
340	55630.6067	54493.6733	53202.04
341	56355.7067	55262.24	53980.84
342	57055.7733	56008.5067	54735.24
343	57665.3733	56493.6733	55378.54
344	58160.84	56934.1067	55821.9733
345	58637.54	57489.44	56171.44
346	59056.6733	57885.74	56523.1733
347	59460.24	58195.4067	56740.24
348	59727.5067	58424.64	57025.4067
349	59990.54	58545.4733	57291.4733
350	60045.7067	58564.4733	57399.6067
351	59964.4067	58527.2067	57401.64
352	59723.4733	58320.74	57255.3733
353	59369.04	58030.4067	56993.14
354	58995.1733	57639.0067	56589.3067
355	58603.9733	57292.2733	56160.5733
356	57994.74	56850.04	55481.1733
357	57247.14	56322.74	54843.5067

Wavelength	smooth Max	smooth TAR	Smooth Tat
333	47872.2567	18507.8233	18426.0233
334	49160.59	18950.4233	18875.8567
335	50356.09	19404.0233	19274.89
336	51440.9567	19848.49	19694.6567
337	52498.7233	20203.0233	19984.7233
338	53348.9233	20539.19	20299.3567
339	54122.9233	20814.49	20656.6567
340	54903.99	21022.5567	20984.3567
341	55550.1567	21258.49	21220.7567
342	56291.0233	21482.99	21465.1233
343	56914.4233	21650.1567	21604.9233
344	57480.49	21853.2567	21754.4567
345	57999.7233	22006.8233	21869.1567
346	58445.49	22143.0233	21980.8567
347	58805.49	22180.9567	22010.49
348	59166.0233	22208.9233	22096.9567
349	59194.3567	22202.4233	22090.8233
350	59239.9233	22235.79	22088.89
351	59128.9567	22188.5233	22040.3567
352	58983.0567	22103.89	22013.49
353	58852.4233	21986.39	21792.8567
354	58557.49	21757.6233	21604.4233
355	57983.8233	21531.39	21354.0233
356	57403.7567	21309.9567	21099.79
357	56587.6233	21005.79	20830.59

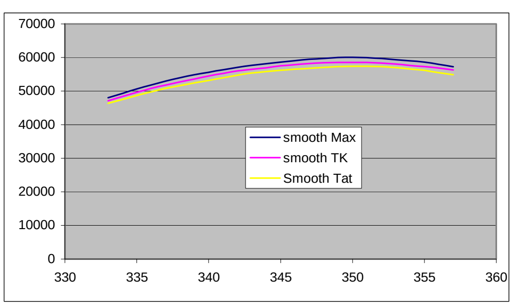

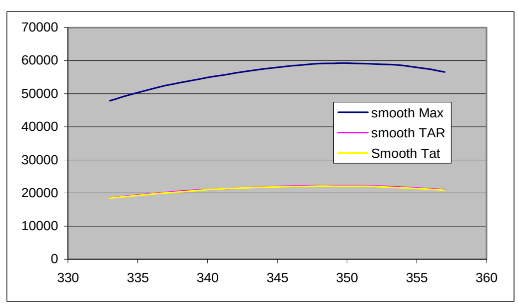

A.7 Competitive Fluorescence Quenching Data: **P2$_1$**

P2 C=C Competitive Quenching Data

Wavelength	smooth BG	smooth Max	smooth TK	Smooth Tat
333	4419.11667	36452.0667	35156.6667	34672.0667
334	4359.18667	37263.9667	35894.0667	35310.7333
335	4267.48667	38136.9	36644.4	35902.3667
336	4182.82333	38810.7667	37307.2667	36535.8333
337	4098.70333	39481.4	38006.6	37077.5333
338	4009.58667	40064.0333	38634.1667	37665.8667
339	3947.72667	40589.5	39096.8333	38091.6
340	3853.92	40989.6333	39534.6	38532.4667
341	3758.17	41439.7667	39943.0333	38952.1667
342	3687.48333	41885.4333	40308.1	39300.5
343	3624.78	42270.2	40708.7667	39598.8
344	3553.16667	42631.3667	40998.6333	39862.0667
345	3515.62333	42904.1	41187.2333	40027.0667
346	3471.92	43080.7333	41404	40254.7
347	3428.55667	43230.2333	41499.5	40477.9333
348	3395.19333	43345.6667	41643.9	40535.3333
349	3349.67	43446.3333	41800.0333	40540.1333
350	3282.88667	43455.5	41893.5333	40580.3667
351	3223.56333	43381.4333	41844.6667	40525.5
352	3183.33333	43290.7333	41707.2333	40465.1333
353	3139.76333	43031	41394.7	40282.0333
354	3080.16333	42565.3333	41054.9	39912.8667
355	3020.63667	42171.0667	40665.5	39507.0333
356	2947.22333	41612.3667	40243.4333	39159.0333
357	2891.57333	41160.9667	39795.6333	38678.3333

Wavelength	smooth BG	smooth Max	smooth TAR	Smooth Tat
333	4160.26333	36733.5667	16711.5667	16595.4
334	4098.33	37627.2333	17020.8667	16836.2667
335	4048.22333	38392.9333	17330.1	17076.4
336	3992.20333	39118.9333	17568.6333	17267.4667
337	3931.69667	39779.9	17760.4	17473.1
338	3883.62667	40312.1	17946.5333	17608.9
339	3814.47	40882.8	18117.0333	17769.9333
340	3736.39	41409.1667	18302.0667	17874.2333
341	3657.73667	41838.6	18474.9	18045.7333
342	3569.93	42182.3	18608.8667	18157.9667
343	3475.86667	42512.6333	18698.8333	18261.8667
344	3410.94	42770.9333	18813.3333	18307.6
345	3359.51	43093.8667	18901.5667	18393.9667
346	3294.3	43415.8333	18873.9333	18450.7333
347	3240.67	43654.8	18850.5333	18512.9
348	3208.06	43778.2667	18833.8	18505.5333
349	3159.78333	43801.5333	18812.3	18491.4333
350	3127.42667	43809.8667	18868.1667	18434.3333
351	3105.31333	43783.9333	18839.4	18365.2667
352	3053.67667	43665.2	18731.1333	18222.2333
353	2989.19	43451.6667	18596	18096.8667
354	2918.43	43033.9	18453.6333	17921.1667
355	2862.51667	42522.5667	18212.3667	17745.1667
356	2804.49333	42111.1333	17936.3	17593.4
357	2765.13333	41675.7	17717.3	17361.7

BG correction

Wavelength	smooth Max	smooth TK	Smooth Tat
333	31996.3067	30700.9067	30216.3067
334	32808.2067	31438.3067	30854.9733
335	33681.14	32188.64	31446.6067
336	34355.0067	32851.5067	32080.0733
337	35025.64	33550.84	32621.7733
338	35608.2733	34178.4067	33210.1067
339	36133.74	34641.0733	33635.84
340	36533.8733	35078.84	34076.7067
341	36984.0067	35487.2733	34496.4067
342	37429.6733	35852.34	34844.74
343	37814.44	36253.0067	35143.04
344	38175.6067	36542.8733	35406.3067
345	38448.34	36731.4733	35571.3067
346	38624.9733	36948.24	35798.94
347	38774.4733	37043.74	36022.1733
348	38889.9067	37188.14	36079.5733
349	38990.5733	37344.2733	36084.3733
350	38999.74	37437.7733	36124.6067
351	38925.6733	37388.9067	36069.74
352	38834.9733	37251.4733	36009.3733
353	38575.24	36938.94	35826.2733
354	38109.5733	36599.14	35457.1067
355	37715.3067	36209.74	35051.2733
356	37156.6067	35787.6733	34703.2733
357	36705.2067	35339.8733	34222.5733

Wavelength	smooth Max	smooth TAR	Smooth Tat
333	32514.89	12492.89	12376.7233
334	33408.5567	12802.19	12617.59
335	34174.2567	13111.4233	12857.7233
336	34900.2567	13349.9567	13048.79
337	35561.2233	13541.7233	13254.4233
338	36093.4233	13727.8567	13390.2233
339	36664.1233	13898.3567	13551.2567
340	37190.49	14083.39	13655.5567
341	37619.9233	14256.2233	13827.0567
342	37963.6233	14390.19	13939.29
343	38293.9567	14480.1567	14043.19
344	38552.2567	14594.6567	14088.9233
345	38875.19	14682.89	14175.29
346	39197.1567	14655.2567	14232.0567
347	39436.1233	14631.8567	14294.2233
348	39559.59	14615.1233	14286.8567
349	39582.8567	14593.6233	14272.7567
350	39591.19	14649.49	14215.6567
351	39565.2567	14620.7233	14146.59
352	39446.5233	14512.4567	14003.5567
353	39232.99	14377.3233	13878.19
354	38815.2233	14234.9567	13702.49
355	38303.89	13993.69	13526.49
356	37892.4567	13717.6233	13374.7233
357	37457.0233	13498.6233	13143.0233

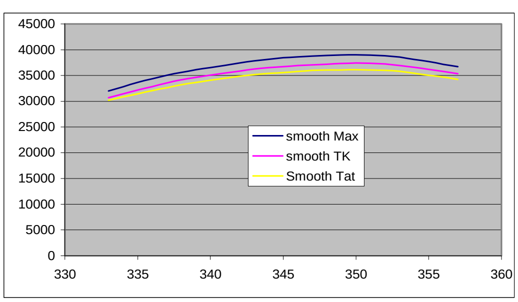

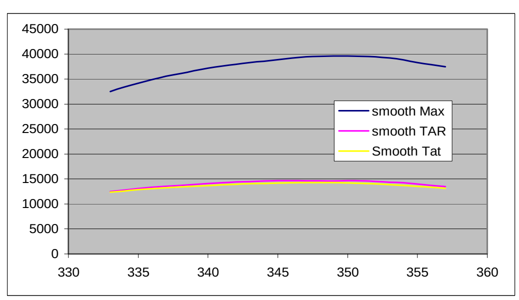

A.8 Competitive Fluorescence Quenching Data: $\mathbf{P2_2}$

P2 C-C Competitive Quenching Data

Wavelength	smooth BG	smooth Max	smooth TK	Smooth Tat
333	4455.76	22712.2	22156.3333	22742.5333
334	4371.80333	23190.5333	22624.1	23104.6
335	4306.21	23590.7333	22986.6333	23524.9333
336	4214.38333	23994.9667	23336.2333	23878.9333
337	4135.97333	24291.7667	23666.1333	24221.2
338	4034.07	24585.5333	23984	24458.6667
339	3974.73667	24941.6667	24298.8667	24707.8333
340	3915.85	25181.6	24584	24944.2333
341	3851.43333	25348.6667	24786.3333	25161.8
342	3765.91333	25496.9667	24968.1	25319.3333
343	3676.08667	25617.3	25145.1	25470.8
344	3581.73	25819.4	25288.1667	25552.6667
345	3532.09667	26092.5667	25480.3667	25694.7
346	3486.23333	26232.6667	25624.1667	25829.9333
347	3436.38	26360.3333	25695.4	25899.3667
348	3397.58	26316.4	25756.0333	25974
349	3366.47667	26265.9333	25754.4667	25995.4667
350	3306.06667	26268.4	25774.2667	25967.7667
351	3265.96667	26226.7667	25760.7333	25920.1667
352	3196.37333	26153.9667	25667.2667	25827.4
353	3125.03	26042.5333	25551.2	25680.5
354	3082.46667	25775.3333	25416.6	25450.1
355	3046.74333	25537.4333	25152.2667	25200.2
356	2989.17333	25268.0667	24895.1333	24927.3333
357	2927.66667	24996.8333	24569.1667	24617.0333

Wavelength	smooth BG	smooth Max	smooth TAR	Smooth Tat
333	4218.67667	21952.5667	10716	10551.7333
334	4141.20333	22376.9333	10781.1667	10622.6333
335	4072.61333	22782.7	10840.2667	10705.7
336	4013.8	23136	10926.4667	10795.1333
337	3953.40667	23443.5	11029.3	10886.5
338	3887.27	23788.9667	11135.1	10934.3
339	3804.69	24092.1	11183.7667	10972.6
340	3728.58333	24367.8667	11224.3667	10997.6
341	3649.73333	24551.4667	11230.5667	10991.6
342	3573.82667	24722.1	11233	10974.8
343	3509.16333	24870.4	11216.3	10950.2333
344	3448.37	25044.7333	11249.6	10952.4667
345	3380.28	25206.8333	11246.9667	10974.1
346	3318.18333	25386.2667	11274.1333	11000.3667
347	3269.08667	25503.9	11245.7	11014.8
348	3227.13667	25545.6333	11232.2	11008.9
349	3202.38333	25513	11211.3	10932.3
350	3160.59333	25506.2333	11157.4333	10899.7667
351	3107.11	25429.6667	11079	10869.1333
352	3050.87667	25378.3	11009.5333	10803.2
353	2976.95333	25214.3667	10908.1333	10704.1333
354	2919.92333	24993.3	10804.6333	10595.8667
355	2860.41667	24747	10688.1667	10435.7667
356	2797.12	24526.7333	10561.1333	10280.8
357	2735.79	24221.2667	10422.9333	10159.3667

BG correction

Wavelength	smooth Max	smooth TK	Smooth Tat
333	18256.44	17700.5733	18286.7733
334	18734.7733	18168.34	18648.84
335	19134.9733	18530.8733	19069.1733
336	19539.2067	18880.4733	19423.1733
337	19836.0067	19210.3733	19765.44
338	20129.7733	19528.24	20002.9067
339	20485.9067	19843.1067	20252.0733
340	20725.84	20128.24	20488.4733
341	20892.9067	20330.5733	20706.04
342	21041.2067	20512.34	20863.5733
343	21161.54	20689.34	21015.04
344	21363.64	20832.4067	21096.9067
345	21636.8067	21024.6067	21238.94
346	21776.9067	21168.4067	21374.1733
347	21904.5733	21239.64	21443.6067
348	21860.64	21300.2733	21518.24
349	21810.1733	21298.7067	21539.7067
350	21812.64	21318.5067	21512.0067
351	21771.0067	21304.9733	21464.4067
352	21698.2067	21211.5067	21371.64
353	21586.7733	21095.44	21224.74
354	21319.5733	20960.84	20994.34
355	21081.6733	20696.5067	20744.44
356	20812.3067	20439.3733	20471.5733
357	20541.0733	20113.4067	20161.2733

Wavelength	smooth Max	smooth TAR	Smooth Tat
333	17733.89	6497.32333	6333.05667
334	18158.2567	6562.49	6403.95667
335	18564.0233	6621.59	6487.02333
336	18917.3233	6707.79	6576.45667
337	19224.8233	6810.62333	6667.82333
338	19570.29	6916.42333	6715.62333
339	19873.4233	6965.09	6753.92333
340	20149.19	7005.69	6778.92333
341	20332.79	7011.89	6772.92333
342	20503.4233	7014.32333	6756.12333
343	20651.7233	6997.62333	6731.55667
344	20826.0567	7030.92333	6733.79
345	20988.1567	7028.29	6755.42333
346	21167.59	7055.45667	6781.69
347	21285.2233	7027.02333	6796.12333
348	21326.9567	7013.52333	6790.22333
349	21294.3233	6992.62333	6713.62333
350	21287.5567	6938.75667	6681.09
351	21210.99	6860.32333	6650.45667
352	21159.6233	6790.85667	6584.52333
353	20995.69	6689.45667	6485.45667
354	20774.6233	6585.95667	6377.19
355	20528.3233	6469.49	6217.09
356	20308.0567	6342.45667	6062.12333
357	20002.59	6204.25667	5940.69

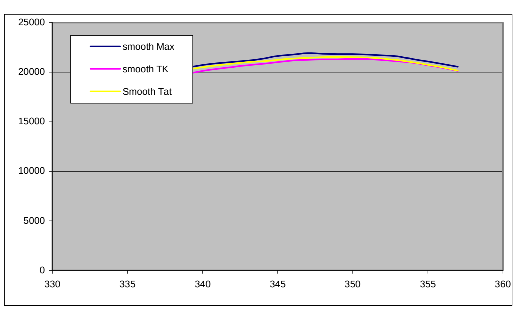

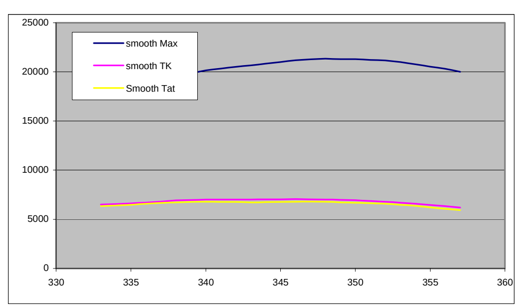

A.9. CD bTAR Binding Study

CD - bTAR Binding Study : all samples at 4 degrees Celsius

wavelenth	TK	bTAR	bTAR-TK	bTat	bTAR/bTat	bTAR/bTat - bTat	P1-1	bTAR/P1-1	bTAR/P1-1 - P1-1	P2-1	bTAR/P2-1	bTAR/P2-1 - P2-1	P2-2	bTAR/P2-2	bTAR/P2-2 - P2-2
300	1.380	1.151	-0.229	1.49172	1.18008	-0.312	1.280	1.183	-0.097	1.269	1.289	0.021	1.437	1.400	-0.036
299	1.352	1.094	-0.258	1.44806	1.02856	-0.420	1.284	1.191	-0.093	1.191	1.286	0.096	1.416	1.424	0.008
298	1.337	1.174	-0.163	1.46075	0.985625	-0.475	1.320	1.204	-0.115	1.255	1.298	0.043	1.450	1.402	-0.048
297	1.360	1.204	-0.157	1.49634	1.00897	-0.487	1.340	1.232	-0.109	1.243	1.319	0.076	1.426	1.405	-0.020
296	1.371	1.186	-0.184	1.48832	1.06776	-0.421	1.320	1.235	-0.085	1.244	1.371	0.128	1.390	1.427	0.037
295	1.361	1.188	-0.173	1.47366	1.13466	-0.339	1.289	1.269	-0.020	1.230	1.398	0.168	1.360	1.461	0.101
294	1.357	1.230	-0.127	1.46885	1.19431	-0.275	1.256	1.316	0.060	1.203	1.448	0.245	1.341	1.493	0.152
293	1.354	1.269	-0.086	1.44041	1.23824	-0.202	1.220	1.380	0.160	1.169	1.496	0.327	1.324	1.543	0.219
292	1.335	1.349	0.013	1.41751	1.26647	-0.151	1.194	1.433	0.238	1.150	1.558	0.408	1.331	1.602	0.271
291	1.311	1.431	0.120	1.3899	1.29007	-0.100	1.171	1.522	0.351	1.132	1.626	0.494	1.336	1.663	0.327
290	1.295	1.539	0.245	1.37666	1.34957	-0.027	1.155	1.609	0.453	1.113	1.716	0.603	1.341	1.744	0.402
289	1.263	1.623	0.360	1.36662	1.42309	0.056	1.136	1.684	0.548	1.113	1.793	0.680	1.320	1.834	0.514
288	1.229	1.698	0.468	1.34295	1.51973	0.177	1.123	1.769	0.645	1.107	1.890	0.783	1.298	1.934	0.636
287	1.199	1.776	0.578	1.33488	1.61369	0.279	1.105	1.864	0.759	1.090	2.002	0.912	1.267	2.042	0.774
286	1.166	1.882	0.715	1.32102	1.71114	0.390	1.088	1.965	0.877	1.073	2.092	1.018	1.227	2.155	0.928
285	1.128	2.000	0.872	1.29261	1.78851	0.496	1.064	2.096	1.032	1.054	2.208	1.154	1.216	2.268	1.051
284	1.103	2.138	1.035	1.28667	1.86038	0.574	1.047	2.216	1.169	1.013	2.317	1.304	1.201	2.389	1.188
283	1.090	2.264	1.174	1.25274	1.9432	0.690	1.030	2.333	1.303	1.001	2.432	1.431	1.183	2.502	1.319
282	1.067	2.388	1.321	1.23075	2.04891	0.818	1.011	2.450	1.438	0.979	2.555	1.576	1.162	2.615	1.452
281	1.040	2.504	1.464	1.20433	2.15832	0.954	0.982	2.601	1.619	0.963	2.684	1.721	1.149	2.734	1.585
280	1.030	2.624	1.594	1.19806	2.30715	1.109	0.945	2.735	1.790	0.937	2.837	1.900	1.120	2.869	1.748
279	0.999	2.746	1.747	1.18159	2.44192	1.260	0.920	2.886	1.966	0.923	2.979	2.057	1.101	3.013	1.912
278	0.966	2.879	1.914	1.15629	2.58883	1.433	0.902	3.045	2.142	0.888	3.133	2.245	1.079	3.195	2.116
277	0.942	3.024	2.082	1.13266	2.72438	1.592	0.890	3.205	2.315	0.856	3.293	2.437	1.050	3.363	2.313
276	0.920	3.185	2.266	1.10199	2.85598	1.754	0.870	3.340	2.470	0.853	3.451	2.598	1.014	3.529	2.515
275	0.888	3.331	2.442	1.07773	2.99636	1.919	0.853	3.485	2.632	0.841	3.586	2.746	1.012	3.689	2.677
274	0.853	3.464	2.611	1.06799	3.1235	2.056	0.846	3.606	2.759	0.830	3.702	2.873	0.989	3.838	2.849
273	0.822	3.555	2.733	1.03664	3.23103	2.194	0.819	3.706	2.887	0.826	3.806	2.980	0.964	3.944	2.980
272	0.804	3.610	2.806	1.00817	3.3227	2.315	0.812	3.811	2.999	0.820	3.884	3.064	0.941	4.012	3.071
271	0.773	3.645	2.872	0.987902	3.38277	2.395	0.792	3.881	3.089	0.804	3.933	3.129	0.943	4.052	3.110
270	0.760	3.671	2.912	0.971914	3.41162	2.440	0.773	3.926	3.153	0.784	3.978	3.193	0.941	4.069	3.128
269	0.741	3.676	2.935	0.946153	3.42093	2.475	0.777	3.954	3.177	0.778	3.989	3.211	0.942	4.069	3.127
268	0.735	3.632	2.897	0.915295	3.419	2.504	0.769	3.938	3.169	0.752	3.969	3.217	0.927	4.044	3.117
267	0.721	3.567	2.846	0.885135	3.362	2.477	0.753	3.874	3.121	0.749	3.902	3.153	0.912	3.979	3.067
266	0.714	3.484	2.770	0.895105	3.28892	2.394	0.738	3.770	3.032	0.745	3.827	3.082	0.880	3.886	3.006
265	0.693	3.375	2.681	0.916101	3.20797	2.292	0.726	3.640	2.914	0.727	3.689	2.962	0.874	3.769	2.895
264	0.673	3.230	2.557	0.8929	3.08283	2.190	0.726	3.453	2.727	0.709	3.538	2.829	0.875	3.601	2.725
263	0.690	3.058	2.368	0.877902	2.95933	2.081	0.716	3.245	2.529	0.703	3.352	2.649	0.876	3.405	2.529
262	0.701	2.855	2.154	0.857554	2.81439	1.957	0.719	3.030	2.311	0.703	3.165	2.462	0.862	3.212	2.350
261	0.692	2.643	1.951	0.842764	2.63973	1.797	0.685	2.781	2.096	0.703	2.930	2.226	0.836	2.997	2.161
260	0.678	2.461	1.783	0.806632	2.43874	1.632	0.651	2.546	1.895	0.680	2.687	2.007	0.800	2.754	1.954
259	0.672	2.260	1.588	0.758364	2.23382	1.475	0.624	2.321	1.697	0.646	2.458	1.812	0.760	2.535	1.774
258	0.646	2.015	1.369	0.724636	2.02808	1.303	0.586	2.116	1.530	0.613	2.209	1.595	0.737	2.288	1.551
257	0.606	1.836	1.230	0.68308	1.79557	1.112	0.528	1.907	1.379	0.620	1.969	1.349	0.696	2.048	1.352
256	0.592	1.623	1.031	0.687361	1.5918	0.904	0.498	1.716	1.218	0.583	1.737	1.154	0.625	1.818	1.193
255	0.557	1.407	0.849	0.676955	1.39472	0.718	0.478	1.521	1.043	0.558	1.523	0.965	0.580	1.605	1.025
254	0.529	1.214	0.684	0.646491	1.23059	0.584	0.477	1.318	0.840	0.511	1.323	0.812	0.545	1.392	0.847
253	0.549	1.040	0.491	0.616417	1.09195	0.476	0.448	1.146	0.697	0.499	1.176	0.677	0.510	1.199	0.689
252	0.524	0.879	0.355	0.591331	0.958734	0.367	0.410	1.017	0.607	0.477	1.047	0.570	0.467	1.042	0.575
251	0.501	0.730	0.229	0.555944	0.819907	0.264	0.352	0.870	0.518	0.437	0.890	0.453	0.418	0.875	0.457
250	0.471	0.637	0.166	0.524304	0.69078	0.166	0.293	0.739	0.446	0.363	0.737	0.374	0.380	0.718	0.337
249	0.446	0.519	0.072	0.477442	0.531412	0.054	0.250	0.618	0.368	0.331	0.629	0.297	0.382	0.595	0.213
248	0.401	0.406	0.005	0.420195	0.379176	-0.041	0.189	0.506	0.317	0.292	0.524	0.232	0.388	0.466	0.079
247	0.361	0.329	-0.032	0.360294	0.243646	-0.117	0.143	0.364	0.221	0.292	0.430	0.138	0.384	0.331	-0.053
246	0.334	0.211	-0.123	0.348246	0.123354	-0.225	0.140	0.257	0.117	0.265	0.311	0.047	0.363	0.221	-0.142
245	0.315	0.128	-0.187	0.32232	0.0176292	-0.305	0.118	0.138	0.021	0.229	0.217	-0.012	0.345	0.127	-0.219
244	0.295	0.057	-0.238	0.28856	-0.0850855	-0.374	0.073	0.024	-0.049	0.195	0.097	-0.098	0.301	0.028	-0.273
243	0.262	-0.013	-0.275	0.235039	-0.199244	-0.434	0.022	-0.065	-0.087	0.176	0.002	-0.174	0.255	-0.086	-0.341
242	0.223	-0.109	-0.332	0.19856	-0.276321	-0.475	-0.048	-0.107	-0.059	0.142	-0.078	-0.220	0.196	-0.174	-0.370
241	0.158	-0.225	-0.382	0.122976	-0.346965	-0.470	-0.150	-0.207	-0.057	0.085	-0.202	-0.287	0.103	-0.268	-0.371
240	0.142	-0.329	-0.471	0.072556	-0.427527	-0.500	-0.211	-0.320	-0.109	0.008	-0.320	-0.328	0.006	-0.341	-0.347
239	0.116	-0.433	-0.549	-0.006621	-0.553635	-0.547	-0.297	-0.456	-0.159	-0.052	-0.419	-0.367	-0.069	-0.416	-0.347
238	0.044	-0.568	-0.612	-0.124228	-0.709953	-0.586	-0.405	-0.598	-0.193	-0.145	-0.520	-0.375	-0.134	-0.491	-0.357
237	-0.019	-0.665	-0.646	-0.224123	-0.837393	-0.613	-0.505	-0.757	-0.252	-0.220	-0.614	-0.394	-0.171	-0.584	-0.413
236	-0.101	-0.721	-0.620	-0.301392	-0.923991	-0.623	-0.580	-0.913	-0.334	-0.324	-0.737	-0.413	-0.251	-0.734	-0.482
235	-0.194	-0.814	-0.620	-0.402936	-0.98545	-0.583	-0.691	-1.070	-0.378	-0.469	-0.821	-0.351	-0.338	-0.854	-0.516
234	-0.341	-0.853	-0.512	-0.518272	-1.11427	-0.596	-0.805	-1.206	-0.401	-0.612	-0.918	-0.306	-0.463	-1.009	-0.546
233	-0.478	-0.928	-0.451	-0.63332	-1.30254	-0.669	-0.922	-1.333	-0.412	-0.741	-1.006	-0.266	-0.606	-1.141	-0.536
232	-0.616	-1.048	-0.431	-0.711011	-1.43067	-0.720	-1.034	-1.425	-0.391	-0.846	-1.049	-0.203	-0.750	-1.250	-0.500
231	-0.739	-1.158	-0.419	-0.851233	-1.56247	-0.711	-1.195	-1.571	-0.376	-0.928	-1.156	-0.228	-0.887	-1.372	-0.485
230	-0.817	-1.272	-0.455	-0.99026	-1.70046	-0.710	-1.307	-1.691	-0.384	-1.046	-1.274	-0.228	-1.051	-1.437	-0.386
229	-0.890	-1.376	-0.487	-1.11368	-1.85241	-0.739	-1.428	-1.831	-0.404	-1.190	-1.364	-0.174	-1.173	-1.479	-0.306
228	-0.979	-1.513	-0.534	-1.29531	-2.00711	-0.712	-1.547	-1.917	-0.370	-1.290	-1.524	-0.235	-1.245	-1.551	-0.306
227	-1.061	-1.569	-0.508	-1.42927	-2.05117	-0.622	-1.695	-1.967	-0.272	-1.404	-1.695	-0.292	-1.406	-1.693	-0.287
226	-1.207	-1.653	-0.446	-1.57382	-2.13576	-0.562	-1.871	-2.063	-0.192	-1.558	-1.907	-0.349	-1.581	-1.866	-0.284
225	-1.352	-1.757	-0.405	-1.71163	-2.30975	-0.598	-2.060	-2.148	-0.088	-1.686	-1.999	-0.314	-1.763	-2.027	-0.263
224	-1.510	-1.842	-0.332	-1.76378	-2.53521	-0.771	-2.197	-2.336	-0.139	-1.828	-2.193	-0.365	-1.884	-2.215	-0.331
223	-1.586	-1.956	-0.370	-1.83729	-2.80332	-0.966	-2.361	-2.484	-0.123	-1.927	-2.358	-0.432	-2.100	-2.433	-0.333
222	-1.614	-2.219	-0.606	-1.9288	-3.05089	-1.122	-2.542	-2.799	-0.257	-2.037	-2.640	-0.603	-2.272	-2.667	-0.395
221	-1.660	-2.503	-0.843	-2.03	-3.35952	-1.330	-2.770	-3.113	-0.343	-2.135	-2.925	-0.791	-2.321	-2.981	-0.659
220	-1.728	-2.772	-1.044	-2.21286	-3.70354	-1.491	-2.836	-3.447	-0.611	-2.279	-3.214	-0.935	-2.465	-3.314	-0.848
219	-1.772	-3.130	-1.358	-2.37165	-4.16675	-1.795	-2.917	-3.852	-0.935	-2.434	-3.495	-1.061	-2.518	-3.626	-1.108
218	-1.813	-3.540	-1.727	-2.53594	-4.55519	-2.019	-2.919	-4.158	-1.239	-2.497	-3.943	-1.446	-2.635	-3.993	-1.358
217	-1.961	-3.880	-1.919	-2.66818	-4.85417	-2.186	-3.075	-4.572	-1.498	-2.546	-4.275	-1.728	-2.791	-4.473	-1.681
216	-2.140	-4.239	-2.099	-2.78463	-5.28679	-2.502	-3.206	-4.953	-1.747	-2.594	-4.640	-2.047	-2.870	-4.945	-2.075
215	-2.258	-4.444	-2.186	-2.96679	-5.57281	-2.606	-3.170	-5.235	-2.064	-2.707	-4.913	-2.206	-3.065	-5.454	-2.389
214	-2.415	-4.647	-2.232	-3.02311	-5.739	-2.716	-3.191	-5.623	-2.432	-2.816	-5.220	-2.404	-3.142	-5.784	-2.642
213	-2.406	-4.837	-2.432	-3.16233	-5.80087	-2.639	-3.249	-5.883	-2.634	-2.944	-5.434	-2.490	-3.369	-6.148	-2.779
212	-2.372	-5.073	-2.701	-3.29498	-5.97649	-2.682	-3.343	-6.177	-2.834	-3.015	-5.663	-2.649	-3.435	-6.395	-2.960
211	-2.426	-5.106	-2.680	-3.46503	-6.02137	-2.556	-3.544	-6.132	-2.588	-3.207	-5.678	-2.471	-3.622	-6.574	-2.953
210	-2.442	-4.993	-2.551	-3.78082	-5.95344	-2.173	-3.561	-6.096	-2.535	-3.297	-5.376	-2.079	-3.773	-6.679	-2.905
209	-2.439	-4.925	-2.486	-3.97528	-5.6608	-1.686	-3.632	-5.773	-2.141	-3.425	-5.306	-1.881	-3.949	-6.590	-2.641
208	-2.360	-4.722	-2.362	-4.06536	-5.57801	-1.513	-3.634	-5.461	-1.828	-3.421	-5.013	-1.592	-4.128	-6.296	-2.167
207	-2.324	-4.195	-1.871	-4.23362	-5.30283	-1.069	-3.718	-5.198	-1.480	-3.402	-4.632	-1.230	-4.297	-5.761	-1.464
206	-2.280	-3.700	-1.420	-4.25937	-5.04866	-0.789	-3.496	-4.603	-1.107	-3.336	-4.052	-0.716	-4.372	-5.238	-0.866
205	-2.182	-2.694	-0.513	-4.40301	-4.53232	-0.129	-3.222	-3.765	-0.543	-3.442	-3.385	0.058	-4.544	-4.740	-0.196
204	-2.140	-1.773	0.367	-4.31293	-3.88518	0.428	-3.233	-2.917	0.317	-3.379	-2.278	1.101	-4.287	-3.931	0.356
203	-1.648	-0.591	1.057	-4.19761	-3.42357	0.774	-3.090	-2.185	0.904	-3.587	-1.424	2.163	-4.496	-2.760	1.736
202	-1.451	0.756	2.207	-4.15506	-1.85178	2.303	-2.901	-1.000	1.901	-3.189	-0.328	2.861	-4.205	-1.477	2.728
201	-1.314	2.866	4.181	-4.06779	-0.606203	3.462	-2.762	0.395	3.157	-2.834	0.273	3.107	-3.918	-0.694	3.223
200	-0.918	2.482	3.399	-3.0859	0.962709	4.049	-2.435	1.911	4.346	-2.115	1.635	3.750	-3.478	0.421	3.899

A.10. CD DATA:Htelo in TBS at 22 ºC

Htelo in TBS at 22 degrees and 90 degrees

Raw Data: TBS background - 5 scans
22 Degrees Celsius

λ	scan 1	scan 2	scan 3	scan 4	scan 5
320	0.99	1.18	1.14	0.95	1.07
319	1.13	0.98	1.19	1.18	1.13
318	1.01	1.16	1.15	1.07	1.16
317	1.14	1.04	1.05	1.27	1.23
316	1.10	0.97	1.17	1.11	1.21
315	1.06	1.06	1.25	0.95	1.12
314	1.15	1.24	1.13	1.29	1.12
313	1.15	1.18	0.91	1.06	1.14
312	1.04	1.03	1.21	0.95	1.16
311	1.24	0.92	1.10	1.18	1.06
310	1.18	1.24	1.14	1.18	1.17
309	1.05	0.88	1.06	1.22	1.02
308	1.10	1.15	1.28	0.88	1.04
307	1.08	1.06	1.11	0.99	1.10
306	1.01	1.23	1.18	1.18	1.01
305	1.24	1.21	1.00	1.05	1.04
304	1.04	1.16	1.10	0.80	1.12
303	1.14	1.12	0.93	1.14	1.01
302	1.07	1.12	1.06	0.96	1.06
301	1.09	1.07	1.06	0.83	1.05
300	1.22	0.96	1.15	1.18	1.15
299	1.08	1.04	0.97	1.05	1.06
298	1.04	1.06	0.93	0.97	1.00
297	0.83	0.96	0.80	1.11	1.03
296	1.04	1.00	1.01	1.12	1.10
295	1.06	1.05	0.92	1.14	1.10
294	1.12	0.84	1.04	0.86	1.14
293	1.15	1.04	0.99	0.75	0.86
292	0.85	0.98	1.14	0.87	0.87
291	1.06	0.87	0.84	0.88	1.05
290	1.20	0.99	0.96	1.15	1.23
289	0.90	1.10	0.87	1.00	0.82
288	0.89	0.94	0.84	0.93	1.01
287	0.94	0.70	0.70	0.75	1.08
286	0.74	0.84	0.89	0.93	0.91
285	0.87	0.97	0.76	0.73	0.90
284	0.93	0.74	0.83	0.54	0.82
283	0.69	0.79	0.72	0.74	0.89
282	0.83	0.79	0.83	0.78	0.85
281	0.82	0.81	0.69	0.98	0.70
280	0.75	0.67	0.65	0.77	0.75
279	0.68	0.68	0.63	0.83	0.64
278	0.67	0.36	0.57	0.74	0.77
277	0.54	0.60	0.74	0.76	0.42
276	0.44	0.61	0.83	0.53	0.72
275	0.59	0.66	0.73	0.77	0.65
274	0.42	0.37	0.44	0.51	0.70
273	0.46	0.61	0.33	0.47	0.26
272	0.41	0.51	0.21	0.34	0.37
271	0.36	0.40	0.64	0.47	0.47
270	0.21	0.27	0.42	0.67	0.19
269	0.71	0.42	0.26	0.63	0.46
268	0.41	0.33	0.62	0.46	0.64
267	0.37	0.74	0.43	0.60	0.59
266	0.42	0.23	0.51	0.26	0.49
265	0.42	0.11	0.50	0.17	0.25
264	0.56	0.34	0.45	0.31	0.46
263	0.15	0.37	0.46	0.35	0.41
262	0.46	0.44	0.49	0.24	0.38
261	0.31	0.23	0.56	0.46	0.51
260	0.29	0.31	0.35	0.17	0.32
259	0.43	0.46	0.40	0.09	0.57
258	0.21	0.13	0.28	0.58	-0.03
257	0.33	0.50	0.28	0.21	0.09
256	0.26	0.41	0.20	0.42	0.13
255	0.32	0.16	0.04	0.14	0.28

Raw Data: Htelo in TBS - 5 scans
22 Degrees Celsius

λ	scan 1	scan 2	scan 3	scan 4	scan 5
320	1.17	1.47	1.31	1.33	1.37
319	1.21	1.40	1.43	1.31	1.39
318	1.27	1.40	1.23	1.32	1.43
317	1.44	1.40	1.45	1.36	1.41
316	1.26	1.35	1.37	1.17	1.16
315	1.33	1.15	1.36	1.23	1.26
314	1.04	1.31	1.37	1.22	1.21
313	1.32	1.31	1.49	1.21	1.26
312	1.19	1.33	1.41	1.67	1.47
311	1.17	1.32	1.38	1.39	1.37
310	1.11	1.23	1.42	1.55	1.33
309	1.55	1.39	1.27	1.34	1.23
308	1.53	1.46	1.36	1.53	1.47
307	1.51	1.29	1.51	1.37	1.58
306	1.27	1.44	1.34	1.59	1.34
305	1.59	1.60	1.48	1.64	1.34
304	1.74	1.50	1.75	1.81	1.69
303	1.53	1.67	1.64	1.51	1.81
302	1.64	1.51	1.79	1.58	1.77
301	1.73	1.88	1.72	1.83	1.67
300	1.93	1.93	1.95	1.70	1.77
299	1.78	1.76	1.83	1.68	1.91
298	1.91	1.86	1.84	1.82	1.60
297	1.72	1.67	1.64	1.79	1.78
296	1.89	1.68	1.79	1.72	1.82
295	1.79	1.62	1.74	1.69	1.82
294	1.79	1.68	1.76	1.94	1.84
293	1.70	1.72	1.87	1.60	1.76
292	1.88	1.69	1.90	1.66	2.01
291	1.82	1.62	1.57	1.87	1.63
290	1.56	1.61	1.84	1.66	1.77
289	1.50	1.49	1.86	1.56	1.55
288	1.35	1.44	1.39	1.21	1.36
287	1.38	1.51	1.42	1.22	1.46
286	1.31	1.10	1.37	1.40	1.31
285	1.37	1.12	1.18	1.41	1.26
284	1.10	1.29	1.16	0.85	1.12
283	0.86	1.05	1.20	1.12	1.18
282	1.04	0.90	1.09	1.03	1.06
281	1.10	0.88	0.78	0.94	0.93
280	0.61	0.68	0.83	0.71	0.87
279	0.45	0.59	0.75	0.70	0.90
278	0.66	0.75	0.61	0.76	0.58
277	0.50	0.51	0.66	0.48	0.38
276	0.33	0.36	0.52	0.55	0.40
275	0.63	0.59	0.35	0.45	0.45
274	0.29	0.37	0.31	0.36	0.31
273	0.18	0.41	0.24	0.19	0.37
272	0.00	0.15	0.17	0.07	-0.13
271	0.07	0.22	-0.02	0.02	-0.03
270	0.10	-0.03	-0.10	-0.07	0.19
269	0.02	-0.27	-0.14	-0.02	-0.13
268	-0.34	-0.20	-0.22	-0.26	-0.07
267	-0.24	-0.44	-0.36	-0.28	-0.22
266	-0.18	0.04	-0.38	-0.13	-0.34
265	-0.36	-0.25	-0.21	-0.62	-0.37
264	-0.58	-0.09	-0.25	-0.13	-0.44
263	-0.07	-0.05	-0.26	-0.50	-0.30
262	-0.16	-0.52	-0.15	-0.22	-0.10
261	-0.13	-0.29	-0.24	-0.06	-0.02
260	-0.02	-0.22	-0.01	-0.24	0.25
259	-0.05	-0.11	-0.02	-0.18	-0.01
258	-0.15	0.14	-0.15	-0.02	0.19
257	-0.13	0.35	-0.03	0.15	0.18
256	0.45	0.21	-0.09	0.28	0.12
255	0.24	0.42	0.53	0.20	0.38

Averaged and Smoothed over 5 points
Htelo in TBS 22 Degrees Celsius

λ	BG	Htelo	Htelo - BG
320	1.07	1.33	0.26
319	1.12	1.35	0.23
318	1.13	1.37	0.24
317	1.12	1.34	0.22
316	1.13	1.29	0.16
315	1.12	1.30	0.19
314	1.12	1.30	0.18
313	1.12	1.30	0.18
312	1.11	1.31	0.20
311	1.10	1.35	0.25
310	1.10	1.37	0.27
309	1.09	1.38	0.28
308	1.10	1.40	0.30
307	1.10	1.44	0.35
306	1.09	1.49	0.41
305	1.07	1.54	0.47
304	1.08	1.60	0.52
303	1.08	1.65	0.58
302	1.07	1.72	0.65
301	1.05	1.77	0.72
300	1.04	1.78	0.74
299	1.04	1.78	0.74
298	1.03	1.80	0.76
297	1.03	1.78	0.75
296	1.02	1.77	0.76
295	0.98	1.76	0.78
294	0.99	1.77	0.78
293	1.00	1.78	0.78
292	1.00	1.76	0.76
291	0.98	1.71	0.73
290	0.96	1.64	0.68
289	0.95	1.56	0.61
288	0.93	1.48	0.55
287	0.89	1.37	0.48
286	0.85	1.30	0.45
285	0.81	1.23	0.41
284	0.81	1.16	0.34
283	0.80	1.08	0.28
282	0.78	0.98	0.20
281	0.75	0.90	0.15
280	0.71	0.79	0.07
279	0.71	0.71	0.00
278	0.68	0.62	-0.06
277	0.64	0.55	-0.09
276	0.59	0.48	-0.11
275	0.56	0.40	-0.16
274	0.51	0.32	-0.19
273	0.47	0.24	-0.23
272	0.43	0.16	-0.28
271	0.43	0.05	-0.38
270	0.44	-0.04	-0.48
269	0.45	-0.12	-0.57
268	0.45	-0.20	-0.65
267	0.44	-0.24	-0.68
266	0.42	-0.29	-0.70
265	0.42	-0.31	-0.73
264	0.38	-0.28	-0.66
263	0.37	-0.25	-0.62
262	0.36	-0.21	-0.57
261	0.36	-0.17	-0.53
260	0.36	-0.11	-0.46
259	0.31	-0.04	-0.35
258	0.30	0.04	-0.26
257	0.28	0.12	-0.16
256	0.26	0.21	-0.06
255	0.26	0.30	0.03

254	0.38	0.31	0.32	0.42	0.33
253	0.23	0.39	0.25	0.23	0.08
252	0.07	0.28	0.15	0.55	-0.14
251	0.26	0.12	0.35	0.19	0.34
250	-0.12	0.13	0.14	0.31	0.41
249	0.38	0.13	0.21	0.18	0.00
248	0.03	-0.08	0.37	0.41	0.15
247	0.27	0.33	0.01	0.31	0.08
246	0.39	0.19	-0.28	-0.08	0.52
245	-0.01	-0.07	0.27	0.08	-0.19
244	0.11	-0.32	-0.29	0.03	0.33
243	0.04	-0.27	-0.05	0.16	0.04
242	0.22	0.11	0.11	-0.30	-0.13
241	-0.10	-0.12	-0.17	0.24	0.23
240	-0.35	-0.24	0.00	-0.30	-0.53
239	-0.31	-0.22	-0.19	-0.42	-0.24
238	-0.31	-0.67	-0.55	-0.50	-0.54
237	-0.15	-0.39	-0.36	-0.71	0.06
236	-0.06	-0.58	-0.29	-0.57	-0.19
235	-0.20	-0.82	-1.00	-0.28	-0.22
234	-1.05	-0.62	-0.65	-0.65	-0.86
233	-1.00	-1.21	-0.82	-1.12	-0.48
232	-1.18	-0.56	-0.58	-1.09	-0.07
231	-0.49	-1.06	-0.35	-1.28	-1.18
230	-1.32	-0.76	-0.43	-1.35	-1.32
229	-0.91	-1.20	-1.64	-1.29	-1.19
228	-1.10	-1.76	-1.35	-1.25	-1.68
227	-1.80	-0.98	-0.83	-1.18	-1.84
226	-0.84	-1.37	-1.56	-1.52	-1.85
225	-1.71	-1.67	-0.83	-2.01	-1.02
224	-2.24	-1.35	-1.15	-1.49	-2.12
223	-1.85	-2.67	-2.10	-0.88	-2.51
222	-2.67	-2.22	-2.46	-1.86	-1.96
221	-1.58	-2.11	-2.19	-2.37	-3.17
220	-2.58	-2.48	-2.51	-2.72	-2.49
219	-2.83	-2.03	-3.18	-2.38	-2.85
218	-3.19	-1.71	-2.72	-2.35	-1.48
217	-1.76	-2.59	-1.37	-2.50	-2.15
216	-1.98	-1.54	-2.75	-2.47	-3.64
215	-2.70	-2.27	-2.75	-2.13	-3.02
214	-3.39	-2.33	-2.48	-3.04	-2.58
213	-3.11	-2.65	-2.68	-2.88	-1.85
212	-3.06	-3.09	-3.00	-2.55	-2.52
211	-3.99	-4.27	-2.91	-4.09	-1.89
210	-3.20	-3.56	-2.59	-2.68	-2.48
209	-1.50	-3.06	-3.86	-2.32	-2.59
208	-2.65	-2.48	-3.25	-3.87	-2.82
207	-4.08	-2.71	-1.60	-4.07	-3.84
206	-3.53	-3.47	-3.27	-4.89	-4.61
205	-2.59	-1.34	-3.24	-2.72	-4.09
204	-3.17	-2.19	-4.76	-2.67	-2.46
203	-2.06	-2.30	-2.56	-2.07	-2.09
202	-2.41	-3.69	-3.80	-1.68	-2.04
201	-1.48	-0.86	-1.80	-1.53	-1.46
200	-1.60	-3.41	-4.20	-3.43	-1.02

254	0.39	0.62	0.02	0.51	0.54
253	0.70	0.50	0.38	0.64	0.13
252	0.69	0.56	0.52	0.54	0.59
251	0.70	0.60	0.70	0.76	0.63
250	0.64	1.02	1.08	0.74	0.45
249	0.72	0.27	0.58	0.61	0.60
248	0.87	0.74	0.93	0.57	0.49
247	0.68	0.90	0.43	0.72	0.76
246	0.64	0.46	0.51	0.84	0.72
245	0.55	0.20	0.56	0.40	0.88
244	0.50	0.52	0.46	0.65	0.63
243	0.49	0.41	0.54	0.75	1.26
242	0.58	0.59	0.59	-0.03	0.54
241	-0.27	0.39	0.52	0.49	0.45
240	-0.16	0.68	0.31	0.52	0.20
239	-0.05	-0.23	0.26	0.25	-0.19
238	-0.13	-0.13	-0.07	0.36	0.32
237	-0.29	-0.13	-0.34	-0.44	-0.45
236	-0.30	-0.55	-0.72	-0.36	0.46
235	-0.62	-0.51	-0.31	-0.65	-0.42
234	-0.58	-0.49	-1.21	-0.62	-0.51
233	-0.42	-0.80	-0.81	-0.26	-1.12
232	-1.25	-0.34	-0.56	-0.76	-1.05
231	-0.83	-1.46	-1.38	-0.58	-0.88
230	-1.18	-0.58	-0.71	-0.78	-0.77
229	-1.17	-1.22	-1.30	-0.84	-1.34
228	-0.61	-1.45	-1.20	-1.10	-0.94
227	-0.99	-0.77	-1.32	-1.29	-0.89
226	-1.36	-1.31	-2.10	-1.72	-1.61
225	-1.64	-0.88	-1.65	-1.41	-1.11
224	-1.26	-2.43	-1.43	-1.55	-0.92
223	-1.67	-1.54	-0.90	-1.70	-1.66
222	-1.88	-2.00	-1.33	-2.41	-1.55
221	-2.09	-1.84	-1.73	-1.60	-1.69
220	-1.53	-0.56	-1.95	-1.38	-2.72
219	-2.04	-2.32	-2.28	-2.11	-2.00
218	-1.56	-1.56	-1.85	-1.96	-1.69
217	-1.37	-1.30	-2.55	-1.13	-1.67
216	-2.77	-1.82	-1.88	-2.20	-1.29
215	-2.62	-1.69	-3.01	-2.38	-0.85
214	-2.23	-3.82	-1.94	-1.57	-1.94
213	-1.30	-1.65	-1.62	-1.69	-2.75
212	-2.49	-3.92	-2.66	-2.05	-2.95
211	-2.39	-1.95	-2.92	-1.32	-2.68
210	-2.58	-2.09	-2.05	-2.61	-2.41
209	-2.41	-1.89	-1.30	-3.15	-3.71
208	-2.42	-3.05	-1.95	-2.72	-1.95
207	-3.07	-3.55	-3.67	-2.90	-3.28
206	-2.97	-1.86	-2.95	-3.86	-2.04
205	-3.66	-2.24	-2.73	-4.03	-3.31
204	-3.27	-0.78	-4.00	-1.85	-2.40
203	-4.53	-2.42	-2.69	-2.55	-5.38
202	-2.70	-1.83	-1.62	-2.82	-3.28
201	0.66	-1.11	-2.15	-4.73	-1.30
200	-1.34	-2.82	0.52	-0.41	-2.09

254	0.25	0.43	0.18
253	0.25	0.51	0.27
252	0.22	0.58	0.36
251	0.21	0.64	0.43
250	0.22	0.68	0.47
249	0.19	0.70	0.51
248	0.17	0.67	0.50
247	0.14	0.66	0.52
246	0.10	0.64	0.55
245	0.09	0.61	0.52
244	0.05	0.60	0.56
243	0.01	0.52	0.51
242	-0.07	0.47	0.54
241	-0.15	0.37	0.51
240	-0.19	0.25	0.45
239	-0.24	0.10	0.34
238	-0.31	-0.07	0.24
237	-0.43	-0.21	0.22
236	-0.51	-0.34	0.17
235	-0.56	-0.51	0.05
234	-0.63	-0.60	0.03
233	-0.71	-0.74	-0.03
232	-0.87	-0.82	0.04
231	-0.98	-0.87	0.11
230	-1.08	-0.97	0.12
229	-1.16	-1.05	0.11
228	-1.24	-1.15	0.08
227	-1.36	-1.22	0.14
226	-1.48	-1.31	0.16
225	-1.59	-1.46	0.14
224	-1.74	-1.49	0.25
223	-1.96	-1.64	0.33
222	-2.20	-1.73	0.46
221	-2.31	-1.73	0.59
220	-2.39	-1.78	0.61
219	-2.41	-1.80	0.61
218	-2.42	-1.89	0.54
217	-2.43	-1.83	0.59
216	-2.41	-1.95	0.47
215	-2.51	-2.05	0.46
214	-2.68	-2.11	0.57
213	-2.82	-2.26	0.56
212	-2.89	-2.28	0.62
211	-2.87	-2.37	0.50
210	-3.03	-2.44	0.59
209	-3.11	-2.62	0.49
208	-3.24	-2.68	0.57
207	-3.18	-2.78	0.40
206	-3.19	-3.01	0.19
205	-3.03	-3.06	-0.03
204	-2.84	-3.05	-0.21
203	-2.36	-2.90	-0.54
202	-2.08	-2.67	-0.59
201	-1.43	-1.73	-0.30
200	-2.73	-1.23	1.51

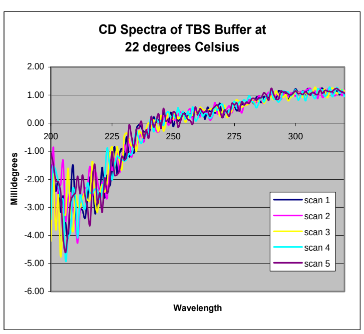

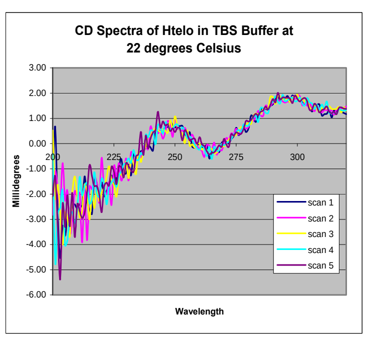

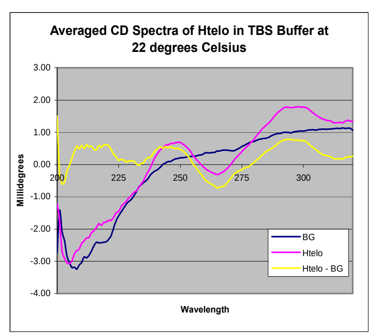

A.11. CD DATA:Htelo in TBS at 90 ºC

Raw Data: TBS background - 5 scans
90 Degrees Celsius

λ	scan 1	scan 2	scan 3	scan 4	scan 5
320	1.09	1.21	1.03	1.21	1.16
319	1.31	1.10	1.29	1.37	1.21
318	1.24	1.11	1.14	1.13	1.38
317	1.09	1.21	1.38	1.28	1.24
316	1.39	1.18	1.23	1.22	1.25
315	1.31	1.23	1.43	1.33	1.19
314	1.08	1.18	1.09	1.16	1.32
313	1.36	1.21	1.26	1.28	1.29
312	1.25	1.17	1.33	1.28	1.19
311	1.31	1.19	1.18	1.12	1.14
310	1.21	1.10	1.18	1.12	1.19
309	1.22	1.21	1.12	1.37	1.16
308	1.24	1.02	1.04	1.42	1.33
307	1.06	1.20	1.30	1.21	1.29
306	1.20	0.97	1.00	1.39	1.03
305	1.26	1.03	1.29	1.13	1.26
304	1.18	1.22	1.14	1.20	1.17
303	1.00	1.14	1.09	1.24	1.18
302	1.11	1.04	1.15	1.12	1.15
301	1.12	1.23	1.02	1.08	1.10
300	1.07	1.13	1.23	1.22	1.34
299	1.00	1.14	1.24	1.26	1.16
298	1.04	0.98	1.18	1.15	1.12
297	0.95	1.08	1.19	0.97	1.24
296	0.94	1.05	1.01	1.13	1.13
295	1.03	0.94	1.00	1.13	1.01
294	1.22	1.01	1.05	0.86	1.01
293	1.16	0.89	1.17	1.13	1.08
292	1.07	0.99	1.19	1.05	1.16
291	1.03	1.10	1.22	1.07	1.15
290	0.95	1.11	0.95	1.17	0.98
289	0.92	1.09	1.13	1.09	0.93
288	0.95	1.13	0.79	0.85	1.00
287	1.01	0.83	0.85	0.96	0.93
286	0.84	0.93	0.90	0.85	0.92
285	0.78	0.84	0.80	0.92	0.67
284	0.90	0.78	0.83	1.00	0.85
283	0.98	0.77	0.66	1.14	1.09
282	0.85	0.66	0.85	0.79	0.94
281	0.64	0.90	0.86	0.83	0.64
280	0.82	0.61	0.73	0.94	0.78
279	0.54	0.80	0.57	0.75	0.82
278	0.61	0.50	0.72	0.91	0.71
277	0.63	0.57	0.55	0.74	0.75
276	0.77	0.76	0.90	0.92	0.75
275	0.57	0.64	0.56	0.62	0.59
274	0.75	0.46	0.58	0.61	0.62
273	0.62	0.59	0.64	0.61	0.45
272	0.74	0.41	0.55	0.69	0.43
271	0.25	0.38	0.46	0.51	0.44
270	0.32	0.53	0.62	0.66	0.50
269	0.52	0.59	0.48	0.39	0.56
268	0.58	0.50	0.63	0.70	0.65
267	0.31	0.57	0.65	0.58	0.29
266	0.61	0.33	0.70	0.51	0.42
265	0.40	0.45	0.63	0.60	0.47
264	0.67	0.39	0.33	0.45	0.20
263	0.45	0.21	0.62	0.37	0.58
262	0.66	0.38	0.70	0.35	0.30
261	0.53	0.43	0.44	0.52	0.28
260	0.27	0.61	0.40	0.55	0.49
259	0.15	0.21	0.51	0.30	0.48
258	0.12	0.21	0.37	0.33	0.34
257	0.49	0.23	0.42	0.74	0.44
256	0.24	0.61	0.44	0.27	0.63
255	0.28	0.41	0.45	0.17	0.30
254	0.44	0.44	0.07	0.83	0.24

Raw Data: Htelo in TBS - 5 scans
90 Degrees Celsius

λ	scan 1	scan 2	scan 3	scan 4	scan 5
320	1.31	1.35	1.40	1.34	1.46
319	1.52	1.49	1.40	1.14	1.29
318	1.54	1.40	1.56	1.36	1.32
317	1.26	1.10	1.37	1.34	1.43
316	1.25	1.33	1.20	1.23	1.18
315	1.10	1.33	1.34	1.41	1.36
314	1.52	1.47	1.34	1.35	1.33
313	1.48	1.30	1.39	1.39	1.23
312	1.43	1.23	1.51	1.25	1.34
311	1.24	1.39	1.56	1.31	1.37
310	1.28	1.20	1.53	1.45	1.42
309	1.60	1.45	1.41	1.37	1.45
308	1.38	1.54	1.21	1.35	1.28
307	1.56	1.42	1.42	1.44	1.46
306	1.42	1.46	1.45	1.39	1.46
305	1.51	1.42	1.24	1.32	1.36
304	1.46	1.56	1.53	1.42	1.41
303	1.41	1.54	1.51	1.56	1.55
302	1.54	1.58	1.45	1.51	1.61
301	1.59	1.53	1.68	1.59	1.48
300	1.59	1.57	1.76	1.49	1.49
299	1.48	1.73	1.71	1.39	1.68
298	1.47	1.56	1.50	1.54	1.67
297	1.59	1.62	1.83	1.65	1.43
296	1.43	1.60	1.64	1.47	1.52
295	1.62	1.68	1.47	1.47	1.64
294	1.82	1.51	1.62	1.63	1.71
293	1.66	1.68	1.58	1.56	1.73
292	1.66	1.60	1.47	1.49	1.45
291	1.52	1.40	1.37	1.44	1.51
290	1.32	1.61	1.62	1.37	1.23
289	1.44	1.41	1.21	1.25	1.44
288	1.27	1.18	1.19	1.30	1.13
287	1.28	1.01	1.18	1.29	1.33
286	1.20	1.06	1.31	1.33	1.21
285	1.30	1.21	1.04	1.06	1.02
284	1.25	0.86	0.97	1.10	0.94
283	1.14	1.08	0.92	1.10	1.01
282	0.90	0.96	0.99	0.76	0.77
281	0.92	0.87	1.16	0.82	0.79
280	0.72	0.77	0.78	0.83	1.02
279	0.87	0.83	0.90	0.68	0.70
278	0.75	0.66	0.96	0.66	0.60
277	0.92	0.95	0.71	0.83	0.79
276	0.86	0.47	0.72	0.71	0.75
275	0.70	0.71	0.89	0.50	0.68
274	0.34	0.62	0.51	0.43	0.55
273	0.47	0.72	0.45	0.50	0.36
272	0.25	0.19	0.33	0.41	0.53
271	0.20	0.50	0.59	0.38	0.35
270	0.37	0.59	0.47	0.30	0.65
269	0.20	0.42	0.20	0.29	0.42
268	0.41	0.07	0.16	0.30	0.21
267	0.22	0.19	0.06	0.28	0.29
266	0.12	0.05	0.31	0.47	0.20
265	0.24	0.18	0.37	0.29	0.55
264	0.07	0.15	0.16	0.36	0.11
263	0.31	0.01	0.26	0.12	0.24
262	0.24	0.23	0.25	0.05	0.21
261	0.10	0.43	0.39	0.18	0.24
260	0.21	0.45	0.14	0.40	0.28
259	0.25	0.29	0.26	0.08	0.30
258	0.36	0.15	0.08	0.40	0.09
257	0.10	0.42	0.46	0.31	0.45
256	0.53	0.35	0.25	0.55	0.00
255	0.53	0.30	0.41	0.58	0.72
254	0.47	0.68	0.59	0.27	0.33

Averaged and Smoothed over 5 points
Htelo in TBS 90 Degrees Celsius

λ	BG	Htelo	Htelo - BG
320	1.14	1.37	0.23
319	1.26	1.37	0.11
318	1.23	1.39	0.16
317	1.26	1.32	0.06
316	1.25	1.32	0.07
315	1.26	1.33	0.07
314	1.24	1.33	0.09
313	1.23	1.35	0.11
312	1.22	1.37	0.15
311	1.22	1.39	0.17
310	1.20	1.40	0.20
309	1.20	1.39	0.20
308	1.19	1.40	0.22
307	1.19	1.41	0.23
306	1.18	1.43	0.24
305	1.16	1.45	0.28
304	1.15	1.47	0.32
303	1.15	1.51	0.36
302	1.15	1.52	0.38
301	1.15	1.56	0.41
300	1.14	1.58	0.45
299	1.13	1.58	0.45
298	1.11	1.58	0.47
297	1.09	1.59	0.51
296	1.06	1.60	0.54
295	1.05	1.60	0.55
294	1.06	1.60	0.54
293	1.07	1.59	0.51
292	1.07	1.54	0.47
291	1.07	1.48	0.42
290	1.06	1.41	0.36
289	1.01	1.34	0.33
288	0.95	1.27	0.32
287	0.92	1.23	0.31
286	0.89	1.17	0.28
285	0.88	1.11	0.24
284	0.86	1.06	0.20
283	0.84	1.01	0.16
282	0.82	0.93	0.11
281	0.78	0.88	0.10
280	0.77	0.84	0.07
279	0.74	0.82	0.09
278	0.71	0.78	0.07
277	0.69	0.75	0.06
276	0.68	0.69	0.01
275	0.64	0.62	-0.02
274	0.61	0.56	-0.05
273	0.56	0.51	-0.06
272	0.54	0.44	-0.10
271	0.51	0.39	-0.12
270	0.52	0.33	-0.19
269	0.52	0.32	-0.20
268	0.52	0.29	-0.23
267	0.51	0.27	-0.24
266	0.51	0.23	-0.29
265	0.48	0.20	-0.28
264	0.48	0.22	-0.26
263	0.46	0.23	-0.23
262	0.44	0.23	-0.21
261	0.41	0.23	-0.18
260	0.41	0.22	-0.19
259	0.40	0.26	-0.14
258	0.40	0.30	-0.10
257	0.38	0.33	-0.05
256	0.36	0.37	0.01
255	0.35	0.41	0.06
254	0.34	0.45	0.10

253	0.15	0.22	0.21	0.21	0.21
252	0.24	0.39	0.09	0.21	0.23
251	0.22	0.53	0.53	0.22	0.25
250	0.53	0.00	0.23	0.18	-0.15
249	0.08	0.11	0.12	0.46	0.07
248	-0.39	0.33	0.19	0.12	0.33
247	0.20	0.05	0.11	-0.08	0.32
246	-0.20	0.28	-0.17	0.00	-0.07
245	0.08	-0.13	0.07	0.17	0.27
244	0.16	0.14	-0.05	0.17	0.17
243	-0.11	-0.20	0.19	0.14	-0.33
242	0.49	-0.12	0.11	0.19	0.19
241	0.22	-0.23	0.27	0.07	-0.33
240	0.28	-0.34	-0.23	-0.24	-0.31
239	-0.43	0.16	0.06	-0.38	0.12
238	-0.31	-0.18	-0.08	0.06	-0.31
237	-0.80	-0.07	-0.35	-0.46	-0.18
236	-0.62	-0.48	-1.11	-0.52	-0.33
235	-0.45	-0.85	-0.48	-0.11	-0.34
234	-0.71	-1.03	-0.31	-0.38	-0.67
233	-0.70	-0.72	-0.13	-0.80	-0.59
232	-1.37	-0.33	-0.84	-1.13	-0.87
231	-1.21	-0.90	-0.60	-1.17	-1.27
230	-1.04	-1.65	-0.91	-1.56	-1.58
229	-1.73	-1.01	-1.26	-1.43	-1.34
228	-1.00	-1.68	-1.37	-0.92	-1.47
227	-1.98	-1.30	-1.68	-2.11	-1.23
226	-1.62	-1.24	-2.07	-1.57	-1.76
225	-0.76	-2.11	-1.71	-1.65	-1.86
224	-2.22	-1.95	-2.66	-1.95	-1.72
223	-1.93	-2.34	-2.05	-2.61	-2.08
222	-1.74	-2.52	-1.94	-2.39	-1.77
221	-2.36	-3.29	-3.13	-2.82	-2.06
220	-2.45	-2.14	-1.53	-2.68	-1.64
219	-3.60	-2.34	-2.79	-2.87	-3.27
218	-3.05	-2.71	-2.29	-2.93	-2.13
217	-2.00	-3.16	-2.60	-2.35	-1.71
216	-2.33	-3.60	-2.64	-2.39	-3.04
215	-3.18	-3.16	-3.05	-3.15	-2.34
214	-2.66	-2.70	-3.33	-3.03	-2.83
213	-3.38	-3.58	-1.48	-3.31	-3.65
212	-3.00	-2.27	-2.38	-3.14	-2.19
211	-2.65	-2.57	-2.50	-2.46	-3.58
210	-3.22	-2.67	-1.54	-2.88	-3.84
209	-5.37	-5.36	-2.59	-4.35	-3.18
208	-1.62	-1.85	-3.80	-4.90	-3.45
207	-2.58	-1.81	-3.24	-3.61	-4.18
206	-2.34	-2.09	-2.97	-4.54	-1.11
205	-3.40	-3.97	-3.67	-2.12	-2.11
204	-4.92	-0.84	-3.73	-3.29	-2.17
203	-0.39	-2.02	-3.15	-3.90	-1.18
202	1.94	-1.82	-4.14	-1.60	-2.27
201	-2.15	-1.11	-1.22	-0.46	-5.62
200	-6.55	-0.82	-1.16	-1.59	2.31

253	0.43	0.30	0.43	0.14	0.73
252	0.43	0.60	0.71	0.22	0.59
251	0.32	0.40	0.30	0.54	0.71
250	0.39	0.49	0.61	0.10	0.58
249	0.24	0.56	0.63	0.46	0.55
248	0.39	-0.09	0.96	0.39	0.49
247	0.25	0.52	-0.12	0.26	0.46
246	0.29	0.08	0.31	0.12	0.32
245	0.45	0.22	-0.18	0.50	0.07
244	0.13	-0.04	-0.03	-0.03	0.06
243	0.32	0.08	-0.06	-0.05	0.37
242	0.11	0.07	-0.06	-0.24	-0.12
241	-0.20	0.01	0.03	0.47	0.19
240	-0.14	-0.29	-0.35	-0.13	-0.14
239	0.05	-0.44	-0.38	-0.02	0.16
238	-0.37	-0.20	-0.18	-0.59	-0.88
237	-0.14	-0.37	-0.55	-0.07	-0.07
236	-0.30	-0.45	-0.49	-0.67	-0.54
235	-0.52	0.04	-0.73	-0.55	-0.25
234	-0.61	-0.90	-0.85	-0.48	-0.35
233	-0.77	-0.73	-0.71	-0.65	-1.19
232	-0.92	-0.87	-0.52	-0.88	-1.18
231	-1.23	-0.76	-1.47	-1.05	-1.37
230	-1.19	-0.91	-0.97	-1.21	-1.16
229	-1.79	-1.29	-1.26	-1.03	-1.28
228	-1.50	-2.26	-1.81	-0.88	-0.83
227	-1.51	-1.76	-1.55	-1.58	-1.80
226	-2.22	-1.08	-1.30	-1.96	-1.72
225	-1.26	-1.40	-2.22	-1.49	-1.60
224	-1.09	-1.95	-1.71	-1.14	-1.66
223	-1.86	-2.00	-2.03	-2.17	-1.69
222	-1.80	-1.71	-2.44	-1.94	-1.98
221	-1.99	-2.93	-1.82	-1.68	-1.63
220	-2.22	-1.53	-0.92	-0.98	-1.24
219	-2.33	-2.04	-2.45	-1.80	-2.74
218	-2.39	-1.29	-2.28	-1.55	-2.84
217	-2.57	-2.41	-1.71	-1.60	-2.30
216	-3.37	-2.85	-1.18	-2.36	-1.30
215	-2.41	-2.04	-1.72	-1.72	-2.48
214	-2.81	-3.30	-3.53	-2.61	-2.81
213	-3.03	-2.47	-3.21	-1.35	-1.94
212	-2.70	-3.05	-3.50	-2.62	-1.94
211	-2.44	-2.41	-4.01	-2.70	-1.90
210	-4.14	-2.27	-2.31	-3.41	-0.27
209	-3.22	-2.94	-3.29	-4.36	-3.91
208	-4.26	-1.84	-4.12	-3.09	-3.01
207	-2.35	-2.54	-3.04	-3.20	-2.72
206	-3.45	-3.18	-3.93	-5.16	-2.46
205	0.27	-0.42	-4.19	-4.53	-3.31
204	-3.41	-4.17	-4.29	-4.55	-1.74
203	-1.73	-3.31	-4.06	-4.93	-2.28
202	-1.65	-0.93	-0.45	-3.69	-4.03
201	-3.24	-3.18	-0.21	-3.96	2.91
200	0.06	-4.30	-5.51	-4.47	-1.62

253	0.32	0.47	0.16
252	0.26	0.49	0.23
251	0.24	0.48	0.25
250	0.20	0.45	0.25
249	0.15	0.43	0.29
248	0.14	0.38	0.24
247	0.08	0.32	0.23
246	0.06	0.24	0.18
245	0.08	0.19	0.11
244	0.06	0.11	0.05
243	0.04	0.08	0.04
242	0.03	0.01	-0.03
241	0.02	-0.05	-0.07
240	-0.08	-0.13	-0.06
239	-0.16	-0.19	-0.03
238	-0.25	-0.26	-0.01
237	-0.35	-0.34	0.01
236	-0.42	-0.43	-0.01
235	-0.49	-0.53	-0.03
234	-0.63	-0.64	-0.02
233	-0.77	-0.75	0.02
232	-0.88	-0.91	-0.03
231	-1.02	-1.05	-0.03
230	-1.21	-1.22	-0.02
229	-1.31	-1.36	-0.05
228	-1.44	-1.43	0.01
227	-1.57	-1.51	0.06
226	-1.65	-1.59	0.06
225	-1.83	-1.74	0.09
224	-1.94	-1.72	0.22
223	-2.13	-1.76	0.36
222	-2.29	-1.81	0.48
221	-2.41	-1.87	0.53
220	-2.49	-1.96	0.53
219	-2.55	-1.94	0.60
218	-2.62	-2.03	0.60
217	-2.75	-2.12	0.63
216	-2.77	-2.27	0.50
215	-2.85	-2.46	0.40
214	-2.70	-2.40	0.29
213	-2.87	-2.55	0.32
212	-3.00	-2.74	0.27
211	-3.09	-2.80	0.30
210	-3.11	-3.00	0.11
209	-3.14	-2.94	0.20
208	-3.22	-3.08	0.14
207	-3.27	-3.23	0.05
206	-3.06	-3.32	-0.27
205	-2.81	-3.09	-0.27
204	-2.57	-2.91	-0.34
203	-2.35	-2.66	-0.30
202	-1.83	-2.10	-0.28
201	-2.11	-1.53	0.58
200	-1.56	-3.17	-1.61

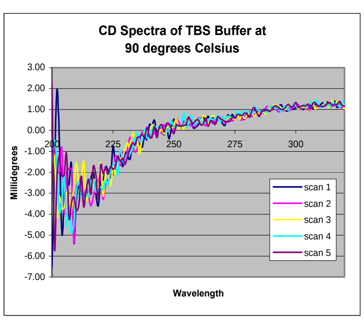

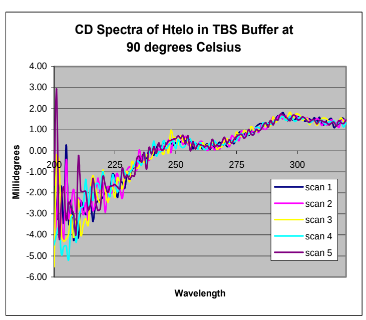

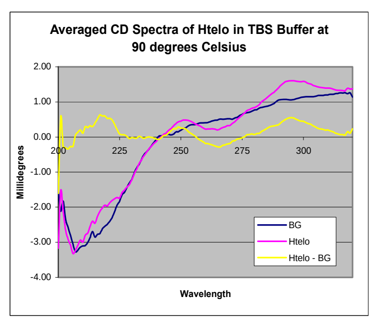

A.12. CD Data: Htelo in No Salt Tris Buffer at 22ºC

Htelo in No Salt Tris Buffer at 22 degrees and 90 degrees

Raw Data: No Salt Tris Buffer background - 5 scans
22 Degrees Celsius

λ	scan 1	scan 2	scan 3	scan 4	scan 5
320	1.95	1.81	1.70	1.91	1.76
319	1.91	1.76	1.92	1.78	1.71
318	2.00	1.88	1.69	1.74	1.71
317	1.79	1.79	1.88	1.87	1.80
316	1.85	1.90	1.98	1.78	1.62
315	2.05	1.98	1.76	1.91	1.60
314	1.97	1.70	1.83	2.04	1.85
313	2.08	1.76	1.67	1.69	1.60
312	1.93	1.81	1.87	1.72	1.75
311	1.89	1.88	1.73	1.80	1.80
310	1.77	1.77	1.85	1.74	1.49
309	2.01	1.91	1.70	1.92	1.66
308	1.89	1.88	1.76	1.85	1.59
307	1.85	1.75	1.78	1.94	1.81
306	1.88	1.82	1.95	1.64	1.79
305	1.87	1.93	1.95	1.97	1.72
304	2.00	2.00	1.76	1.80	1.70
303	1.73	1.82	1.68	1.79	1.65
302	1.79	1.78	1.64	1.75	1.70
301	1.75	1.86	1.51	1.66	1.70
300	1.72	1.66	1.77	1.55	1.55
299	1.76	1.70	1.62	1.61	1.42
298	1.97	1.86	1.72	1.47	1.63
297	1.75	1.70	1.64	1.67	1.52
296	1.73	1.55	1.65	1.47	1.54
295	1.78	1.72	1.50	1.82	1.58
294	1.71	1.55	1.57	1.56	1.38
293	1.59	1.48	1.68	1.65	1.43
292	1.62	1.56	1.40	1.49	1.67
291	1.50	1.60	1.64	1.24	1.63
290	1.65	1.59	1.55	1.19	1.26
289	1.64	1.53	1.51	1.50	1.44
288	1.63	1.36	1.37	1.44	1.33
287	1.61	1.59	1.35	1.37	1.55
286	1.48	1.42	1.30	1.47	1.46
285	1.55	1.37	1.52	1.29	1.22
284	1.29	1.41	1.25	1.32	1.30
283	1.43	1.37	1.29	1.24	1.26
282	1.36	1.31	1.42	1.13	1.25
281	1.14	1.25	1.34	1.14	1.17
280	1.19	1.25	1.21	1.37	0.98
279	1.11	1.08	1.13	1.03	0.97
278	1.31	1.14	1.13	1.07	1.25
277	1.27	1.13	1.26	1.15	0.89
276	1.17	1.21	1.29	1.13	0.86
275	1.05	1.09	1.17	0.99	1.16
274	1.08	1.01	1.07	0.98	1.10
273	1.07	1.15	1.06	1.07	0.85
272	0.79	0.87	0.78	0.93	0.71
271	0.90	0.78	1.01	0.80	0.68
270	1.01	0.89	0.59	0.78	0.77
269	1.06	0.73	0.94	0.95	0.71
268	0.78	0.95	0.76	0.84	0.65
267	0.90	0.62	0.90	0.82	0.84
266	0.68	0.60	0.66	0.70	0.71
265	0.74	0.63	0.87	0.66	0.74
264	0.87	0.80	0.61	0.67	0.67
263	0.61	0.68	0.50	0.72	0.30
262	0.74	0.66	0.80	0.58	0.49
261	0.84	0.81	0.88	0.63	0.57
260	0.87	0.59	0.53	0.44	0.69
259	0.43	0.68	0.45	0.28	0.82
258	0.29	0.11	0.49	0.57	0.49
257	0.44	0.45	0.63	0.33	0.30
256	0.33	0.35	0.54	0.56	0.19
255	0.46	0.12	0.67	0.30	0.70
254	0.46	0.30	0.31	0.28	0.37

Raw Data: Htelo in No Salt Tris Buffer - 5 scans
22 Degrees Celsius

λ	scan 1	scan 2	scan 3	scan 4	scan 5
320	1.84	1.61	1.66	1.62	1.55
319	1.76	1.70	1.74	1.56	1.52
318	1.62	1.74	1.70	1.49	1.54
317	1.76	1.70	1.64	1.66	1.51
316	1.54	1.52	1.63	1.70	1.56
315	1.67	1.69	1.68	1.51	1.59
314	1.61	1.55	1.66	1.50	1.39
313	1.35	1.61	1.63	1.63	1.62
312	1.74	1.55	1.54	1.69	1.39
311	1.78	1.66	1.63	1.64	1.52
310	1.78	1.76	1.63	1.58	1.65
309	1.81	1.91	1.70	1.55	1.64
308	1.90	1.85	1.56	1.58	1.49
307	1.42	1.61	1.43	1.67	1.53
306	1.81	1.59	1.57	1.44	1.61
305	1.68	1.64	1.44	1.35	1.69
304	1.59	1.57	1.56	1.46	1.44
303	1.64	1.64	1.63	1.60	1.46
302	1.62	1.67	1.65	1.78	1.51
301	1.63	1.69	1.68	1.53	1.46
300	1.56	1.60	1.62	1.64	1.44
299	1.74	1.41	1.59	1.55	1.50
298	1.54	1.57	1.43	1.60	1.43
297	1.56	1.57	1.66	1.57	1.34
296	1.69	1.48	1.55	1.65	1.22
295	1.66	1.52	1.75	1.54	1.62
294	1.66	1.52	1.51	1.61	1.42
293	1.54	1.55	1.64	1.43	1.52
292	1.54	1.53	1.39	1.35	1.32
291	1.52	1.58	1.42	1.37	1.38
290	1.39	1.39	1.39	1.17	1.47
289	1.35	1.25	1.33	1.30	1.38
288	1.36	1.36	1.36	1.24	1.17
287	1.25	1.32	1.38	1.03	1.19
286	1.34	1.23	1.14	1.43	1.22
285	1.11	1.37	1.06	1.07	1.17
284	1.01	1.11	1.39	1.04	1.08
283	0.91	1.08	0.93	1.26	1.17
282	1.04	1.17	1.33	0.98	1.05
281	1.32	1.17	1.02	1.06	0.87
280	1.07	1.15	1.17	1.08	0.96
279	1.09	0.96	1.11	1.05	0.91
278	1.24	1.06	0.77	0.99	0.98
277	1.10	1.08	0.78	0.80	1.01
276	1.10	1.10	0.91	1.13	0.78
275	0.99	1.06	1.00	0.86	0.96
274	1.20	0.99	0.74	1.00	0.79
273	1.05	1.16	0.89	0.83	0.68
272	0.97	1.14	0.96	1.21	0.73
271	0.82	1.07	0.98	1.02	0.95
270	0.76	1.05	1.20	0.90	0.90
269	0.72	0.93	0.72	1.03	0.81
268	0.54	0.90	0.93	1.03	1.05
267	0.99	1.03	0.99	0.91	0.67
266	1.00	1.06	0.78	0.97	0.78
265	0.95	0.86	1.16	0.77	0.87
264	0.94	1.00	0.99	1.06	1.14
263	1.05	1.03	0.84	0.94	0.90
262	0.94	0.70	0.90	0.90	1.03
261	1.04	1.10	1.02	0.90	0.43
260	1.06	0.70	1.03	0.96	0.85
259	0.94	1.00	1.03	0.83	1.46
258	1.08	1.07	0.96	0.71	1.02
257	0.79	0.94	0.77	0.78	0.65
256	0.88	0.87	0.80	0.60	0.68
255	0.85	1.00	0.75	0.67	0.88
254	0.74	0.78	0.32	0.99	0.63

Averaged and Smoothed over 5 points
Htelo in No Salt Tris Buffer 22 Degrees Celsius

λ	BG	Htelo	Htelo - BG
320	1.83	1.65	-0.17
319	1.82	1.65	-0.16
318	1.81	1.64	-0.17
317	1.82	1.63	-0.19
316	1.83	1.61	-0.23
315	1.84	1.59	-0.25
314	1.83	1.58	-0.24
313	1.82	1.59	-0.23
312	1.81	1.62	-0.18
311	1.80	1.64	-0.16
310	1.78	1.65	-0.14
309	1.79	1.66	-0.13
308	1.82	1.64	-0.18
307	1.83	1.61	-0.22
306	1.83	1.59	-0.24
305	1.84	1.58	-0.26
304	1.81	1.57	-0.24
303	1.77	1.58	-0.19
302	1.74	1.59	-0.14
301	1.71	1.58	-0.13
300	1.67	1.57	-0.10
299	1.66	1.57	-0.10
298	1.66	1.55	-0.11
297	1.65	1.55	-0.09
296	1.63	1.55	-0.09
295	1.62	1.55	-0.08
294	1.59	1.54	-0.05
293	1.56	1.51	-0.05
292	1.54	1.48	-0.06
291	1.52	1.42	-0.09
290	1.49	1.37	-0.12
289	1.49	1.34	-0.15
288	1.47	1.30	-0.17
287	1.44	1.25	-0.19
286	1.42	1.21	-0.22
285	1.39	1.17	-0.22
284	1.36	1.14	-0.21
283	1.31	1.12	-0.19
282	1.25	1.10	-0.16
281	1.22	1.07	-0.15
280	1.19	1.05	-0.13
279	1.17	1.04	-0.13
278	1.14	1.02	-0.12
277	1.14	0.99	-0.15
276	1.12	0.97	-0.15
275	1.08	0.96	-0.12
274	1.03	0.97	-0.06
273	0.97	0.96	0.00
272	0.91	0.95	0.04
271	0.88	0.94	0.06
270	0.84	0.93	0.09
269	0.80	0.91	0.11
268	0.79	0.91	0.12
267	0.78	0.91	0.14
266	0.73	0.93	0.19
265	0.71	0.93	0.23
264	0.69	0.94	0.25
263	0.69	0.94	0.26
262	0.66	0.96	0.30
261	0.63	0.96	0.33
260	0.57	0.94	0.37
259	0.54	0.92	0.39
258	0.50	0.90	0.40
257	0.44	0.87	0.43
256	0.39	0.85	0.45
255	0.38	0.81	0.43
254	0.35	0.71	0.36

253	0.56	0.31	0.62	0.11	0.21
252	0.36	0.48	0.18	0.08	0.40
251	0.31	0.37	0.86	-0.12	0.25
250	0.19	0.37	0.09	0.48	0.30
249	0.40	0.74	0.42	0.20	0.59
248	0.06	0.18	0.26	0.31	-0.04
247	0.31	0.18	0.14	0.09	0.00
246	0.15	-0.03	0.12	0.04	0.32
245	0.32	0.41	0.16	0.15	0.10
244	0.22	-0.13	-0.07	0.05	-0.37
243	0.21	0.08	0.02	-0.43	-0.05
242	-0.23	-0.03	0.18	0.06	-0.09
241	-0.36	-0.20	-0.31	-0.10	-0.09
240	0.04	-0.13	-0.28	-0.19	-0.48
239	-0.01	-0.29	0.16	-0.25	-0.42
238	-0.51	-0.28	0.02	-0.22	-0.23
237	-0.32	-1.04	-0.50	-0.50	-0.18
236	-0.72	-0.92	-0.80	-0.82	-0.33
235	-0.80	-0.56	-0.35	-0.93	-0.46
234	-1.12	-1.26	-1.19	-1.23	-0.89
233	-0.84	-1.00	-1.33	-0.87	-0.94
232	-1.40	-1.39	-0.72	-1.41	-1.14
231	-1.45	-1.34	-1.02	-1.02	-1.67
230	-1.81	-1.20	-1.74	-1.50	-1.44
229	-2.26	-1.41	-1.64	-2.01	-1.79
228	-1.70	-1.85	-1.90	-2.01	-2.20
227	-1.98	-2.96	-1.99	-1.89	-2.00
226	-2.01	-1.81	-1.54	-1.50	-1.90
225	-2.42	-1.94	-2.48	-2.25	-2.15
224	-2.67	-2.39	-2.50	-2.68	-1.94
223	-1.96	-2.70	-1.95	-2.63	-2.61
222	-2.31	-2.55	-3.59	-2.83	-2.35
221	-3.05	-2.41	-3.47	-2.53	-2.80
220	-3.34	-2.87	-3.42	-2.73	-2.70
219	-2.22	-2.98	-2.51	-4.03	-3.08
218	-2.65	-3.11	-3.91	-3.96	-3.09
217	-3.54	-3.78	-3.32	-4.26	-3.30
216	-4.09	-3.90	-3.43	-3.41	-3.85
215	-3.11	-3.07	-3.09	-3.97	-4.43
214	-3.82	-3.86	-3.48	-3.01	-4.36
213	-4.18	-3.54	-4.33	-3.90	-3.94
212	-4.05	-3.61	-4.03	-3.14	-4.17
211	-3.89	-3.82	-3.67	-4.52	-4.66
210	-4.20	-3.78	-5.15	-4.47	-5.34
209	-4.03	-3.56	-5.15	-4.00	-4.69
208	-4.40	-3.56	-3.68	-4.34	-5.15
207	-3.49	-5.38	-5.54	-3.73	-3.47
206	-3.42	-4.34	-4.62	-5.41	-4.78
205	-4.02	-4.29	-3.60	-2.64	-4.54
204	-4.72	-6.41	-4.49	-5.29	-1.68
203	-3.52	-2.31	-5.37	-5.46	-3.39
202	-4.33	-4.76	-2.39	-3.40	-3.48
201	-4.00	-3.00	-3.71	-3.18	-5.01
200	-4.19	-2.60	-1.92	-4.82	-3.08

253	0.50	0.72	0.83	0.92	0.57
252	0.79	0.64	0.83	0.42	0.62
251	0.29	0.80	0.34	0.34	0.27
250	-0.04	0.42	0.07	0.19	-0.05
249	0.41	0.42	0.24	0.35	0.05
248	-0.18	0.14	0.49	0.15	0.36
247	0.07	0.09	-0.11	0.02	0.28
246	0.21	0.33	0.01	0.35	0.08
245	0.29	0.05	-0.09	0.15	-0.33
244	-0.25	-0.16	-0.53	0.00	-0.09
243	-0.18	-0.42	0.02	-0.35	-0.43
242	-0.15	-0.03	-0.28	-0.38	-0.35
241	-0.64	-0.32	-0.25	-0.67	-0.33
240	-0.44	-0.02	-0.47	-0.41	-0.16
239	-0.67	-0.79	-0.76	-0.40	-0.90
238	-0.77	-0.64	-0.87	-0.59	-1.01
237	-0.70	-0.67	-0.69	-0.89	-0.67
236	-0.90	-0.88	-0.48	-1.12	-1.10
235	-1.08	-1.21	-1.09	-1.39	-1.10
234	-0.59	-0.93	-1.13	-1.06	-1.11
233	-1.28	-0.72	-1.13	-1.43	-1.14
232	-1.25	-1.94	-1.50	-1.28	-1.14
231	-1.18	-1.43	-1.69	-1.52	-1.03
230	-1.53	-1.46	-0.46	-1.25	-2.24
229	-1.68	-1.75	-1.12	-2.18	-1.75
228	-1.44	-1.41	-1.14	-1.88	-1.62
227	-1.76	-2.24	-2.24	-1.78	-1.59
226	-2.38	-2.23	-1.89	-2.38	-2.06
225	-2.23	-2.38	-1.99	-1.58	-1.49
224	-2.45	-2.22	-2.18	-2.18	-2.54
223	-1.28	-1.64	-1.15	-2.11	-2.05
222	-2.28	-2.00	-2.29	-2.59	-2.06
221	-2.26	-2.15	-3.02	-1.70	-2.57
220	-2.66	-2.93	-2.90	-1.58	-3.05
219	-2.49	-2.77	-2.73	-2.11	-3.01
218	-0.50	-2.10	-2.66	-1.96	-1.82
217	-2.53	-2.48	-1.58	-2.41	-2.15
216	-3.10	-2.24	-3.33	-1.93	-1.73
215	-2.47	-1.96	-2.09	-3.40	-2.37
214	-4.26	-3.03	-3.74	-2.77	-2.43
213	-2.76	-3.00	-3.78	-3.18	-2.30
212	-3.72	-3.05	-3.45	-3.72	-2.87
211	-3.30	-1.66	-3.81	-3.33	-3.57
210	-3.55	-3.26	-2.82	-4.17	-4.27
209	-4.33	-1.97	-3.85	-3.47	-2.24
208	-3.08	-4.07	-5.23	-3.26	-5.59
207	-6.00	-5.81	-2.53	-4.02	-3.41
206	-5.11	-4.27	-5.40	-4.70	-6.06
205	-5.40	-4.17	-4.17	-4.37	-1.56
204	-4.54	-5.21	-4.90	-4.71	-3.99
203	-5.72	-4.92	-2.67	-7.10	-5.96
202	-3.64	-3.14	-6.65	-3.53	-5.31
201	-5.86	-4.62	-3.39	-4.10	-6.76
200	-5.34	-7.44	-4.08	-5.79	-5.85

253	0.37	0.63	0.26
252	0.36	0.55	0.19
251	0.34	0.43	0.09
250	0.29	0.33	0.03
249	0.29	0.26	-0.03
248	0.25	0.18	-0.07
247	0.20	0.10	-0.10
246	0.15	0.06	-0.09
245	0.09	-0.02	-0.11
244	0.01	-0.11	-0.11
243	-0.02	-0.19	-0.16
242	-0.06	-0.30	-0.24
241	-0.11	-0.41	-0.30
240	-0.20	-0.48	-0.28
239	-0.23	-0.59	-0.36
238	-0.35	-0.70	-0.35
237	-0.48	-0.80	-0.32
236	-0.61	-0.91	-0.30
235	-0.77	-1.03	-0.27
234	-0.92	-1.08	-0.17
233	-1.07	-1.21	-0.13
232	-1.21	-1.29	-0.07
231	-1.43	-1.35	0.08
230	-1.58	-1.48	0.10
229	-1.69	-1.61	0.08
228	-1.87	-1.78	0.09
227	-1.98	-1.84	0.14
226	-2.10	-1.93	0.17
225	-2.21	-1.99	0.22
224	-2.35	-2.06	0.29
223	-2.48	-2.23	0.24
222	-2.62	-2.24	0.37
221	-2.83	-2.25	0.58
220	-3.00	-2.30	0.70
219	-3.18	-2.25	0.93
218	-3.33	-2.36	0.97
217	-3.47	-2.36	1.11
216	-3.58	-2.49	1.10
215	-3.66	-2.60	1.06
214	-3.80	-2.86	0.95
213	-3.91	-3.05	0.86
212	-4.01	-3.17	0.84
211	-4.11	-3.29	0.82
210	-4.29	-3.60	0.69
209	-4.30	-3.75	0.55
208	-4.34	-3.96	0.39
207	-4.39	-4.25	0.14
206	-4.30	-4.47	-0.18
205	-4.22	-4.56	-0.34
204	-4.17	-4.62	-0.45
203	-4.02	-4.60	-0.59
202	-3.78	-4.78	-0.99
201	-3.78	-4.95	-1.17
200	-3.32	-5.70	-2.38

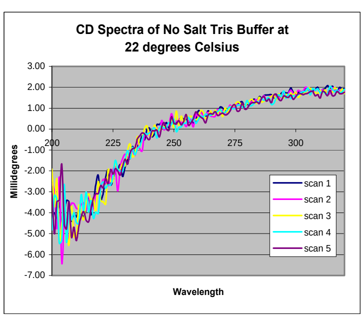

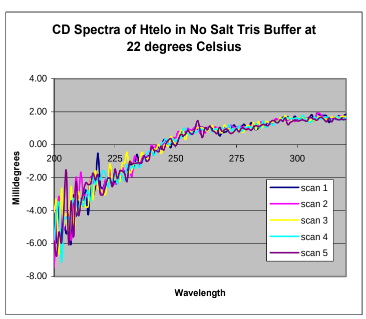

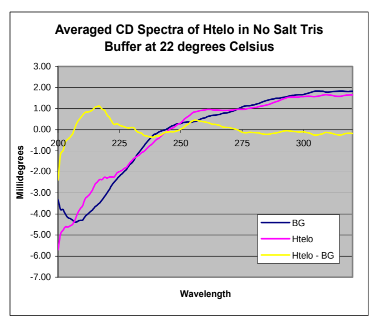

A.13. CD Data: Htelo in No Salt Tris Buffer at 90 ºC

Raw Data: No Salt Tris Buffer background - 5 scans
90 Degrees Celsius

λ	scan 1	scan 2	scan 3	scan 4	scan 5
320	1.82	1.55	1.66	1.76	1.29
319	1.86	1.51	1.62	1.51	1.47
318	1.50	1.51	1.62	1.60	1.72
317	1.58	1.52	1.57	1.46	1.49
316	1.75	1.54	1.59	1.49	1.55
315	1.61	1.48	1.66	1.55	1.47
314	1.75	1.75	1.53	1.59	1.51
313	1.70	1.60	1.50	1.56	1.47
312	1.64	1.74	1.50	1.64	1.63
311	1.59	1.65	1.64	1.49	1.67
310	1.52	1.61	1.52	1.46	1.56
309	1.51	1.62	1.57	1.68	1.59
308	1.58	1.65	1.45	1.55	1.37
307	1.67	1.57	1.36	1.40	1.50
306	1.74	1.51	1.41	1.49	1.47
305	1.45	1.38	1.57	1.62	1.62
304	1.60	1.65	1.51	1.44	1.46
303	1.70	1.51	1.57	1.44	1.65
302	1.80	1.56	1.59	1.60	1.55
301	1.38	1.50	1.66	1.67	1.70
300	1.45	1.62	1.56	1.32	1.38
299	1.46	1.57	1.52	1.56	1.53
298	1.30	1.67	1.38	1.46	1.36
297	1.44	1.72	1.47	1.43	1.41
296	1.48	1.45	1.50	1.47	1.55
295	1.50	1.57	1.52	1.50	1.50
294	1.40	1.29	1.50	1.36	1.37
293	1.53	1.59	1.40	1.50	1.59
292	1.69	1.35	1.61	1.38	1.39
291	1.56	1.63	1.32	1.37	1.24
290	1.22	1.47	1.57	1.47	1.48
289	1.33	1.22	1.29	1.49	1.47
288	1.49	1.30	1.47	1.28	1.39
287	1.41	1.17	1.30	1.50	1.41
286	1.36	1.34	1.50	1.27	1.20
285	1.46	1.28	1.20	1.14	1.33
284	1.39	1.22	1.33	1.36	1.33
283	1.34	1.28	0.90	1.13	1.23
282	1.00	1.08	1.18	1.20	1.27
281	1.18	1.15	1.22	1.28	1.14
280	1.08	1.08	1.07	1.08	1.19
279	1.18	1.16	1.19	1.24	1.37
278	1.20	0.95	1.47	0.91	1.29
277	1.07	1.09	1.20	0.95	1.01
276	0.98	1.21	1.00	0.99	0.78
275	1.10	1.00	1.02	1.24	1.15
274	1.06	0.81	1.25	0.85	1.16
273	1.13	0.97	0.96	1.12	1.14
272	1.27	0.89	0.87	0.83	0.84
271	0.92	0.99	0.96	1.05	0.98
270	1.01	0.83	1.01	1.12	0.86
269	1.11	1.05	0.85	0.97	1.07
268	0.77	0.90	0.85	0.95	0.72
267	0.93	1.13	0.74	0.75	0.79
266	0.88	0.74	0.86	0.93	0.90
265	0.65	0.90	1.03	0.75	0.88
264	1.10	0.78	0.92	1.01	0.65
263	0.83	1.12	0.78	0.95	0.99
262	0.75	0.73	1.07	0.75	0.72
261	0.94	0.80	0.69	0.63	0.76
260	0.96	0.98	0.90	0.88	0.72
259	0.80	0.77	0.95	1.05	0.86
258	0.73	0.29	0.73	0.80	0.67
257	0.83	0.65	0.84	0.76	0.67
256	1.08	0.58	0.75	0.48	0.64
255	0.83	0.80	0.58	0.55	0.90
254	0.58	0.73	0.86	0.73	0.58

Raw Data: Htelo in No Salt Tris Buffer - 5 scans
90 Degrees Celsius

λ	scan 1	scan 2	scan 3	scan 4	scan 5
320	1.59	1.63	1.60	1.50	1.45
319	1.65	1.59	1.63	1.57	1.26
318	1.45	1.43	1.47	1.29	1.41
317	1.51	1.47	1.39	1.53	1.36
316	1.41	1.56	1.44	1.41	1.53
315	1.55	1.49	1.45	1.38	1.57
314	1.49	1.61	1.51	1.35	1.32
313	1.45	1.30	1.40	1.41	1.25
312	1.46	1.47	1.43	1.41	1.37
311	1.39	1.36	1.54	1.37	1.30
310	1.43	1.56	1.40	1.32	1.51
309	1.55	1.28	1.43	1.38	1.54
308	1.31	1.47	1.52	1.36	1.15
307	1.42	1.45	1.36	1.38	1.43
306	1.50	1.14	1.25	1.16	1.27
305	1.27	1.39	1.52	1.45	1.45
304	1.32	1.34	1.42	1.31	1.36
303	1.30	1.25	1.36	1.25	1.59
302	1.34	1.57	1.47	1.26	1.36
301	1.28	1.38	1.35	1.37	1.31
300	1.53	1.31	1.24	1.36	1.29
299	1.26	1.34	1.24	1.26	1.18
298	1.35	1.32	1.35	1.27	1.29
297	1.30	1.28	1.32	1.27	1.37
296	1.35	1.40	1.45	1.36	1.43
295	1.22	1.19	1.41	1.42	1.31
294	1.62	1.31	1.32	1.53	1.31
293	1.40	1.43	1.26	1.42	1.42
292	1.30	1.24	1.31	1.43	1.39
291	1.28	1.30	1.23	1.18	1.19
290	1.23	1.22	1.38	1.18	1.12
289	1.27	1.21	1.36	1.40	1.33
288	1.43	1.20	1.23	1.29	1.17
287	1.11	1.46	1.22	1.16	1.26
286	1.17	1.28	1.23	1.01	1.13
285	0.98	1.28	1.18	1.04	1.41
284	0.95	1.07	1.07	1.06	1.01
283	1.17	1.21	1.04	1.06	1.09
282	1.02	1.13	1.24	1.20	1.11
281	1.26	1.25	0.95	1.14	0.99
280	1.11	1.20	0.94	1.00	1.02
279	1.09	1.12	1.07	1.43	0.83
278	1.23	0.85	0.75	0.77	0.85
277	0.90	1.17	1.02	0.95	1.13
276	1.33	0.88	0.84	1.11	0.75
275	1.14	1.04	1.15	1.05	0.57
274	0.95	0.94	1.05	1.08	0.89
273	1.34	0.91	0.85	0.76	0.86
272	0.91	1.07	0.95	0.77	0.80
271	0.68	1.00	0.89	0.82	1.14
270	0.81	0.71	0.91	0.79	1.13
269	1.13	0.91	0.90	0.72	0.65
268	0.73	0.69	0.92	0.48	0.68
267	1.12	0.92	0.72	0.82	1.03
266	0.77	0.57	0.78	0.84	0.64
265	0.72	0.99	1.01	0.68	0.76
264	0.91	0.69	0.85	0.79	0.91
263	0.75	0.71	0.58	0.66	0.77
262	0.91	0.80	0.51	0.74	0.56
261	0.65	0.67	0.53	0.48	0.91
260	0.86	0.61	0.94	0.80	0.97
259	0.95	0.53	0.61	0.44	0.54
258	0.69	0.61	0.53	0.82	0.84
257	0.50	0.49	0.64	0.88	0.61
256	0.48	0.56	0.73	0.47	0.62
255	0.50	0.23	0.45	0.71	0.43
254	0.36	0.62	0.42	0.37	0.06

Averaged and Smoothed over 5 points
Htelo in No Salt Tris Buffer 90 Degrees Celsius

λ	BG	Htelo	Htelo - BG
320	1.62	1.55	-0.06
319	1.59	1.54	-0.05
318	1.57	1.45	-0.11
317	1.56	1.45	-0.10
316	1.56	1.45	-0.11
315	1.58	1.44	-0.15
314	1.59	1.43	-0.16
313	1.60	1.44	-0.16
312	1.60	1.42	-0.18
311	1.59	1.42	-0.17
310	1.57	1.40	-0.17
309	1.55	1.40	-0.16
308	1.54	1.39	-0.14
307	1.52	1.37	-0.15
306	1.52	1.37	-0.16
305	1.55	1.36	-0.19
304	1.55	1.36	-0.18
303	1.57	1.36	-0.21
302	1.56	1.35	-0.21
301	1.55	1.34	-0.21
300	1.53	1.32	-0.20
299	1.52	1.32	-0.20
298	1.49	1.32	-0.17
297	1.47	1.33	-0.14
296	1.47	1.35	-0.12
295	1.48	1.36	-0.12
294	1.48	1.36	-0.12
293	1.47	1.34	-0.13
292	1.46	1.33	-0.13
291	1.44	1.31	-0.13
290	1.42	1.29	-0.14
289	1.40	1.26	-0.14
288	1.38	1.23	-0.14
287	1.36	1.21	-0.15
286	1.33	1.19	-0.14
285	1.29	1.16	-0.14
284	1.25	1.12	-0.13
283	1.22	1.12	-0.09
282	1.20	1.10	-0.10
281	1.18	1.08	-0.10
280	1.15	1.06	-0.09
279	1.13	1.05	-0.08
278	1.12	1.02	-0.10
277	1.11	1.00	-0.11
276	1.08	0.98	-0.10
275	1.05	0.97	-0.08
274	1.01	0.96	-0.06
273	1.02	0.97	-0.05
272	1.01	0.91	-0.10
271	0.99	0.89	-0.09
270	0.95	0.86	-0.09
269	0.92	0.83	-0.09
268	0.89	0.83	-0.07
267	0.90	0.82	-0.08
266	0.88	0.80	-0.08
265	0.86	0.77	-0.09
264	0.84	0.77	-0.08
263	0.88	0.76	-0.12
262	0.86	0.72	-0.13
261	0.84	0.72	-0.12
260	0.81	0.70	-0.11
259	0.78	0.69	-0.10
258	0.77	0.66	-0.11
257	0.75	0.61	-0.15
256	0.72	0.55	-0.17
255	0.66	0.49	-0.18
254	0.64	0.46	-0.18

253	0.35	0.51	0.65	0.38	0.71
252	0.58	0.81	0.45	0.57	0.60
251	0.21	0.83	0.56	0.60	0.59
250	0.56	0.37	0.80	0.97	0.39
249	0.09	0.96	0.41	0.52	0.71
248	0.27	0.42	0.37	0.83	0.78
247	0.56	0.73	0.31	0.51	0.59
246	0.23	0.27	0.57	0.71	0.47
245	0.21	0.18	0.60	0.45	0.32
244	0.60	0.09	0.47	0.10	0.50
243	0.64	0.31	0.31	0.26	0.59
242	0.28	0.15	0.40	0.14	0.60
241	0.42	0.36	0.52	0.40	0.72
240	0.05	0.69	0.14	0.20	0.58
239	0.22	0.20	0.02	0.13	-0.07
238	0.04	-0.14	0.28	-0.01	-0.02
237	-0.36	-0.13	0.16	-0.14	-0.22
236	0.08	-0.16	0.22	-0.12	0.25
235	0.19	-0.16	-0.33	-0.92	0.00
234	-0.01	-0.07	-0.50	-0.03	-0.03
233	0.17	-0.62	-0.55	-0.39	-0.32
232	-0.66	-0.96	-0.39	-0.67	-0.64
231	-0.51	-0.40	-0.56	-1.14	-1.44
230	-0.38	-1.23	-0.89	-1.49	-1.26
229	-1.02	-0.25	-0.92	-0.74	-0.93
228	-1.19	-1.58	-1.46	-0.43	-0.85
227	-1.40	-0.81	-1.10	-0.83	-1.07
226	-1.53	-0.44	-1.34	-1.14	-1.36
225	-1.30	-1.05	-1.02	-1.42	-1.31
224	-1.43	-1.30	-0.75	-1.56	-0.40
223	-0.71	-1.78	-2.00	-1.27	-1.05
222	-1.54	-1.05	-2.02	-1.12	-1.70
221	-1.49	-1.73	-2.23	-1.20	-1.56
220	-1.27	-1.80	-1.99	-2.20	-2.08
219	-0.88	-1.87	-1.15	-2.68	-2.34
218	-1.21	-1.24	-1.79	-1.43	-1.68
217	-2.35	-1.26	-2.11	-2.18	-2.23
216	-2.11	-1.90	-3.30	-2.35	-1.92
215	-0.99	-1.90	-1.68	-2.05	-2.44
214	-1.13	-2.49	-2.11	-2.21	-2.31
213	-1.36	-1.37	-1.62	-1.88	-2.20
212	-2.09	-3.26	-1.57	-3.10	-2.25
211	-1.94	-2.55	-1.11	-2.94	-3.57
210	-2.89	-2.32	-2.93	-1.69	-1.75
209	-2.07	-3.16	-1.56	-1.61	-2.64
208	-3.22	-2.89	-2.17	-1.65	-2.56
207	-2.17	-3.64	-1.89	-1.60	-2.89
206	-1.78	-3.97	-3.27	-0.75	0.29
205	-2.12	-0.77	-0.57	-2.73	-2.19
204	-3.56	-0.36	-1.18	-2.12	-0.35
203	-2.87	-0.38	-2.10	-1.96	-1.96
202	-3.13	-4.10	0.78	-1.56	-0.49
201	1.80	0.22	-1.28	-0.44	-3.77
200	-4.84	1.03	-2.06	1.88	-0.40

253	0.20	0.44	0.36	0.55	0.40
252	0.52	0.39	0.50	0.28	0.24
251	0.38	0.21	0.14	0.61	0.36
250	0.06	0.28	-0.09	0.64	0.19
249	-0.15	0.34	0.06	0.30	-0.29
248	0.41	0.14	0.25	0.13	-0.44
247	0.42	0.20	-0.01	0.09	-0.09
246	0.02	0.42	0.25	-0.15	0.17
245	-0.20	-0.14	-0.31	-0.56	-0.03
244	0.11	0.05	-0.43	0.12	0.25
243	0.04	-0.19	-0.55	0.05	0.07
242	-0.04	0.00	-0.17	-0.49	0.02
241	-0.40	-0.67	-0.56	-0.15	-0.01
240	-0.58	-0.39	-0.30	-0.09	-0.23
239	-0.37	-0.35	-0.07	-0.24	-0.33
238	-0.59	-0.46	-0.32	-0.27	-0.45
237	-0.47	-0.27	-0.71	-0.61	-0.28
236	-0.82	-0.39	-0.57	-0.91	-0.49
235	-0.67	-0.88	-1.18	-0.72	-0.77
234	-0.60	-0.71	-1.20	-0.44	-0.46
233	-0.81	-0.73	-1.33	-0.27	-1.17
232	-1.50	-1.14	-0.83	-1.29	-0.75
231	-1.41	-1.23	-1.64	-1.61	-1.13
230	-0.59	-1.14	-1.17	-0.86	-1.69
229	-1.12	-1.23	-1.63	-1.69	-1.02
228	-1.68	-0.70	-1.30	-1.35	-1.15
227	-1.41	-1.80	-1.29	-1.50	-1.29
226	-1.67	-1.34	-1.00	-1.94	-2.41
225	-1.27	-1.75	-1.72	-2.32	-2.40
224	-1.42	-1.99	-1.79	-0.84	-1.67
223	-1.60	-1.99	-2.09	-2.10	-1.80
222	-1.68	-1.78	-1.68	-2.29	-2.48
221	-2.42	-1.86	-1.99	-1.72	-1.48
220	-2.24	-2.75	-2.33	-1.03	-1.38
219	-2.60	-2.75	-1.54	-2.55	-2.36
218	-2.04	-2.63	-1.66	-1.56	-1.96
217	-1.78	-1.68	-1.53	-2.86	-1.50
216	-1.58	-1.90	-1.26	-1.61	-2.17
215	-1.96	-1.59	-1.50	-2.53	-1.31
214	-2.66	-2.76	-1.38	-2.85	-1.81
213	-2.65	-1.63	-2.55	-1.85	-1.75
212	-2.77	-1.68	-2.45	-4.23	-2.45
211	-2.67	-1.84	-4.06	-1.75	-2.61
210	-1.42	-3.46	-4.82	-2.86	-2.09
209	-3.38	-3.13	-2.52	-3.11	-3.75
208	-2.30	-3.97	-1.77	-2.18	-2.60
207	-3.22	-2.23	-1.26	-1.69	-3.69
206	-3.48	-2.90	-1.98	-1.73	-3.27
205	-3.35	-3.83	-4.07	-2.64	-5.04
204	-1.79	-4.58	-1.98	-3.54	-3.80
203	-3.01	-0.89	-4.88	-0.81	-2.40
202	-4.76	-3.17	-1.34	0.09	-5.43
201	-3.44	-1.23	-0.35	-3.10	-2.00
200	-3.22	-4.15	-5.43	-1.71	-2.14

253	0.63	0.39	-0.25
252	0.60	0.32	-0.27
251	0.58	0.26	-0.32
250	0.57	0.24	-0.32
249	0.55	0.17	-0.38
248	0.53	0.11	-0.42
247	0.49	0.05	-0.44
246	0.44	0.02	-0.42
245	0.41	-0.02	-0.43
244	0.42	-0.08	-0.49
243	0.40	-0.14	-0.54
242	0.38	-0.20	-0.57
241	0.31	-0.24	-0.55
240	0.27	-0.26	-0.53
239	0.17	-0.38	-0.55
238	0.08	-0.44	-0.53
237	0.02	-0.51	-0.52
236	-0.08	-0.56	-0.48
235	-0.16	-0.72	-0.56
234	-0.30	-0.84	-0.54
233	-0.43	-0.97	-0.54
232	-0.58	-1.06	-0.48
231	-0.74	-1.13	-0.38
230	-0.86	-1.20	-0.34
229	-1.00	-1.35	-0.35
228	-1.04	-1.41	-0.37
227	-1.06	-1.47	-0.41
226	-1.10	-1.57	-0.47
225	-1.15	-1.71	-0.56
224	-1.28	-1.75	-0.47
223	-1.40	-1.88	-0.48
222	-1.48	-1.95	-0.47
221	-1.54	-2.01	-0.46
220	-1.70	-2.02	-0.32
219	-1.81	-2.00	-0.19
218	-1.90	-1.95	-0.06
217	-1.88	-1.90	-0.02
216	-1.90	-1.93	-0.03
215	-1.97	-1.96	0.01
214	-2.08	-2.04	0.04
213	-2.14	-2.31	-0.17
212	-2.15	-2.55	-0.40
211	-2.27	-2.71	-0.44
210	-2.40	-2.68	-0.29
209	-2.40	-2.76	-0.36
208	-2.31	-2.93	-0.62
207	-2.13	-2.90	-0.77
206	-2.08	-2.99	-0.91
205	-1.93	-2.84	-0.91
204	-1.70	-2.92	-1.22
203	-1.61	-2.79	-1.18
202	-1.49	-2.38	-0.89
201	-0.69	-2.03	-1.33
200	-0.88	-3.33	-2.45

CD Spectra of No Salt Tris Buffer at 90 degrees Celsius

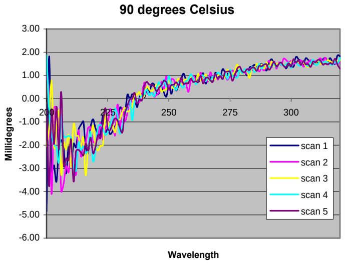

CD Spectra of Htelo in No Salt Tris Buffer at 90 degrees Celsius

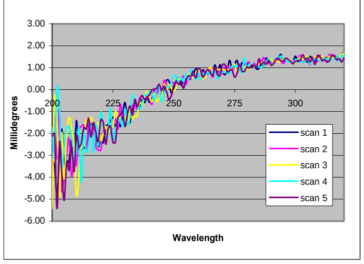

Averaged CD Spectra of Htelo in No Salt Tris Buffer at 90 degrees Celsius